

PL-TR-97-2141

MFD-FR-97-15920

**FURTHER ANALYSES OF REGIONAL SEISMIC DATA  
RECORDED FROM THE SOVIET PNE PROGRAM:  
IMPLICATIONS WITH RESPECT TO CTBT  
MONITORING**

**J. R. Murphy  
D. D. Sultanov  
B. W. Barker**

**I. O. Kitov  
M. E. Marshall**

**Maxwell Technologies, Incorporated  
8888 Balboa Avenue  
San Diego, CA 92123-1506**

**October 1997**

19980422 112

**Final Report  
August 1995 - August 1997**

**DTIC QUALITY INSPECTED 4**

**Approved for public release; distribution unlimited.**



**PHILLIPS LABORATORY  
Directorate of Geophysics  
AIR FORCE MATERIEL COMMAND  
HANSCOM AFB, MA 01731-3010**

SPONSORED BY  
Air Force Technical Applications Center  
Directorate of Nuclear Treaty Monitoring  
Project Authorization T/5101

MONITORED BY  
Phillips Laboratory  
CONTRACT No. F19628-95-C-0109

The views and conclusions contained in this document are those of the authors and should not be interpreted as representing the official policies, either express or implied, of the Air Force or U.S. Government.

This technical report has been reviewed and is approved for publication.

  
JAMES C. BATNS  
Contract Manager

  
CHARLES P. PIKE, Deputy Director  
Integration and Operations Division

This report has been reviewed by the ESD Public Affairs Office (PA) and is releasable to the National Technical Information Service (NTIS).

Qualified requestors may obtain copies from the Defense Technical Information Center. All others should apply to the National Technical Information Service.

If your address has changed, or you wish to be removed from the mailing list, or if the addressee is no longer employed by your organization, please notify PL/IM, 29 Randolph Road, Hanscom AFB, MA 01731-3010. This will assist us in maintaining a current mailing list.

Do not return copies of the report unless contractual obligations or notices on a specific document requires that it be returned.

REPORT DOCUMENTATION PAGE			Form Approved OMB No. 0704-0188	
Public reporting burden for this collection of information is estimated to average 1 hour per response, including the time for reviewing instructions, searching existing data sources, gathering and maintaining the data needed, and completing and reviewing the collection of information. Send comments regarding this burden estimate or any other aspect of this collection of information, including suggestions for reducing this burden, to Washington Headquarters Services, Directorate for Information Operations and Reports, 1216 Jefferson Davis Highway, Suite 1204, Arlington, VA 22202-4302, and to the Office of Management and Budget, Paperwork Reduction Project (0704-0188), Washington, DC 20503.				
1. AGENCY USE ONLY (Leave blank)	2. REPORT DATE October, 1997	3. REPORT TYPE AND DATES COVERED Final Report 8/95 - 8/97		
4. TITLE AND SUBTITLE Further Analyses of Regional Seismic Data Recorded From the Soviet PNE Program: Implications With Respect to CTBT Monitoring			5. FUNDING NUMBERS Contract No. F19628-95-C-0109 PE 35999F PR 5101 TA GM WU AE	
6. AUTHOR(S) J. R. Murphy, D. D. Sultanov*, B. W. Barker, I. O. Kitov* and M. E. Marshall			8. PERFORMING ORGANIZATION REPORT NUMBER MFD-FR-97-15920	
7. PERFORMING ORGANIZATION NAME(S) AND ADDRESS(ES) Maxwell Technologies, Inc. 8888 Balboa Avenue San Diego, CA 92123-1514			10. SPONSORING/MONITORING AGENCY REPORT NUMBER PL-TR-97-2141	
9. SPONSORING/MONITORING AGENCY NAME(S) AND ADDRESS(ES) Phillips Laboratory 29 Randolph Road Hanscom AFB, MA 01731-3010  Contract Manager: James Battis/GPI				
11. SUPPLEMENTARY NOTES  *Institute for Dynamics of the Geospheres, Russian Academy of Sciences				
12a. DISTRIBUTION/AVAILABILITY STATEMENT Approved for public release; distribution unlimited			12b. DISTRIBUTION CODE	
13. ABSTRACT (Maximum 200 words)  This report summarizes the result of a joint research program which has been carried out by scientists from Maxwell Technologies, Inc. and the Russian Institute for Dynamics of the Geospheres to use regional seismic data recorded from Soviet PNE tests to assess the transportability of regional discriminants. More specifically, the goal of the study has been to use these PNE data to derive improved, quantitative bounds on the ranges of regional seismic signal characteristics which might be expected from underground nuclear tests conducted under the variety of source and propagation path conditions which must be considered in global monitoring of the CTBT. Broadband data recorded at the Borovoye Geophysical Observatory in Central Asia from 29 of these PNE tests in the distance range from about 7 to 9 degrees have now been processed and analyzed in detail. The characteristics of the explosion source coupling inferred from this analysis indicate systematic variations with source yield, depth of burial and medium which are generally consistent with those predicted by the Mueller/Murphy source model. Moreover, the L <sub>g</sub> /P spectral ratios determined from these observed Borovoye PNE data generally decline to average values (over)				
14. SUBJECT TERMS Seismic Discrimination Nuclear Explosion			15. NUMBER OF PAGES	
Regional Soviet PNE Borovoye			CTBT Monitoring Source Coupling	
17. SECURITY CLASSIFICATION OF REPORT UNCLASSIFIED			16. PRICE CODE	
18. SECURITY CLASSIFICATION OF THIS PAGE UNCLASSIFIED		19. SECURITY CLASSIFICATION OF ABSTRACT UNCLASSIFIED		20. LIMITATION OF ABSTRACT UNLIMITED

CLASSIFIED BY:

DECLASSIFY ON:

13. ABSTRACT (Continued)

of 1 or less at frequencies above about 3 Hz and, therefore, typically appear explosion-like at high frequencies over this entire range of source and propagation path conditions.

## Table of Contents

1.0	Introduction.....	1
2.0	Overview of Regional Seismic Data Recorded at the Borovoye Geophysical Observatory From Soviet PNE Tests.....	4
3.0	Regional Phase Spectra and Discrimination .....	13
4.0	Theoretical Modeling Analysis of Near-Regional Seismic Data Recorded From Selected PNE Events .....	48
5.0	Summary and Conclusions .....	64
	5.1 Summary .....	64
	5.2 Conclusions .....	65
	References .....	68

## List of Illustrations

1. Locations of representative Soviet PNE events (large squares) shown as overlays to a shaded topographic map of the former Soviet Union and surrounding countries. The small squares correspond to the ISC seismicity for the region for the period 1988-1990..... 2
2. Map locations of selected Soviet PNE tests which were recorded at the Borovoye digital station in Kazakhstan..... 5
3. Vertical component regional signals recorded at Borovoye from selected Soviet PNE events in Groups I and II. Note the strong dependence of the Pg/Pn ratios on station to source azimuth (Az) for these explosions at comparable distances from the Borovoye station.. ..... 8
4. Map of types of crust in the Borovoye region. A sample of representative crustal types is shown in Figure 5..... 10
5. Comparison of the subsurface velocity models corresponding to representative crustal types from Figure 4..... 12
6. Comparison of the frequency dependent yield (n) and depth (m) scaling exponents derived from the covariance analysis of Borovoye data recorded from the 21 PNE events of Groups I, II, A and B with the corresponding values predicted by the Mueller/Murphy explosion source model..... 19
7. Comparison of the frequency dependent yield (n) and depth (m) scaling exponents derived from the covariance analysis of Borovoye data recorded from the non-clay PNE events of Groups I, II, A and B with the corresponding values predicted by the Mueller/Murphy explosion source model..... 24
8. Comparison of the frequency dependent yield (n) and depth (m) scaling exponents derived from the covariance analysis

	of Borovoye RMS spectral amplitude levels defined over short and long time windows.....	26
9	Illustration of the effects of explosion yield (left) and depth of burial (right) on the regional phase spectra predicted by the non-clay covariance model for the Group I Pn phase.....	27
10	Comparison of regional phase spectra predicted for a 10 kt underground nuclear explosion at a depth of 1000 m using the covariance analysis results for the four selected groups of Soviet PNE events recorded at the Borovoye station.....	29
11	Regional phase spectral ratios for fixed yield and depth of burial, Group II/Group I. Note that the enhancement of the Group II Pg amplitudes with respect to Group I is limited to low frequencies and that it is associated with a corresponding broadband decrease in relative Pn amplitude.....	30
12	Frequency dependent amplitude attenuation as a function of epicentral distance ( $\Delta$ ) relative to Group II ( $\Delta = 10.2^\circ$ ) inferred from the statistical covariance analyses of Pn (left) and Sn (right) PNE data recorded at the Borovoye station...	32
13	Frequency dependent amplitude attenuation as a function of frequency relative to Group II ( $\Delta = 10.2^\circ$ ) inferred from statistical covariance analyses of P coda (left) and Pg (right) PNE data recorded at Borovoye.....	33
14	Comparison of the frequency dependent Lg amplitude attenuation as a function of epicentral distance relative to Group II ( $\Delta = 10.2^\circ$ ) inferred from statistical covariance analyses of PNE data recorded at the Borovoye station (left) and from Mitchell's (1996) coda Q estimates for Central Asia (right).....	34
15	Ratios of observed to predicted (Group A covariance model) Borovoye regional phase spectra for selected Azgir explosions. Note that the observed Azgir Lg spectral amplitude levels are quite consistent with those of Group A explosions at comparable distances outside the Caspian Basin.	36

16	Ratios of observed to predicted (Group A covariance model) Borovoye regional phase spectra for selected Astrakhan explosions. Note that the observed Astrakhan Lg spectral amplitude levels are quite consistent with those of Group A explosions at comparable distances outside the Caspian Basin.	37
17	Comparison of estimates of covariance model prediction uncertainties ( $\sigma$ ) versus frequency for various assumed levels of regional calibration.....	40
18	Observed Lg/Pn spectral ratios corresponding to the different groups of Soviet PNE events recorded at the Borovoye station.....	41
19	Observed Lg/Pg spectral ratios corresponding to the different groups of Soviet PNE events recorded at the Borovoye station.....	42
20	Observed Sn/Pn spectral ratios corresponding to the different groups of Soviet PNE events recorded at the Borovoye station.....	43
21	Observed Sn/Pg spectral ratios corresponding to the different groups of Soviet PNE events recorded at the Borovoye station.....	44
22	Comparison of estimates of covariance model prediction uncertainties ( $\sigma$ ) versus frequency for the different regional phase spectral ratios.....	46
23	Average Lg/Pg spectral ratios corresponding to the different groups of Soviet PNE events recorded at the Borovoye station.....	47
24	Comparison of observed (solid) and synthetic (dashed) near-regional, vertical component displacements for the PNE event of 7/21/84, which was a 13.5 kt explosion at a depth of 846 m in salt.....	53

25	Comparison of observed (solid) and synthetic (dashed) near-regional, vertical component displacements for the PNE event of 8/10/77, which was an 8.5 kt explosion at a depth of 499 m in granite. ....	55
26	Comparison of observed (solid) and synthetic (dashed) near-regional, vertical component displacements for the PNE event of 9/17/84, which was an 10 kt explosion at a depth of 557 m in granite. ....	56
27	Comparison of observed (solid) and synthetic (dashed) near-regional, vertical component displacements for the PNE event of 7/18/85, which was an 8.5 kt explosion at a depth of 772 m in granite ....	57
28	Comparison of observed (solid) and synthetic (dashed) near-regional, vertical component displacements for the PNE event of 10/02/74, which was a 1.7 kt explosion at a depth of 98 m in limestone.....	58
29	Comparison of observed (solid) and synthetic (dashed) near-regional, vertical component displacements for the PNE event of 9/02697, which was a 7.6 kt explosion at a depth of 1212 m in granite.....	59
30	Comparison of observed (solid) and synthetic (dashed) near-regional, vertical component displacements for the PNE event of 4/11/72, which was a 14 kt explosion at a depth of 1720 m in limestone ....	60
31	Comparison of observed (solid) and synthetic (dashed) near-regional, vertical component displacements for the PNE event of 4/18/87, which was a 3.2 kt explosion at a depth of 2055 m in limestone. ....	61
32	Comparison of observed (solid) and synthetic (dashed) near-regional, vertical component displacements for the PNE event of 6/18/85, which was a 2.5 kt explosion at a depth of 2859 m in sandstone. ....	63

## 1. INTRODUCTION

In order to discriminate the regional seismic signals produced by underground nuclear explosions from those produced by earthquakes, rockbursts and conventional mining explosions of comparable magnitude, it is necessary to know the range of nuclear explosion signal variation that can be expected as a function of source and propagation path conditions over the entire ranges of these conditions which may be encountered in global test monitoring under the CTBT. However, most of the empirical regional discrimination studies which have been conducted to date have focused on analyses of seismic signals recorded from underground tests conducted at the few major nuclear test sites, and these sample only limited ranges of the variables of interest. This constitutes a serious limitation in that existing theoretical simulation models have not yet proven capable of fully explaining the observed characteristics of the various proposed empirical discriminants and, therefore, their extrapolation to applications in new environments is subject to considerable uncertainty. In an attempt to overcome these limitations of previous analyses, we have been working with scientists from the Russian Institute for Dynamics of the Geospheres (IDG) to use regional seismic data recorded from the extensive Soviet Peaceful Nuclear Explosion (PNE) testing program to better quantify the variability of regional discriminants over ranges of explosion source and propagation path conditions which may be more representative of the diversity which will be encountered in global CTBT monitoring.

From its inception in the mid 1960's, the Soviet PNE program utilized nuclear explosions in a variety of commercial and scientific applications. Over 120 explosions were conducted in this series up until its cessation in 1988 and the locations of these tests were widely dispersed throughout the territories of the former Soviet Union. This fact is graphically illustrated in Figure 1 where the locations of a representative subset of these explosions are shown as overlays (large squares) to a gray-scale topographic map of the former Soviet Union and surrounding countries. The ISC seismicity database for the area for the period 1988-1990 is also included as an overlay (small squares) to this map to illustrate

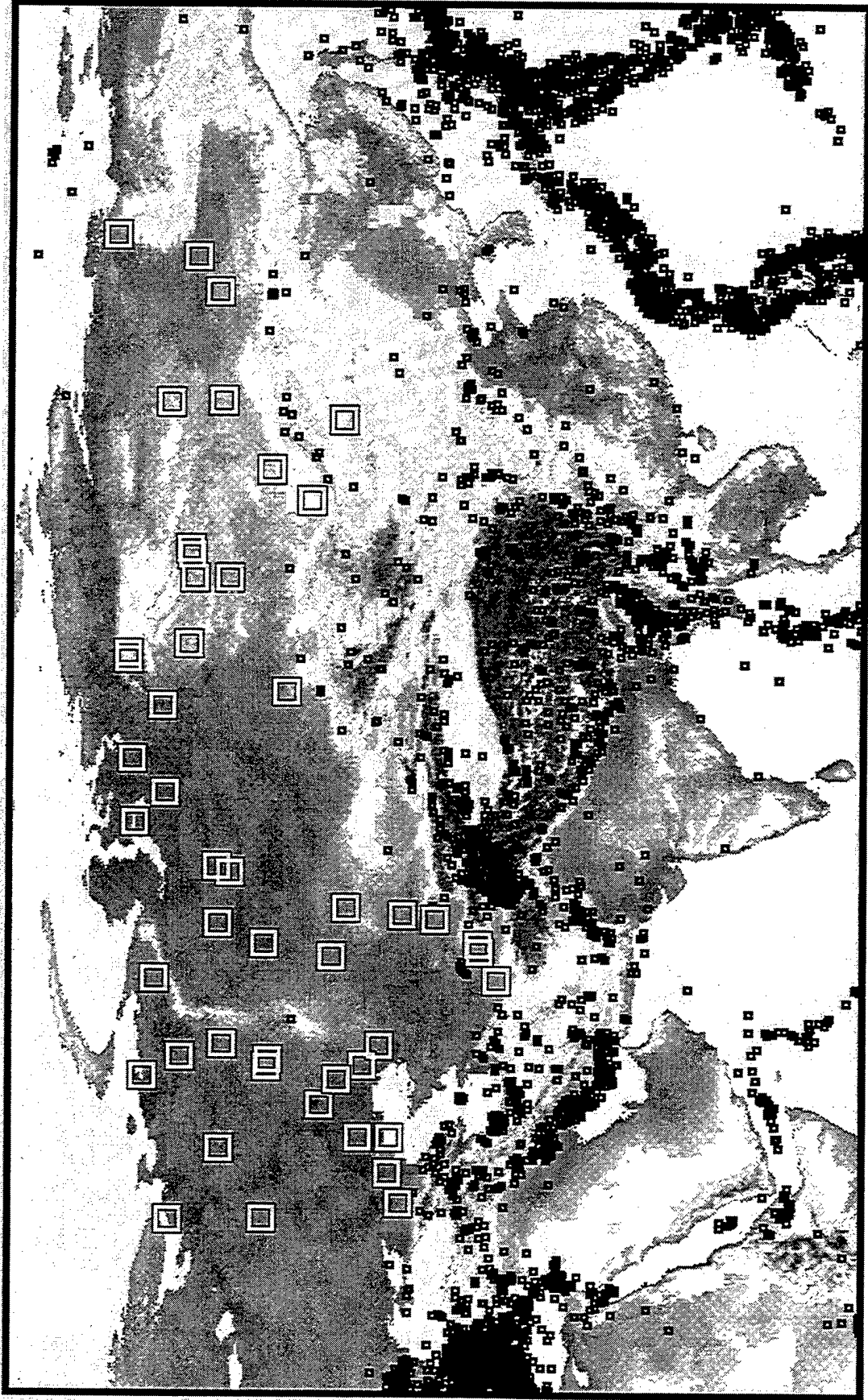


Figure 1. Locations of representative Soviet PNE events (large squares) shown as overlays to a shaded topographic map of the former Soviet Union and surrounding countries. The small squares correspond to the ISC seismicity for the period 1988-1990.

the tectonic variability of the PNE test environments. The PNE explosions were conducted in a wide variety of geologic emplacement media (e.g. salt, clay, sandstone, granite, limestone, dolomite) and are representative of broad ranges in yield (0.01 to 140 kt) and source depth (31 to 2860 m). Moreover, because of the tremendous geologic and tectonic diversity represented within the territories of the former Soviet Union, regional data recorded from these tests sample propagation path characteristics encompassing a range extending from tectonically active to stable continental interior regimes. Thus, regional data recorded from these tests represent a unique resource for use in seismic verification studies of underground nuclear testing. The objective of the research described in this report is to improve seismic discrimination capability through in-depth analyses of regional seismic data recorded from these Soviet PNE tests.

This report presents a summary of the research investigations which have been conducted in an attempt to better define the regional seismic characteristics of underground nuclear explosions conducted over wide ranges of source and propagation path conditions. The regional seismic data recorded at the Borovoye Geophysical Observatory from a selected sample of Soviet PNE events are reviewed in Section 2, where available information regarding the explosive source conditions and propagation path characteristics are also presented and analyzed in a preliminary fashion. This is followed in Section 3 by the presentation of a detailed spectral analysis of these Borovoye data and a subsequent investigation of source scaling and propagation path effects on the regional phase spectra and the discriminants derived from them. In Section 4, some near-regional seismic data recorded from a selected sample of PNE events are presented and theoretically simulated in an attempt to better define the effects of explosion source conditions on seismic coupling efficiency. The report concludes with Section 5, which contains a summary and statement of conclusions regarding the transportability of regional seismic discriminants for use in the identification of underground nuclear explosions over the ranges of source conditions which must be considered in global test monitoring of the CTBT.

## **2. OVERVIEW OF REGIONAL SEISMIC DATA RECORDED AT THE BOROVOYE GEOPHYSICAL OBSERVATORY FROM SOVIET PNE TESTS**

Over the past several years, data recorded at the Borovoye digital seismic station in Central Asia from a number of Soviet nuclear tests have been made available by the IDG (Adushkin and An, 1990; Laushkin *et al.*, 1995) for analysis by the seismic verification community. The Borovoye Geophysical Observatory is located in North Kazakhstan (53.08°N, 70.25°E) and is one of the oldest digitally recording seismic observatories in the world, having initiated digital recording in 1966. A variety of long-period and short-period seismic systems have been deployed at this station over the years (Kim and Ekström, 1996), including some relatively broadband systems which were recorded with digitization rates in the 30-40 sample/second range. Thus, dynamic range permitting, these data provide potential resolution of seismic frequency content to 10 Hz and higher. For most of the Soviet PNE tests, these Borovoye recordings represent the highest quality regional seismic data which are available for detailed analysis.

A preliminary analysis of an initial sample of Borovoye data recorded from 11 Soviet PNE events in the narrow epicentral distance range extending from 7.2 to 11.0 degrees was described in our previous, interim report on this project (Murphy *et al.*, 1996). For the purposes of the present investigation these initial data have been supplemented by the Borovoye recordings from an additional 18 Soviet PNE events, giving a composite sample consisting of 29 explosions located in the regional distance range extending from 7.2 to 19.1 degrees from the Borovoye station. The map locations of these selected explosions with respect to the Borovoye station are shown in Figure 2 where it can be seen that they are widely distributed throughout the territories of the former Soviet Union. Thus, their regional propagation paths to the Borovoye station sample diverse ranges of crust and upper mantle structures which can potentially provide some valuable constraints on the types of seismic characteristics which may be expected in global CTBT monitoring.

The source parameters of these selected PNE events are listed in Table 1 where they have been divided into subsets (i.e., Groups I, II, A, B, Azgir and

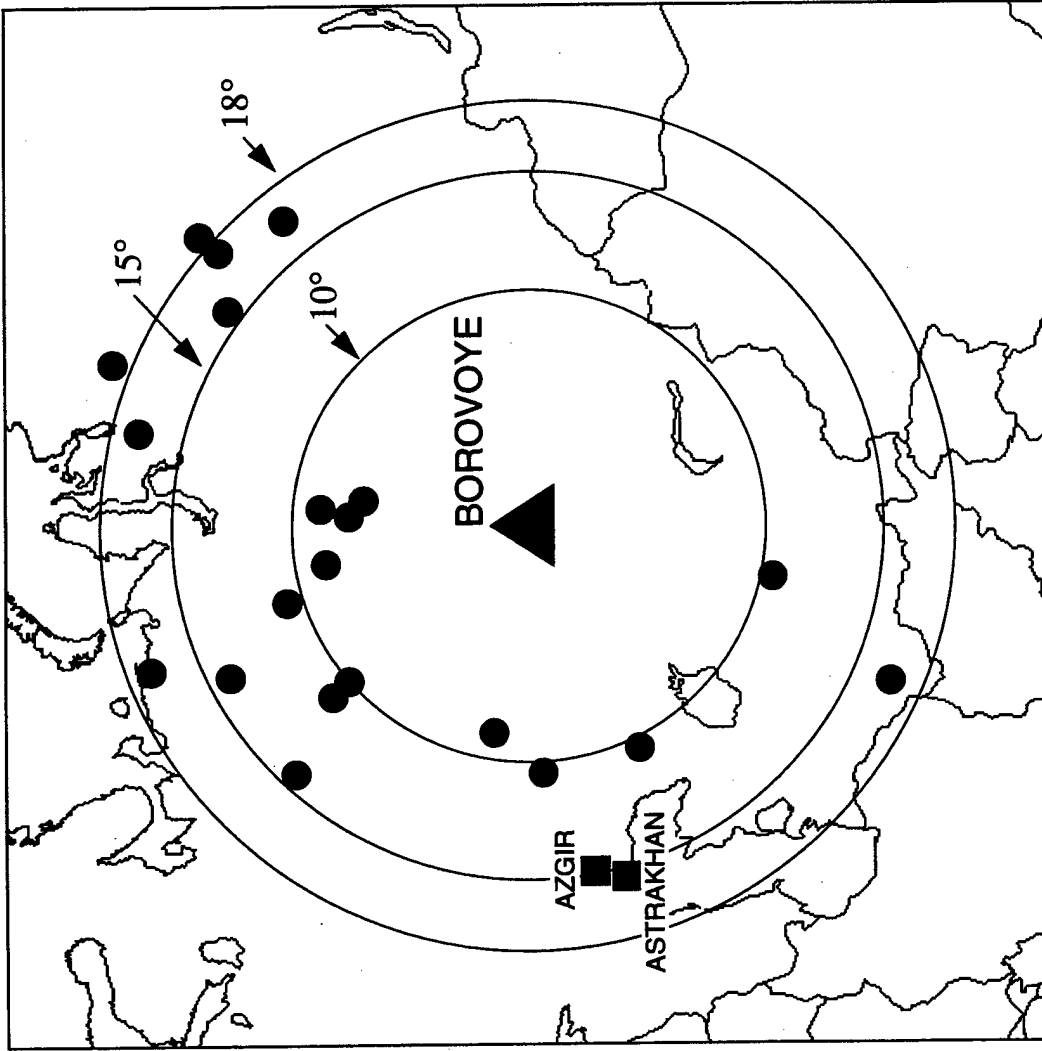


Figure 2. Map locations of selected Soviet PNE tests which were recorded at the Borovoye station in Kazakhstan.

**Table. 1 Source Characteristics of Selected Soviet PNE Events**

<b>Group I (<math>\bar{\Delta} = 10.2^\circ</math>)</b>						
Date	Latitude	Longitude	W,kt	h,m	Medium	$\Delta,^\circ$
08/15/73	42.78	67.41	6.3	600	clay	10.5
10/26/73	53.66	55.38	10	2026	dolomite	8.3
09/02/81	60.62	55.59	3.2	2088	limestone	11.0
07/21/84	51.36	53.32	13.5	846	salt	10.6
04/19/87	60.25	57.08	3.2	2015	limestone	10.4
10/03/87	47.61	56.23	8.5	1000	salt	10.5
<b>Group II (<math>\bar{\Delta} = 8.6^\circ</math>)</b>						
Date	Latitude	Longitude	W,kt	h,m	Medium	$\Delta,^\circ$
10/17/78	63.19	63.43	23	593	sandstone	10.7
10/04/79	60.68	71.46	21	837	clay	7.7
12/10/80	61.69	67.00	15	2485	sandstone	8.8
08/25/84	61.88	72.09	8.5	726	clay	8.9
06/18/85	60.17	72.50	2.5	2859	argillite	7.2
<b>Group A (<math>\bar{\Delta} = 15.6^\circ</math>)</b>						
Date	Latitude	Longitude	W,kt	h,m	Medium	$\Delta,^\circ$
04/11/72	37.37	62.00	14	1720	argillite	16.7
11/01/80	60.82	97.57	8.0	720	dolomite	16.7
09/25/82	64.31	91.83	8.5	554	gabbro	15.8
08/11/84	65.03	55.19	9.5	759	clay	14.2
09/06/88	61.36	48.09	7.5	793	dolomite	14.6
<b>Group B (<math>\bar{\Delta} = 18.0^\circ</math>)</b>						
Date	Latitude	Longitude	W,kt	h,m	Medium	$\Delta,^\circ$
07/26/77	69.58	90.38	13	879	salt	19.1
08/20/77	64.11	99.56	8.5	592	tuff	18.9
05/25/81	68.21	53.66	37.6	1511	clay	17.2
10/22/81	63.79	97.55	8.5	581	dolomite	17.7
09/04/82	69.21	81.65	16	960	sandstone	17.0
<b>Astrakhan (<math>\bar{\Delta} = 15.5^\circ</math>)</b>						
Date	Latitude	Longitude	W,kt	h,m	Medium	$\Delta,^\circ$
10/08/80	46.71	48.22	8.5	1050	salt	15.5
09/26/81	46.78	48.25	8.5	1050	salt	15.5
10/16/82	46.73	48.20	8.5	974	salt	15.5
09/24/83	46.78	48.32	8.5	1050	salt	15.4
10/27/84	46.77	48.31	3.2	1000	salt	15.5
<b>Azgir (<math>\bar{\Delta} = 15.0^\circ</math>)</b>						
Date	Latitude	Longitude	W,kt	h,m	Medium	$\Delta,^\circ$
09/30/77	48.14	47.85	9.3	1503	salt	15.0
07/14/79	47.81	48.10	21	982	salt	15.1
10/24/79	47.81	48.16	33	982	salt	15.0

Astrakhan), such that the explosions in each subset are located in a fairly narrow, common distance range. Note also from Table 1 that, although the explosions in the Astrakhan and Azgir groups are located at distances from Borovoye which are very comparable to those of the Group A events, they have been classified as separate groups in order to assess any propagation path effects which may be related to their locations within the Caspian Basin. With regard to source parameters, the data of Table 1 indicate that these selected explosions sample wide ranges of source media (i.e., sandstone, clay, salt, limestone/dolomite, argillite and gabbro) and source depth (i.e., 554-2859 m) and that they are predominantly low yield, overburied explosions of the type which represent the greatest challenge to seismic monitoring of the CTBT.

The broadband, vertical component seismic data recorded at the Borovoye station from the explosions of Table 1 were displayed and characterized in our previous report (Murphy *et al.*, 1996). In that report, data from the 11 explosions of Table 1 which lie in the epicentral distance range extending from 7.2 to 11.0 degrees were analyzed in detail as a single group, in view of the fact that both predicted and observed attenuation effects appear to be fairly small over this limited distance range. However, as is indicated in Table 1, these data have been separated into two groups (i.e., Groups I and II) for the purposes of the present analysis. This subdivision is based on the observation that, although these events are all distributed over the same narrow band in epicentral distance, those explosions located north of Borovoye (i.e., Group II) consistently produce recordings at that station having broadband  $P_g/P_n$  ratios which are significantly larger than those observed from the other PNE events at comparable distances along different azimuths (i.e., Group I). This fact is documented in Figure 3 which shows a comparison of the vertical component, broadband signals recorded at Borovoye from the 11 PNE events of Groups I and II. In this figure, the data are displayed as a function of group velocity and it can be seen that, if we denote the arrivals in the 6 to 5 km/sec window as  $P_g$  and those in the 8 to 6 km/sec window as  $P_n$ , then the broadband  $P_g/P_n$  amplitude ratios are clearly much larger for the five explosions of Group II than they are for the six explosions of Group I.

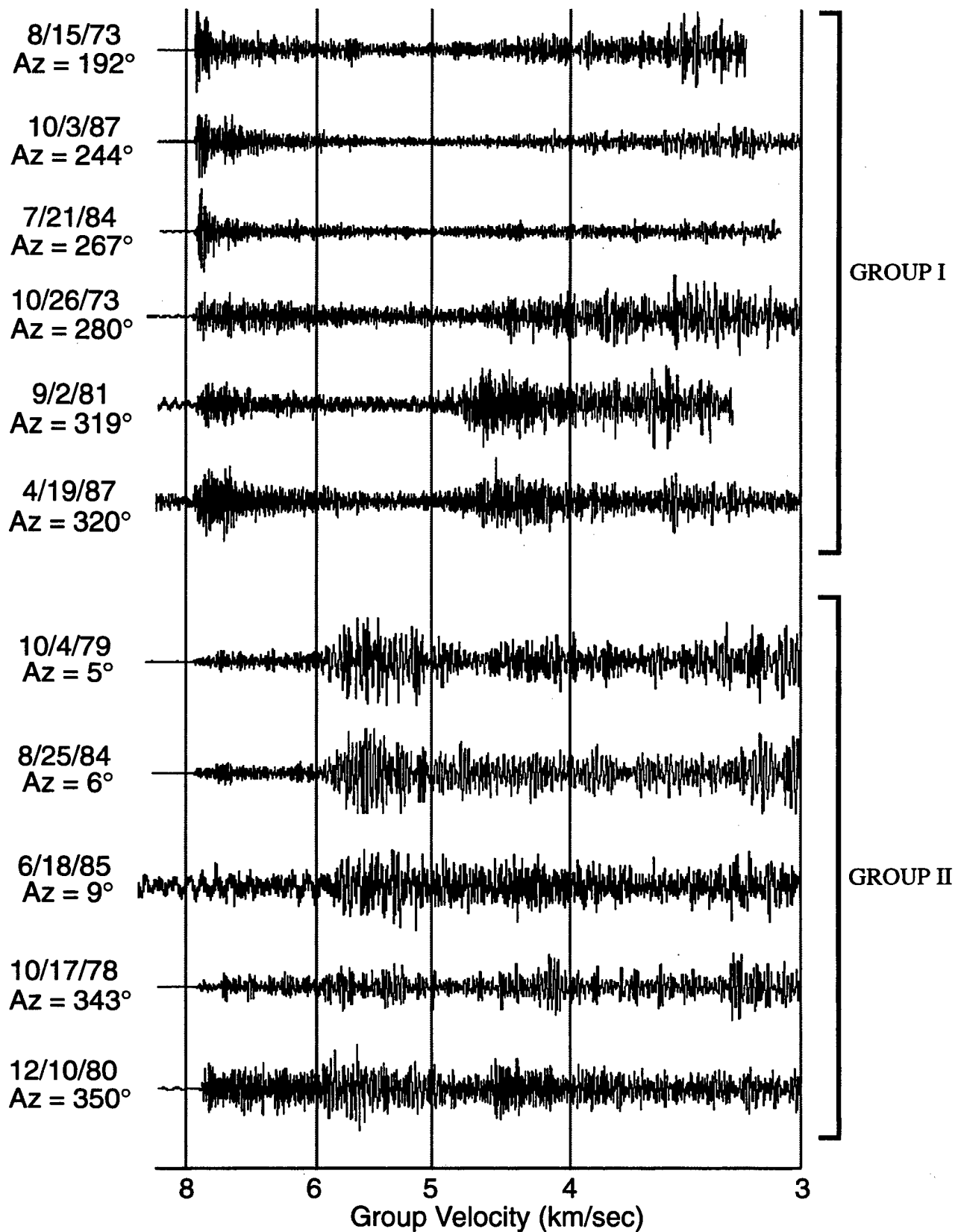


Figure 3. Vertical component regional signals recorded at Borovoye from selected Soviet PNE events in Groups I and II. Note the strong dependence of the  $P_g/P_n$  ratios on station to source azimuth (Az) for these explosions at comparable distances from the Borovoye station.

The systematic variability of the seismic signatures shown in Figure 3 is somewhat surprising in that all the propagation paths involved are predominantly across platform regions of the stable continental interior of Central Asia. In this sense, these observations provide some cautionary warnings regarding the reliability of regionalizations of seismic propagation characteristics on the basis of generalized geophysical data. The region surrounding the Borovoye station is particularly relevant to such an assessment in that, not only is the crustal structure thought to be relatively simple throughout the region, but the area was also extensively studied during the Soviet Deep Seismic Sounding (DSS) program in which seismic data from various PNE tests were recorded along numerous linear profiles crossing this area. Thus, the area has been unusually well-characterized with respect to the delineation of crustal structures which might affect regional seismic propagation characteristics.

Tectonically, the region encompassing the locations of the Group I and Group II PNE events and their seismic propagation paths to the Borovoye station are situated within platforms. Thus, the Borovoye seismic station and the southernmost PNE event of 8/15/73 are situated within the ancient crystalline massif of the Kazakh platform, while the northernmost explosions of Group II are located within the West Siberian platform. The remaining explosions of Group I are located within the Pre-Urals Depression, a transition zone from the Russian platform to the Urals Mountains (i.e., 10/26/73, 9/02/81, 4/19/87) and at the eastern edge of the Caspian Depression (i.e., 7/21/84, 10/03/87).

A simplified characterization of the variation in crustal structure across this region is shown in Figure 4, where the different symbols denote variations in the generalized, three layered crustal model which has been developed by Russian geophysicists on the basis of analyses of DSS and other data (Zverev and Kosminskyaya, 1980; Belousov *et al.*, 1991). This simplified model consists of an upper "granitic-gneiss" layer with P wave velocities in the range 5.8 to 6.4 km/sec, an intermediate "granulite-gneiss" layer with P wave velocities in the range 6.5 to 6.7 km/sec and a lowermost "granulite-basalt" layer characterized by velocities in the range 6.8 to 7.4 km/sec. In areas where it is required, this basic model is extended by adding a surface sediment layer of variable thickness and velocity. Also shown on Figure 4 are the locations (circles) of the Group I and

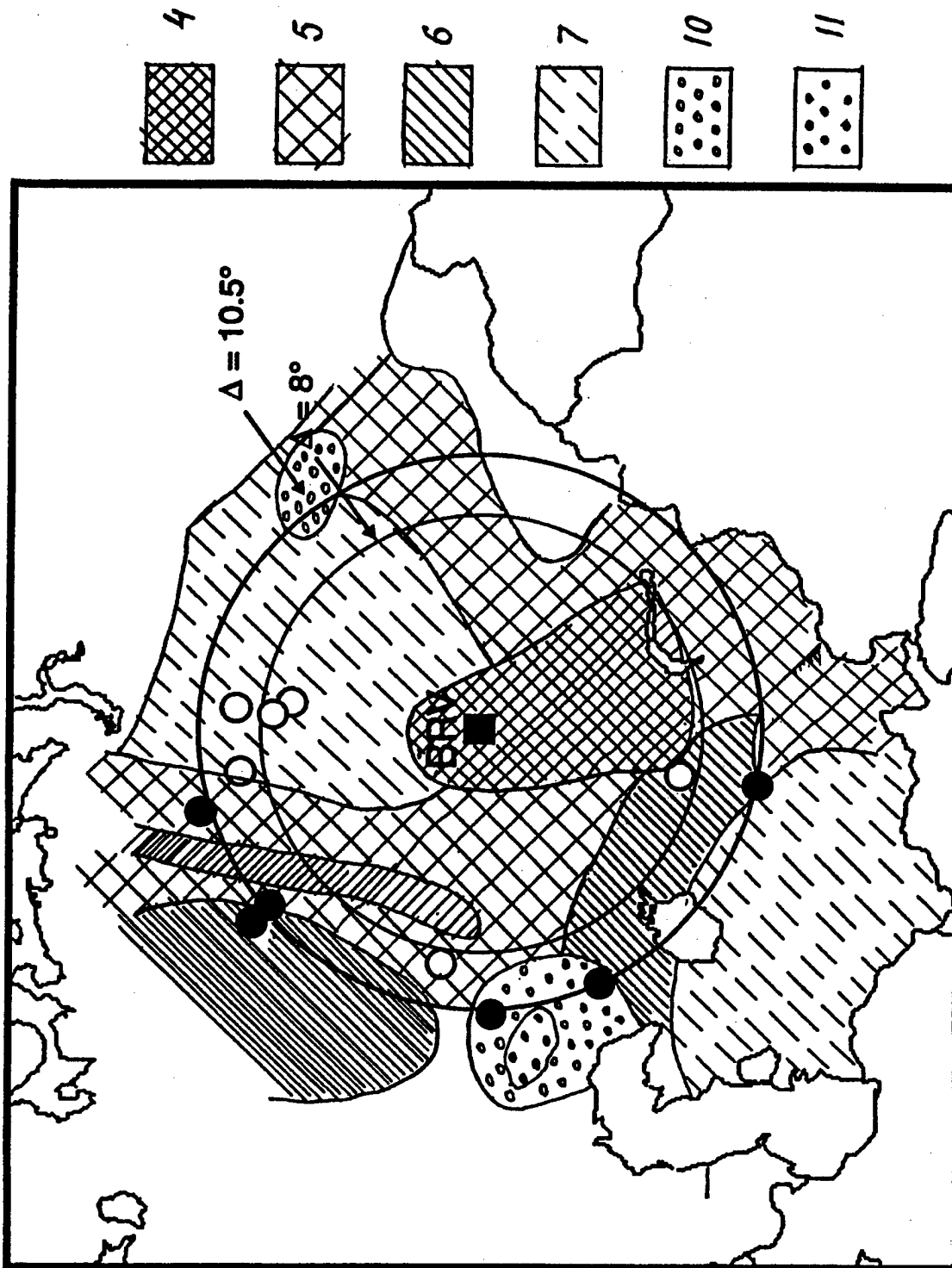


Figure 4. Map of types of crust in the Borovoye region. A sample of representative crustal types is shown in Figure 5.

Group II PNE events and it can be seen that the regional seismic propagation paths from these explosion locations to the Borovoye station are predominantly across regions characterized as crustal types labeled 4, 5, 6 and 7. The subsurface velocity models corresponding to these four crustal types are displayed in Figure 5 where it can be seen that the thicknesses of the individual layers and the associated total crustal thicknesses vary somewhat between them. Thus, for example, the total crustal thickness of model 7, which characterizes most of the propagation paths from the Group II event locations to the Borovoye station, is significantly less than that of model 4, which makes up most of the propagation path from the southernmost Group I PNE event of 8/15/73 to the Borovoye station (i.e., 53 versus 37 km). However, given the similarities of the inferred velocity structures for these two crustal models and the fact that the upper mantle  $P_n$  velocity has been determined to be 8.1 km/sec or higher over most of this area, it seems unlikely that such relatively minor structural differences can explain the observed dramatic variations in the broadband  $P_g/P_n$  amplitude ratios. Moreover, with reference to Figures 4 and 5, it appears that the propagation paths to Borovoye associated with some of the Group I event locations are more similar to those characteristic of the Group II event locations than to those characteristic of other Group I event locations. Thus, even in this relatively simple and extensively studied region, it is not a simple matter to predict the regional phase propagation characteristics in a manner suitable for nuclear monitoring purposes. It follows that extrapolations and interpolations of the results of analyses of limited seismic calibration data based on regional geophysical models may be subject to significant uncertainties which will have to be factored into the event screening process under the CTBT.

All the Borovoye data corresponding to the PNE events of Table 1 were carefully previewed by an experienced analyst to assess data quality and suitability for digital signal processing. As in our previous study (Murphy *et al.*, 1996), although the data were found to be of generally good quality, close examination revealed a number of instances of spikes, data dropouts and clipping which would seriously contaminate any data analysis results at high frequency. In cases where such data problems were isolated as single points, they were corrected using simple interpolation of the adjacent data points. In those few cases where the data problems were too complex to be remedied by such simple

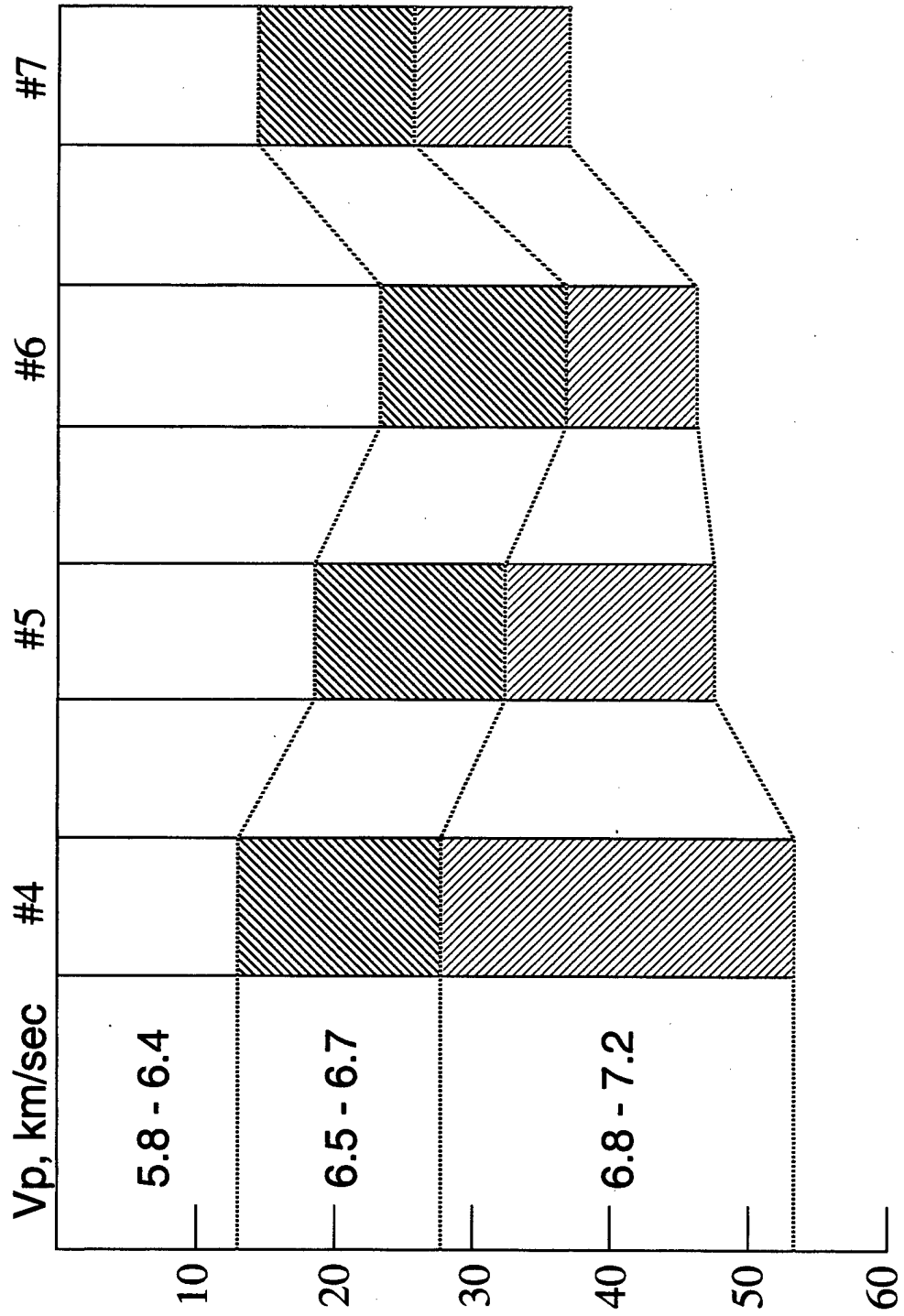


Figure 5. Comparison of the subsurface velocity models corresponding to representative crustal types from Figure 4.

data interpolation, the time windows containing high frequency spikes were duly noted and avoided in subsequent spectral analyses of those data traces.

### 3. REGIONAL PHASE SPECTRA AND DISCRIMINATION

Much research has been conducted over the past several decades in attempts to characterize the regional seismic signals observed from underground nuclear explosions and earthquakes. Because of data availability limitations, most of the initial U.S. research in this area focused on analyses of data recorded from explosions at the Nevada Test Site (Blandford and Klouda, 1980; Blandford, 1981; Murphy and Bennett, 1982; Chael, 1988; Taylor *et al.*, 1988; Bennett and Murphy, 1986). These investigations were generally productive and led to rough characterizations of the different seismic phases observed in this particular region, as well as the identification of some diagnostic differences in the spectral composition of the  $L_g$  phases observed from earthquakes and explosions (Murphy and Bennett, 1982; Taylor *et al.*, 1988) which formed the basis for the definition of discriminants (i.e.,  $L_g$  spectral ratio,  $L_g/P$  spectral ratio) which have proved to be applicable in a number of other testing environments. However, in general, the applicability of many of the results of these empirical characterization studies to other testing environments has been viewed with caution, due to the rather unique source and propagation path features of the Basin and Range Province of the Western U.S. In more recent years, some regional data have started to become available from underground nuclear explosions at the principal Soviet test sites at Semipalatinsk and Novaya Zemlya and at the Chinese test site at Lop Nor, and these data have been extensively processed and analyzed in attempts to assess their utility for event identification purposes (Ringdal and Hokland, 1987; Bennett *et al.*, 1993; Baumgardt, 1990; Taylor and Denny, 1991). These studies documented differences in the excitation of regional signals for different source types in Eurasia, but they also showed that propagation effects sometimes made the effects ambiguous or difficult to observe. In particular, it has been noted that there are some significant differences in the relative phase amplitudes and spectral composition of the signals observed from explosions at the different test sites and this has increased the level of concern regarding the transportability of simple empirical discriminants to new testing regimes.

Coincident with the empirical studies referenced above, extensive research has been on-going in attempts to define robust theoretical models which can be used to quantitatively explain the observed characteristics of these regional signals (McLaughlin *et al.*, 1993; Stump and Reinke, 1991; Taylor and Randall, 1989; Barker *et al.*, 1990). Although much progress has been made as a result of these theoretical investigations, the problem has proved to be complex and there are still important features of the observed regional waveforms which are only roughly and incompletely accounted for by existing simulation models. For example, it has proved to be very difficult to theoretically account for observed variations of S and  $L_g$  excitation levels and spectral composition for explosions in different environments and such variations can effect the performance of a number of proposed regional discriminants. Thus, it is not possible at the present time to confidently predict, either empirically or theoretically, how nuclear explosion regional seismic signals can be expected to vary over the range of source and propagation path conditions of potential interest in global test monitoring. Data recorded at regional distances from the extensive Soviet PNE test program provide the best available resource for evaluating such variability in regional discriminant performance.

The Borovoye data corresponding to the selected PNE events of Table 1 have been processed to obtain estimates of the different regional phase spectra for each event. In the first step of this processing, the data and pre-signal noise windows for each event were bandpass filtered using a Gaussian comb of filters spaced at intervals of 0.25 Hz between 0.5 and 10 Hz, where each filter is characterized by a Q value of  $6 f_c$ , with  $f_c$  the filter center frequency. Filters of this type have been used by us and a number of other investigators in previous studies (Murphy *et al.*, 1989; Murphy *et al.*, 1996) and have been found to provide spectral estimates which are useful for purposes of seismic analysis. Note that, although the digitization rates for the Borovoye data are nominally high enough to support signal analyses to 10 Hz or higher, we have established an upper limit of 5 Hz for the purposes of the present study. This reflects our conclusion that the combination of limitations in the dynamic range of the original data, uncertainties in high frequency instrument response characteristics and the decrease in the signal-to-noise ratios with increasing frequency leads to a significant increase in the uncertainty associated with the reduction of the higher

frequency data. For purposes of the regional phase analyses, the filter outputs for each recording were sorted into six distinct time windows and the spectral amplitudes at each center frequency were estimated by computing RMS values from the instrument-corrected filter outputs in each of the designated windows. In the interests of simplicity and consistency, these regional phase time windows were defined in terms of apparent group velocity intervals as follows: (1) pre-signal noise, (2)  $V_g > 7$  km/sec, (3)  $6 < V_g < 7$  km/sec, (4)  $5 < V_g < 6$  km/sec, (5)  $4 < V_g < 5$  km/sec, and (6)  $3 < V_g < 4$  km/sec. For purposes of subsequent discussion, these six time windows will be identified as pre-signal noise,  $P_n$ ,  $P_{\text{coda}}$ ,  $P_g$ ,  $S_n$ , and  $L_g$ , respectively. Although there are individual cases in which refined time windows could be specified that would more precisely isolate particular regional phases of interest, this simple windowing procedure was employed throughout as a test of its potential utility for routine seismic discrimination purposes.

The first priority in the analysis of the Borovoye regional phase spectra is the estimation of their dependence on the characteristics of the explosion seismic source function. As in our previous analysis (Murphy *et al.*, 1996), it has been assumed that this source function, denoted  $S(\omega)$ , can be approximated as a product of simple power law relations of the form

$$S(\omega) \sim W^{n(\omega)} h^{m(\omega)} \quad (1)$$

where  $W$  and  $h$  are the explosion yield and depth of burial, respectively. In contrast to the previous analysis, however, the Borovoye data recorded from the PNE events of Table 1 represent a wide range of epicentral distance and, therefore, the effects of the differences in propagation paths can't be ignored and they must be explicitly estimated and separated from the source effects. This has been accomplished using statistical covariance techniques in which our model describing the variations in the observed spectra for each regional phase  $p$  is:

$$A_{p,k}(\omega) = \beta_{p,k}(\omega) W^{n(\omega)} h^{m(\omega)} \quad (2)$$

where  $k = 1, \dots, K$  denotes the designated subgroups of Table 1 (e.g., Group A, Group B, etc.). The  $n_p(\omega)$ ,  $m_p(\omega)$  and  $\beta_{p,k}(\omega)$  are simultaneously estimated from the observed spectral data using covariance analysis procedures based on the

least-squares fit criterion (Murphy and O'Brien, 1977). As was the case in the previous analysis of a smaller data set (Murphy *et al.*, 1996), the yield and depth scaling exponents derived from this larger data set have been found to be roughly independent of phase type, at least within their rather large estimated uncertainty bounds. That is, these spectral data are consistent with the hypothesis that, to first order, all of these regional phases are produced from a single explosion P wave source function through linear conversion processes. Thus, as has been noted previously (Murphy, 1977), this observation implies that the entire regional waveform, including both P and S wave phases, can be approximately scaled for explosion yield and depth effects using scaling laws derived from a spherically symmetric P wave source model. This approximation greatly simplifies the estimation of the frequency dependent effects of variations in explosion source characteristics on the regional phase spectral data used for event identification.

It follows from the above discussion that, if the yield and depth scaling exponents can be assumed to be independent of regional phase type, then the scaling model represented by equation (2) simplifies to

$$A_{p,k}(\omega) = \beta_{p,k}(\omega) W^{n(\omega)} h^{m(\omega)} \quad (3)$$

where the coefficients  $\beta_{p,k}(\omega)$  represent the average spectral amplitude levels for each phase  $p$  and epicentral distance group  $k$  (i.e., the frequency dependent propagation path effects for each phase). The regional phase spectral scaling coefficients derived from a covariance analysis of the Borovoye data recorded from the 21 Soviet PNE events of Groups I, II, A and B are listed in Table 2 for each of the five regional phases which have been analyzed using the scaling model of equation of (3). The yield and depth scaling exponents resulting from this analysis are also plotted as a function of frequency in Figure 6, where they are compared with the corresponding values predicted by the Mueller/Murphy (M/M) explosion source model (Mueller and Murphy, 1971; Murphy, 1977). It can be seen from this figure that the model predictions are generally consistent with the experimentally derived values within the estimated 95% uncertainty bounds on those values, except at low frequency where the statistically inferred depth dependence is significantly larger at the 95% level than that predicted by the M/M model. A similar discrepancy was noted in our previous analysis of the initial,

**Table 2. Frequency dependent regional phase scaling coefficients derived from the covariance analysis of Borovoye data recorded from the 21 PNE events of Groups I,II,A and B.**

f(Hz)	n(f)	m(f)	B <sub>I</sub> (P <sub>n</sub> )	B <sub>II</sub> (P <sub>n</sub> )	B <sub>A</sub> (P <sub>n</sub> )	B <sub>B</sub> (P <sub>n</sub> )
0.50	0.919	-0.950	3.024	2.852	2.759	2.878
0.75	1.137	-1.191	3.619	3.192	3.152	3.166
1.00	1.278	-1.064	3.104	2.615	2.559	2.565
1.25	1.212	-0.917	2.628	2.299	2.175	2.191
1.50	1.192	-0.875	2.435	2.138	2.111	1.955
1.75	1.284	-0.846	2.202	1.944	1.961	1.618
2.00	1.275	-0.723	1.811	1.471	1.511	1.104
2.25	1.230	-0.599	1.422	0.951	0.992	0.566
2.50	1.161	-0.521	1.204	0.618	0.644	0.272
2.75	1.188	-0.398	0.753	0.146	0.238	-0.166
3.00	1.120	-0.299	0.465	-0.075	-0.019	-0.475
3.25	1.111	-0.257	0.364	-0.102	-0.159	-0.666
3.50	1.007	-0.322	0.672	0.126	0.077	-0.430
3.75	0.921	-0.304	0.626	0.133	0.020	-0.327
4.00	0.825	-0.262	0.470	0.060	-0.092	-0.397
4.25	0.886	-0.116	-0.112	-0.530	-0.608	-1.003
4.50	0.912	-0.088	-0.200	-0.697	-0.808	-1.209
4.75	0.841	-0.060	-0.269	-0.737	-0.864	-1.342
5.00	0.764	0.015	-0.483	-0.933	-1.056	-1.577

f(Hz)	B <sub>I</sub> (P <sub>coda</sub> )	B <sub>II</sub> (P <sub>coda</sub> )	B <sub>A</sub> (P <sub>coda</sub> )	B <sub>B</sub> (P <sub>coda</sub> )	B <sub>I</sub> (P <sub>e</sub> )	B <sub>II</sub> (P <sub>e</sub> )	B <sub>A</sub> (P <sub>e</sub> )	B <sub>B</sub> (P <sub>e</sub> )
0.50	2.905	2.925	2.474	2.423	2.780	3.512	2.360	2.346
0.75	3.409	3.248	2.811	2.744	3.244	3.904	2.680	2.647
1.00	2.851	2.632	2.225	2.075	2.727	3.036	2.093	1.933
1.25	2.409	2.345	1.799	1.655	2.261	2.602	1.661	1.502
1.50	2.187	2.188	1.705	1.515	2.032	2.402	1.511	1.324
1.75	1.964	1.959	1.533	1.229	1.800	2.150	1.329	1.023
2.00	1.584	1.510	1.084	0.679	1.418	1.595	0.869	0.475
2.25	1.222	1.027	0.661	0.174	1.045	1.136	0.420	-0.090
2.50	1.027	0.798	0.347	-0.091	0.832	0.793	0.109	-0.323
2.75	0.549	0.346	-0.128	-0.513	0.340	0.309	-0.374	-0.730
3.00	0.224	0.045	-0.309	-0.842	-0.017	-0.006	-0.603	-1.049
3.25	0.096	-0.135	-0.466	-1.097	-0.166	-0.135	-0.751	-1.280
3.50	0.312	0.164	-0.286	-0.817	0.068	0.145	-0.553	-1.061
3.75	0.263	0.121	-0.342	-0.770	0.054	0.119	-0.613	-1.045
4.00	0.171	0.029	-0.401	-0.857	-0.039	0.013	-0.696	-1.089
4.25	-0.413	-0.498	-0.925	-1.384	-0.619	-0.605	-1.221	-1.625
4.50	-0.553	-0.639	-1.103	-1.549	-0.732	-0.773	-1.408	-1.778
4.75	-0.552	-0.741	-1.179	-1.645	-0.813	-0.848	-1.509	-1.836
5.00	-0.747	-0.976	-1.415	-1.876	-1.046	-1.136	-1.735	-2.033

**Table 2. Continued.**

f(Hz)	B <sub>I</sub> (S <sub>n</sub> )	B <sub>II</sub> (S <sub>n</sub> )	B <sub>A</sub> (S <sub>n</sub> )	B <sub>B</sub> (S <sub>n</sub> )	B <sub>I</sub> (L <sub>p</sub> )	B <sub>II</sub> (L <sub>p</sub> )	B <sub>A</sub> (L <sub>p</sub> )	B <sub>B</sub> (L <sub>p</sub> )
0.50	2.971	3.449	2.517	2.407	3.345	3.484	2.734	2.374
0.75	3.453	3.884	2.913	2.703	3.813	3.864	3.047	2.639
1.00	2.904	3.075	2.333	2.030	3.172	3.123	2.413	1.876
1.25	2.444	2.620	1.799	1.577	2.609	2.586	1.892	1.346
1.50	2.259	2.435	1.595	1.349	2.355	2.309	1.601	1.075
1.75	2.014	2.154	1.415	1.011	2.051	2.053	1.359	0.758
2.00	1.602	1.618	1.007	0.500	1.504	1.516	0.911	0.249
2.25	1.172	1.126	0.553	0.044	1.046	1.039	0.442	-0.255
2.50	0.895	0.899	0.195	-0.251	0.769	0.752	0.106	-0.537
2.75	0.425	0.415	-0.313	-0.729	0.235	0.248	-0.523	-1.016
3.00	0.093	0.039	-0.561	-0.998	-0.126	-0.091	-0.830	-1.310
3.25	-0.090	-0.120	-0.701	-1.215	-0.322	-0.290	-0.950	-1.508
3.50	0.183	0.111	-0.487	-1.023	-0.112	-0.034	-0.769	-1.303
3.75	0.157	0.126	-0.534	-1.027	-0.154	-0.018	-0.896	-1.293
4.00	0.019	0.098	-0.612	-1.076	-0.271	-0.083	-0.968	-1.300
4.25	-0.525	-0.483	-1.124	-1.645	-0.866	-0.638	-1.466	-1.793
4.50	-0.662	-0.633	-1.356	-1.825	-1.018	-0.761	-1.678	-1.969
4.75	-0.765	-0.663	-1.467	-1.877	-1.051	-0.824	-1.746	-2.035
5.00	-0.982	-0.865	-1.657	-2.050	-1.325	-1.087	-1.934	-2.233

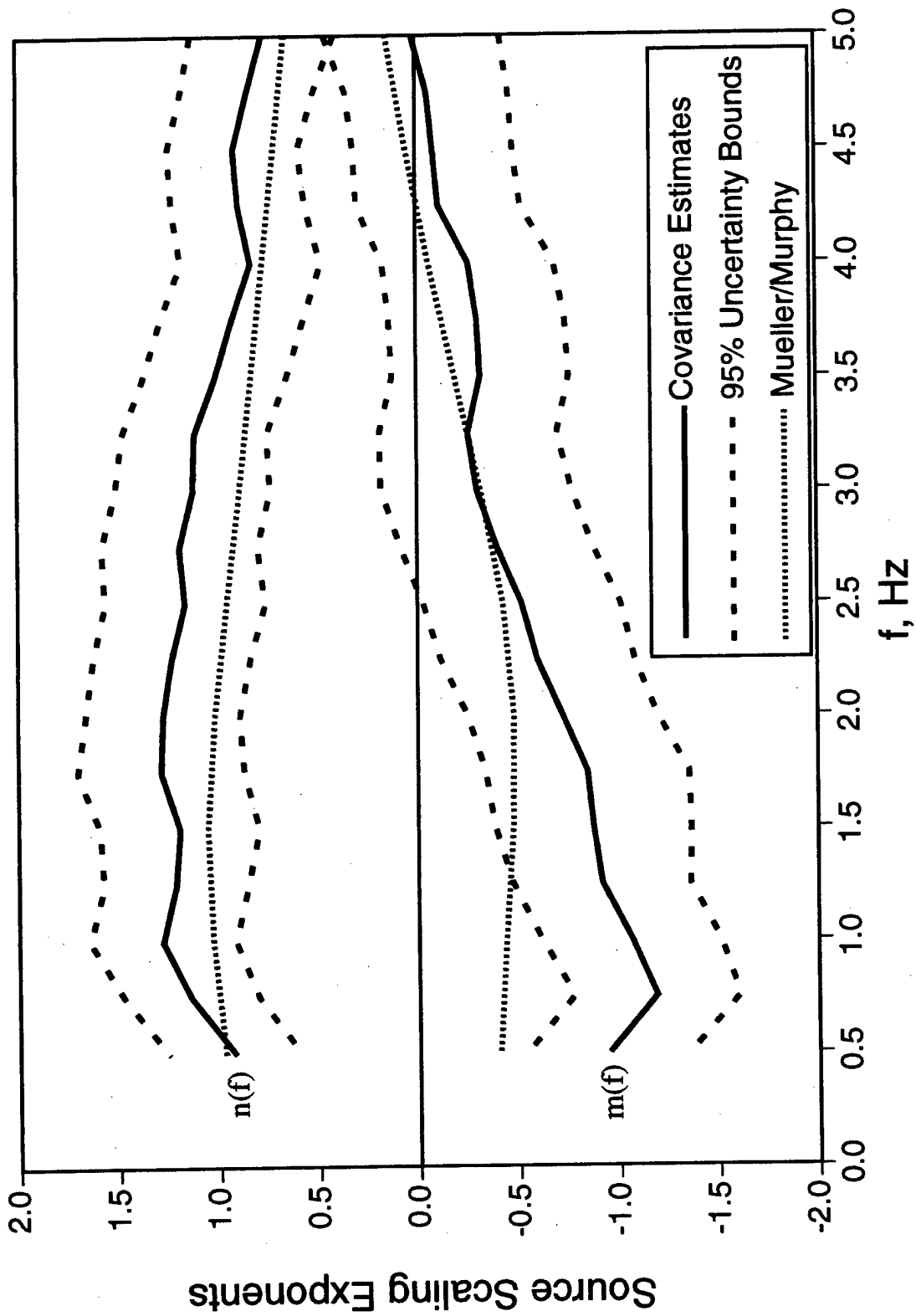


Figure 6. Comparison of the frequency dependent yield ( $n$ ) and depth ( $m$ ) scaling exponents derived from the covariance analysis of Borovoye data recorded from the 21 PNE events of Groups I, II, A and B with the corresponding values predicted by the Mueller/Murphy explosion source model.

smaller sample of Borovoye data (Murphy *et al.*, 1996) and, consequently, it merits further investigation.

One simplification which was employed in the above analysis which needs to be evaluated is the assumption that the seismic source coupling efficiency is the same in all the sampled source media. Clearly, if this is not approximately true, the scaling results of Table 2 and Figure 6 could be biased by source medium. The scaling coefficients of Table 2 were used together with Eq. (3) to predict the regional phase spectra corresponding to each of the selected 21 PNE events. Ratios of observed-to-predicted spectra were then computed and logarithmically averaged over the frequency band extending from 0.5 to 5.0 Hz. The resulting values for the five phases were then logarithmically averaged to obtain a measure of source coupling efficiency for each event. These final average ratio values for the 21 selected PNE events are listed in order of increasing observed/predicted ratio value in Table 3. It can be seen from this table that the values of this coupling parameter vary from about 0.5 to 2.0, with average ratios less than 1.0 corresponding to cases where the source coupling is low, and those with average ratios greater than 1.0 to cases where the source coupling is high, relative to the average values represented by the covariance model predictions. Note, for example that the three explosions in sandstone are associated with low, intermediate and higher than average values, indicating that the coupling in this medium shows no systematic difference from the average. In fact, the only consistent dependence on source medium is observed for the explosions in clay, which correspond to the five highest values in this table. Moreover, it can be seen that within this clay subgroup, the offset increases with decreasing yield, consistent with the  $m_b$ /yield results reported by Sultanov *et al.* (1993) for explosions in that medium. These results are also consistent with the alternate seismic source model for explosions in clay which was proposed by Murphy and Barker (1994) on the basis of their analyses of network-averaged teleseismic P wave spectral data. More generally, the results of these previous teleseismic studies suggested that explosive coupling in clay represents the only significant outlier among the various source media sampled by the Soviet PNE events, a conclusion which is also consistent with the regional analysis results of Table 3.

**Table 3. Comparison of Relative Source Coupling Efficiency as Inferred From Average Ratios of Observed to Predicted (Covariance Model) Regional Phase Spectra for Selected Soviet PNE Events Recorded at the Borovoye Station.**

Event	Medium	W,kt	h,m	Average: $\frac{\text{Observed}}{\text{Predicted}}$ 0.5 - 5.0 Hz
09/25/82	gabbro	8.5	554	0.48
10/17/78	sandstone	23	593	0.49
09/02/81	limestone	3.2	2088	0.74
07/21/84	salt	13.5	846	0.74
09/04/82	sandstone	16	960	0.79
04/19/87	limestone	3.2	2015	0.81
10/03/87	salt	8.5	1000	0.87
08/20/77	tuff	8.5	592	0.89
07/26/77	salt	13	879	0.94
11/01/80	dolomite	8	720	0.95
04/11/72	argillite	14	1720	0.95
06/18/85	argillite	2.5	2859	0.98
09/06/88	dolomite	7.5	793	1.09
10/22/81	dolomite	8.5	581	1.10
10/26/73	dolomite	10	2026	1.11
12/10/80	sandstone	15	2485	1.12
05/25/81	clay	37.6	1511	1.24
10/04/74	clay	21	827	1.33
08/25/84	clay	8.5	726	1.38
08/11/84	clay	9.5	759	1.74
08/15/73	clay	6.3	600	2.09

On the basis of the results of the coupling analysis summarized in Table 3, the covariance analysis was repeated using the subset of the Borovoye spectral data which remained after the removal of the data from the five explosions in clay. The resulting revised scaling coefficients are listed in Table 4, and the associated yield and depth scaling exponents are plotted as functions of frequency in Figure 7 where they are again compared with the corresponding values predicted by the M/M source model. Note that the low frequency depth exponents inferred from this revised covariance analysis change significantly with respect to those shown in Figure 6 and that, in this case, the predicted M/M yield and depth scaling exponents are completely consistent with the experimentally

**Table 4. Frequency dependent regional phase scaling coefficients derived from the covariance analysis of Borovoye data recorded from the non-clay PNE events of Groups I,II,A and B.**

f(Hz)	n(f)	m(f)	$B_I(P_n)$	$B_{II}(P_n)$	$B_A(P_n)$	$B_B(P_n)$
0.50	0.937	-0.618	1.864	1.819	1.689	1.865
0.75	1.198	-0.810	2.266	1.905	1.920	1.979
1.00	1.289	-0.792	2.112	1.845	1.761	1.723
1.25	1.214	-0.520	1.247	1.058	1.018	1.053
1.50	1.301	-0.231	0.222	-0.204	0.066	0.066
1.75	1.360	-0.326	0.425	-0.009	0.298	0.076
2.00	1.298	-0.318	0.413	0.005	0.246	-0.079
2.25	1.228	-0.169	-0.028	-0.582	-0.321	-0.683
2.50	1.124	-0.148	-0.060	-0.678	-0.449	-0.831
2.75	1.206	0.039	-0.781	-1.421	-1.059	-1.460
3.00	1.098	-0.010	-0.524	-1.135	-0.854	-1.297
3.25	1.085	-0.076	-0.251	-0.727	-0.694	-1.192
3.50	0.975	-0.156	0.137	-0.422	-0.443	-0.900
3.75	0.896	-0.095	-0.049	-0.585	-0.607	-0.915
4.00	0.809	-0.113	-0.052	-0.449	-0.520	-0.792
4.25	0.905	0.009	-0.553	-0.999	-0.982	-1.357
4.50	0.930	0.113	-0.894	-1.409	-1.414	-1.808
4.75	0.885	0.173	-1.094	-1.579	-1.600	-2.059
5.00	0.805	0.206	-1.156	-1.671	-1.681	-2.168

f(Hz)	$B_I(P_{coda})$	$B_{II}(P_{coda})$	$B_A(P_{coda})$	$B_B(P_{coda})$	$B_I(P_g)$	$B_{II}(P_g)$	$B_A(P_g)$	$B_B(P_g)$
0.50	1.760	1.893	1.390	1.437	1.640	2.333	1.309	1.369
0.75	2.053	1.980	1.543	1.573	1.905	2.569	1.441	1.470
1.00	1.874	1.810	1.392	1.226	1.751	2.103	1.252	1.079
1.25	1.052	1.026	0.614	0.491	0.887	1.194	0.488	0.328
1.50	-0.015	-0.151	-0.385	-0.448	-0.178	0.068	-0.541	-0.644
1.75	0.193	0.097	-0.184	-0.349	0.020	0.281	-0.364	-0.569
2.00	0.189	0.077	-0.240	-0.516	0.042	0.183	-0.448	-0.737
2.25	-0.236	-0.492	-0.701	-1.105	-0.393	-0.369	-0.951	-1.346
2.50	-0.202	-0.496	-0.782	-1.198	-0.397	-0.469	-1.061	-1.397
2.75	-0.918	-1.221	-1.459	-1.803	-1.135	-1.197	-1.733	-2.037
3.00	-0.701	-0.933	-1.181	-1.636	-0.953	-0.995	-1.467	-1.882
3.25	-0.496	-0.703	-1.026	-1.617	-0.737	-0.734	-1.283	-1.798
3.50	-0.229	-0.355	-0.809	-1.289	-0.455	-0.413	-1.034	-1.516
3.75	-0.428	-0.545	-0.952	-1.372	-0.625	-0.615	-1.223	-1.627
4.00	-0.331	-0.407	-0.845	-1.290	-0.531	-0.520	-1.155	-1.524
4.25	-0.844	-0.931	-1.336	-1.769	-1.039	-1.089	-1.642	-1.999
4.50	-1.234	-1.403	-1.721	-2.173	-1.410	-1.519	-2.049	-2.369
4.75	-1.377	-1.560	-1.920	-2.394	-1.629	-1.704	-2.247	-2.537
5.00	-1.447	-1.580	-2.035	-2.484	-1.720	-1.835	-2.327	-2.611

Table 4. Continued.

f(Hz)	B <sub>I</sub> (S <sub>n</sub> )	B <sub>II</sub> (S <sub>n</sub> )	B <sub>A</sub> (S <sub>n</sub> )	B <sub>B</sub> (S <sub>n</sub> )	B <sub>I</sub> (L <sub>g</sub> )	B <sub>II</sub> (L <sub>g</sub> )	B <sub>A</sub> (L <sub>g</sub> )	B <sub>B</sub> (L <sub>g</sub> )
0.50	1.835	2.255	1.424	1.382	2.209	2.200	1.633	1.360
0.75	2.127	2.507	1.614	1.519	2.468	2.460	1.741	1.437
1.00	1.958	2.107	1.407	1.198	2.210	2.165	1.469	1.042
1.25	1.100	1.236	0.551	0.378	1.267	1.172	0.630	0.145
1.50	0.049	0.055	-0.471	-0.642	0.128	-0.082	-0.492	-0.932
1.75	0.273	0.228	-0.306	-0.594	0.256	0.141	-0.363	-0.846
2.00	0.282	0.170	-0.350	-0.737	0.147	0.116	-0.461	-0.974
2.25	-0.227	-0.342	-0.858	-1.218	-0.396	-0.442	-1.005	-1.520
2.50	-0.304	-0.395	-0.983	-1.321	-0.470	-0.523	-1.136	-1.603
2.75	-1.011	-1.141	-1.702	-2.029	-1.223	-1.297	-2.012	-2.294
3.00	-0.807	-0.996	-1.469	-1.823	-1.058	-1.105	-1.769	-2.092
3.25	-0.647	-0.796	-1.277	-1.715	-0.903	-0.919	-1.538	-1.983
3.50	-0.321	-0.501	-1.012	-1.477	-0.647	-0.602	-1.311	-1.729
3.75	-0.494	-0.641	-1.166	-1.622	-0.832	-0.749	-1.572	-1.843
4.00	-0.416	-0.455	-1.090	-1.511	-0.754	-0.630	-1.414	-1.698
4.25	-0.891	-0.982	-1.574	-2.028	-1.276	-1.118	-1.882	-2.153
4.50	-1.310	-1.330	-2.017	-2.418	-1.682	-1.495	-2.338	-2.516
4.75	-1.555	-1.467	-2.232	-2.590	-1.849	-1.690	-2.511	-2.690
5.00	-1.618	-1.500	-2.296	-2.629	-1.980	-1.816	-2.538	-2.755

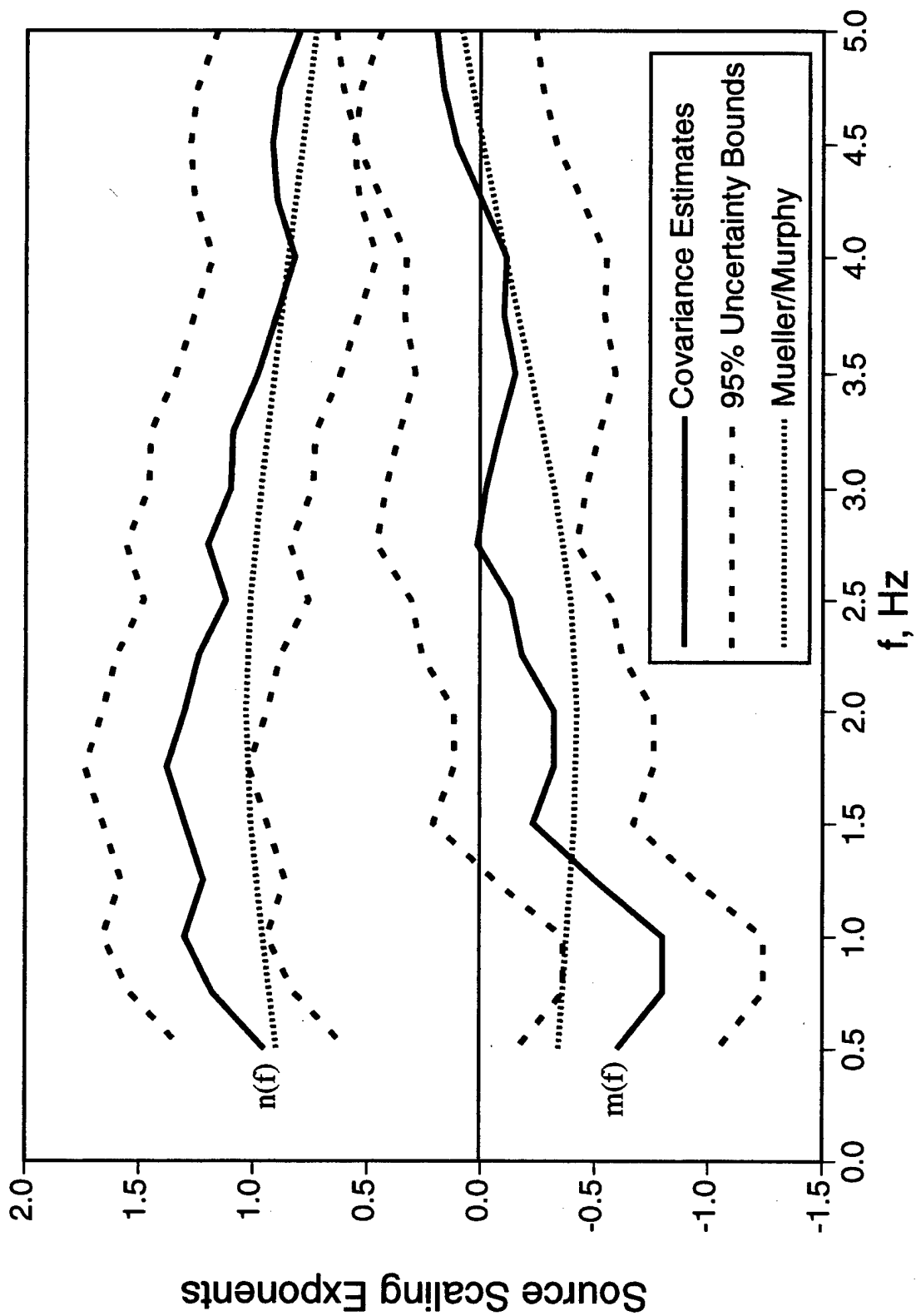


Figure 7. Comparison of the frequency dependent yield ( $n$ ) and depth ( $m$ ) scaling exponents derived from the covariance analysis of Borovoye data recorded from the non-clay PNE events of Groups I, II, A and B with the corresponding values predicted by the Mueller/Murphy explosion source model.

determined values, within the statistical uncertainty of those mean values. We conclude that the Mueller/Murphy explosion source scaling model is consistent with these observed Borovoye PNE regional phase spectral data within the rather large existing uncertainty bounds. More precise data will be required in order to determine whether the observed discrepancy in the average depth scaling exponents at low frequencies is significant enough to warrant modification of that explosion source model.

Another issue that needs to be considered concerns the definition of spectral amplitude which has been employed in the above analyses of the Borovoye data. That is, do the RMS values of the narrowband filter outputs computed over the long time windows defined by the selected group velocity limits accurately represent the spectral amplitude levels of the individual regional phases? In an attempt to answer this question, the RMS spectral amplitude levels were estimated over 5-second windows of the filter outputs and the maximum of these 5-second values was determined for each group velocity window. These short-term maximum values were then taken to represent the spectral amplitude levels of the different regional phases and the covariance analysis was repeated using the data from the non-clay explosions of Groups I, II, A and B. The results of this analysis are summarized in Figure 8 where the derived yield and depth scaling exponents as functions of frequency are compared with the corresponding values from Figure 7, which were derived using the original definition of spectral amplitude level. It can be seen from Figure 8 that these two sets of scaling exponents are remarkably similar, which indicates that the source scaling analysis results are robust and not dependent on the details of the spectral estimation procedure. More generally, these results also suggest that phase association based on rough group velocity windows may be adequate for verification purposes, which would greatly simplify semi-automated analyses of the large volumes of seismic data which will have to be considered in global monitoring of the CTBT.

The effects of variations in explosion yield and depth of burial on the regional phase spectra predicted by the non-clay covariance model are illustrated in Figure 9 for the Group I  $P_n$  phase. Note that although the overall spectral shapes depend on phase and group, the relative source effects shown here are common to all phases and groups for the model represented by Eq. (3). It

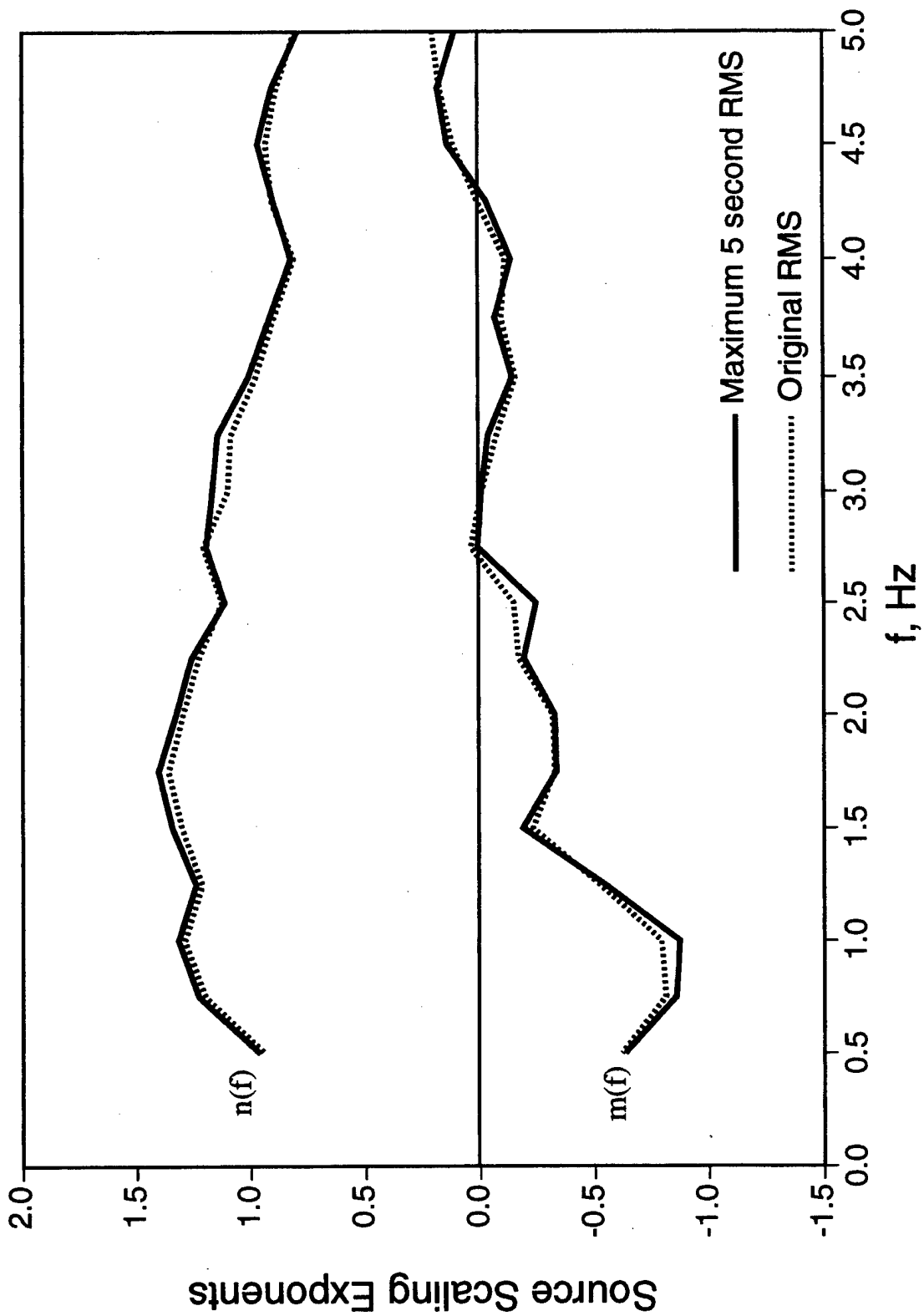


Figure 8. Comparison of the frequency dependent yield ( $n$ ) and depth ( $m$ ) scaling exponents derived from the covariance analysis of Borovoye RMS spectral amplitude levels defined over short and long time windows.

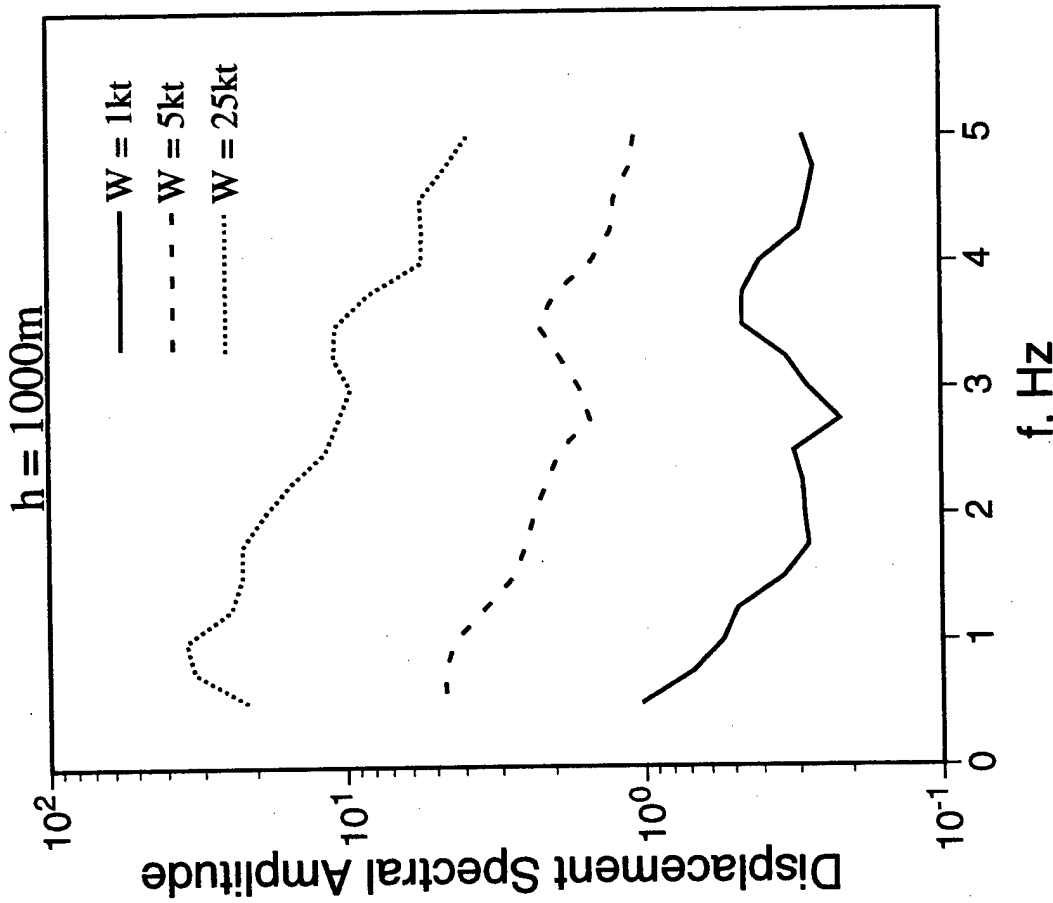
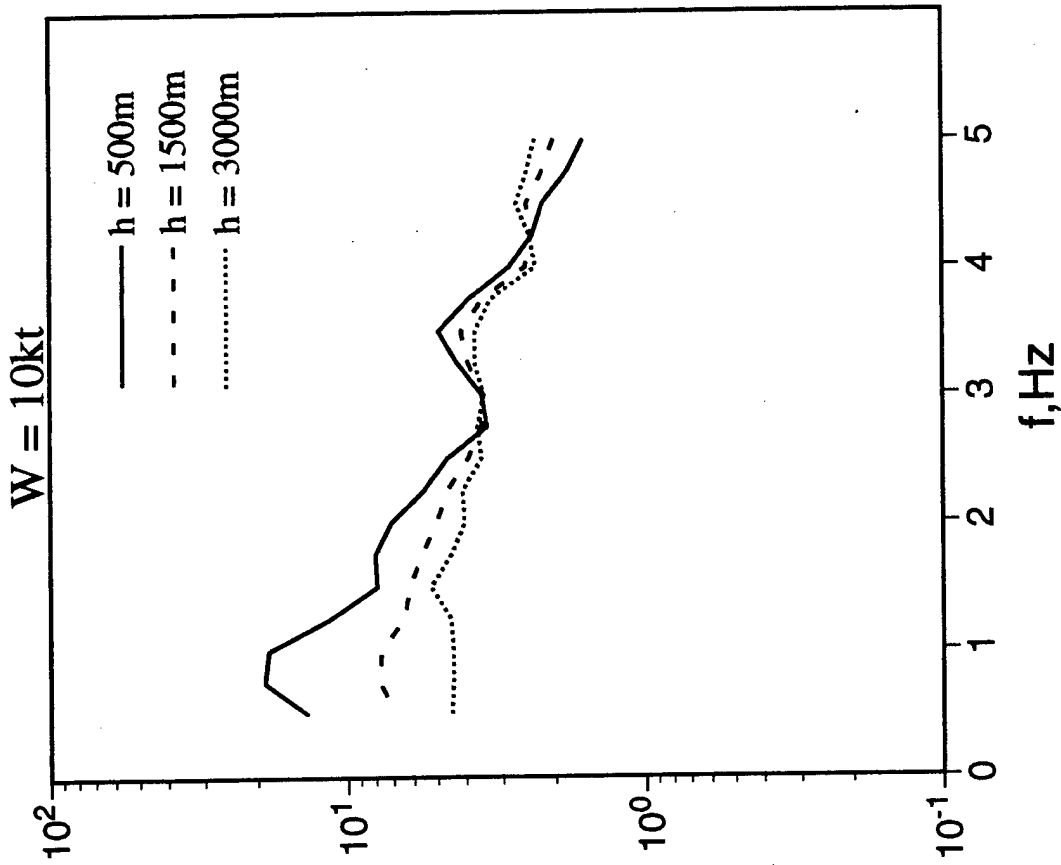


Figure 9. Illustration of the effects of explosion yield (left) and depth of burial (right) on the regional phase spectra predicted by the non-clay covariance model for the Group I Pn phase.

can be seen from Figure 9 that the low frequency ( $f < 2$  Hz) regional phase spectral amplitudes are predicted to increase more rapidly with increasing explosion yield and to decrease more rapidly with increasing source depth of burial than the higher frequency spectral amplitudes, as would be expected on the basis of the results shown in Figure 7. In particular, at a fixed yield, this source model predicts that the regional phase spectral amplitude levels at frequencies near 1 Hz can be expected to decrease by more than a factor of 4 as the source depth increases over the range from about 500 to 3000 m sampled by our Borovoye data set. This is a potentially significant reduction in seismic signal level which will have to be accounted for in any assessments of verification capability.

The corresponding propagation path effects inferred from the covariance analysis of the Borovoye regional phase spectral data are represented by the frequency dependent coefficients  $\beta_k(\omega)$  which have been estimated for each group  $k$ . In the following discussion we will focus on the total sample coefficients from Table 2, although the effects estimated using the non-clay sample coefficients of Table 3 are essentially identical. Figure 10 shows a comparison of the Borovoye regional phase spectra predicted for Groups I, II, A and B by the covariance model for the sample average yield and depth of burial of 10 kt and 1000 m, respectively. This display summarizes the average estimated frequency dependent propagation path effects on the five different regional phases over the sampled epicentral distance range extending from 7.2 to 19.1 degrees. It can be seen from this figure that the initial  $P_n$  phase has the largest amplitude over this entire frequency band for the more distant Group A and B events, while the spectral amplitudes of the various phases are more nearly comparable for the closer events of Groups I and II. This is particularly evident for Group II, for which the predicted spectral amplitude levels for all five regional phases are essentially identical for frequencies above about 1.5 Hz.

Another way of visualizing these same propagation effects is to compute phase spectral ratios between groups for fixed values of yield and depth of burial. As an example, phase spectral ratios for Group II relative to Group I are shown in Figure 11. Note that the average  $P_g$  phase amplitudes associated with the Group II propagation paths are indeed significantly larger than those associated with the Group I propagation paths, consistent with the broadband time domain

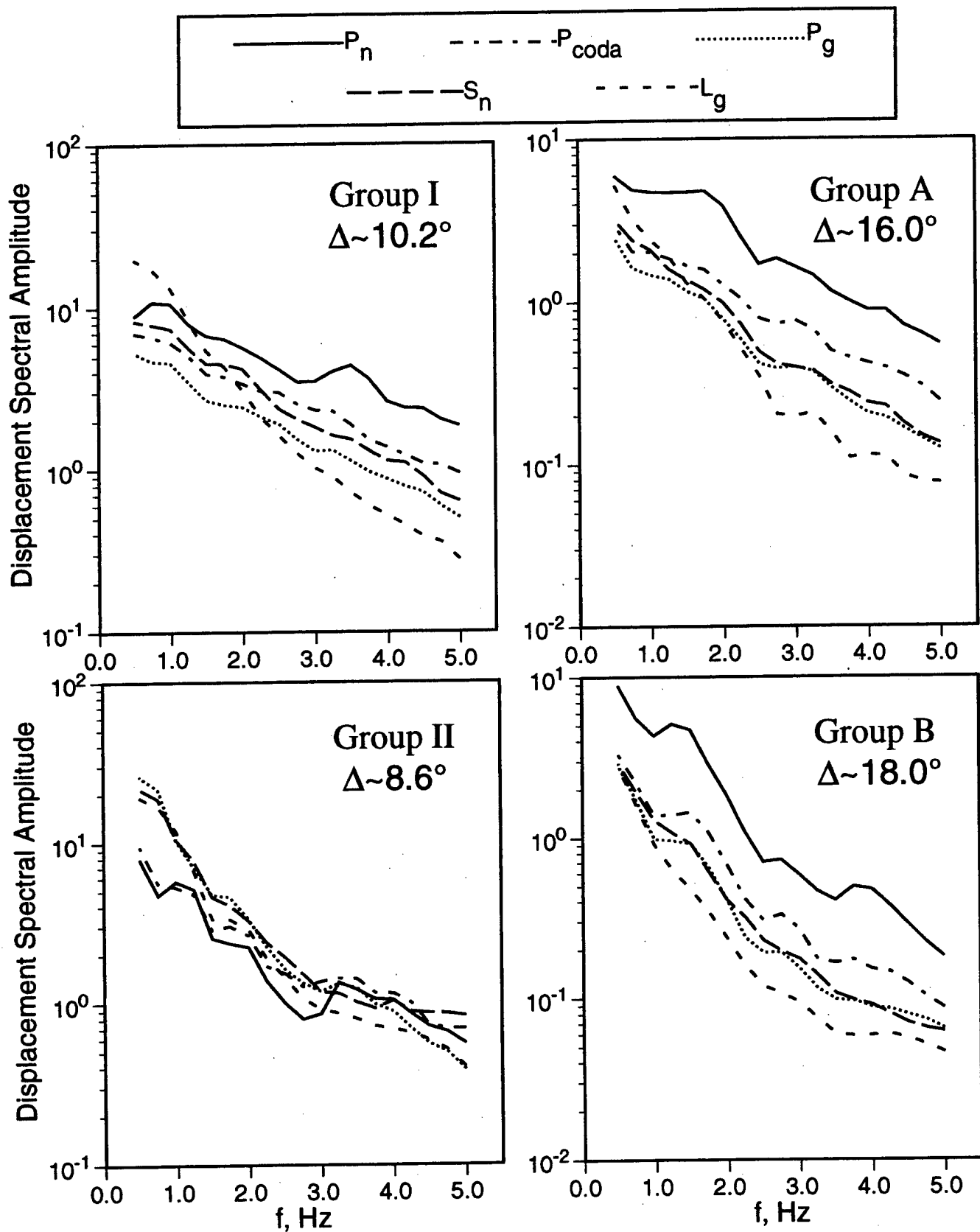


Figure 10. Comparison of regional phase spectra predicted for a 10 kt underground nuclear explosion at a depth of 1000 m using the covariance analysis results for the four selected groups of Soviet PNE events recorded at the Borovoye station.

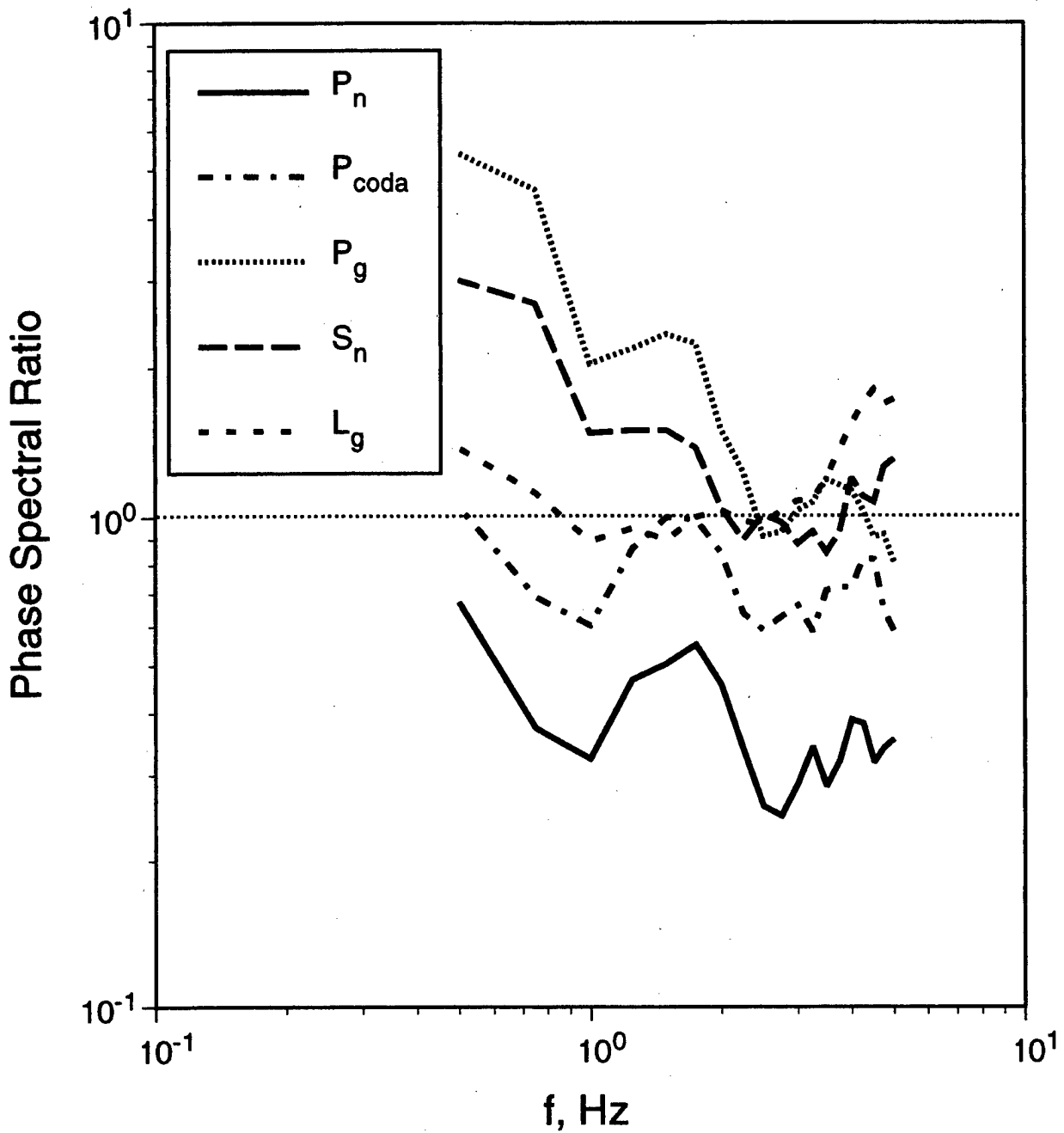


Figure 11. Regional phase spectral ratios for fixed yield and depth of burial, Group II / Group I. Note that the enhancement of the Group II  $P_g$  amplitudes with respect to Group I is limited to low frequencies and that it is associated with a corresponding broadband decrease in relative  $P_n$  amplitude.

data shown in Figure 3. However, it is interesting to note from this figure that this  $P_g$  enhancement is actually a fairly narrowband effect, being largest at 0.5 Hz and decreasing rapidly with increasing frequency until it vanishes at around 2.5 Hz. In fact, the most persistent difference shown in Figure 11 is for the  $P_n$  phase spectral amplitude level, which is lower for Group II than for Group I over the entire frequency band extending from 0.5 to 5.0 Hz. Thus, the large differences in the time domain  $P_g/P_n$  ratios between Groups I and II noted previously in conjunction with the discussion of Figure 3 are attributable to propagation path effects on both  $P_g$  and  $P_n$ , which is rather surprising given the similarities in average crustal structures for the two groups referenced in Section 2.

Yet another way of visualizing these propagation path effects is presented in Figures 12-14 where the phase spectral ratios of the other groups with respect to Group I are plotted versus average group epicentral distance for selected frequency components. The results for the  $P_n$  phase are shown in Figure 12 where again it is evident that the Group II (i.e.,  $\Delta = 8.6^\circ$ )  $P_n$  spectral amplitude levels are lower than the corresponding Group II (i.e.,  $\Delta = 10.2^\circ$ ) amplitude levels over the entire displayed frequency band. Similarly, for the  $P_g$  phase shown in Figure 13, the Group II levels are higher than those for Group I at low frequencies and comparable at higher frequencies, in agreement with the ratios shown in Figure 11. More generally, the P phase results shown in Figures 12 and 13 are consistent with some systematic increase in distance attenuation with increasing frequency. Surprisingly, however, the corresponding results for the  $L_g$  phase shown in Figure 14 show little evidence of any such systematic frequency dependence. This observation seems to be inconsistent with conventional models of  $L_g$  attenuation. Thus, for example, Figure 14 also provides a comparison of this observed  $L_g$  attenuation inferred from the statistical covariance analysis of the Borovoye data (left) with the corresponding  $L_g$  attenuation predicted using Mitchell's (Mitchell *et al.*, 1996) coda Q values for Central Asia (right). It can be seen from this figure that, while the average observed amplitude decrease with distance over this frequency band is qualitatively consistent with the model prediction, the observed frequency dependence is much less pronounced than the predicted. Additional detailed analyses will be required to develop a quantitative understanding of this discrepancy, but in the meantime this example suggests that some degree of caution should be exercised in applying results of inversions of earthquake data to

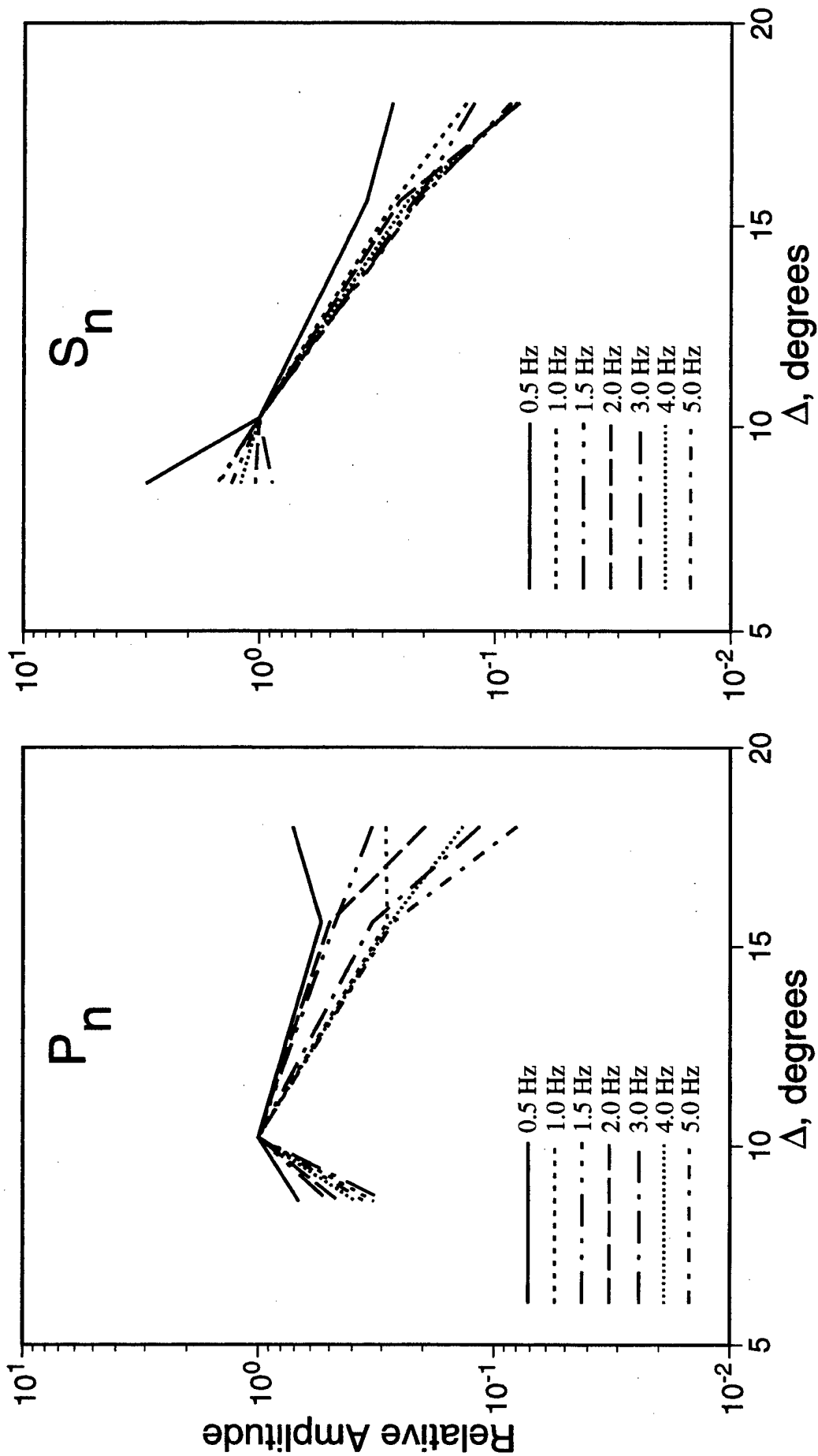


Figure 12. Frequency dependent amplitude attenuation as a function of epicentral distance ( $\Delta$ ) relative to Group II ( $\bar{\Delta}=10.2^\circ$ ) inferred from the statistical covariance analyses of Pn (left) and Sn (right) PNE data recorded at the Borovoye station.

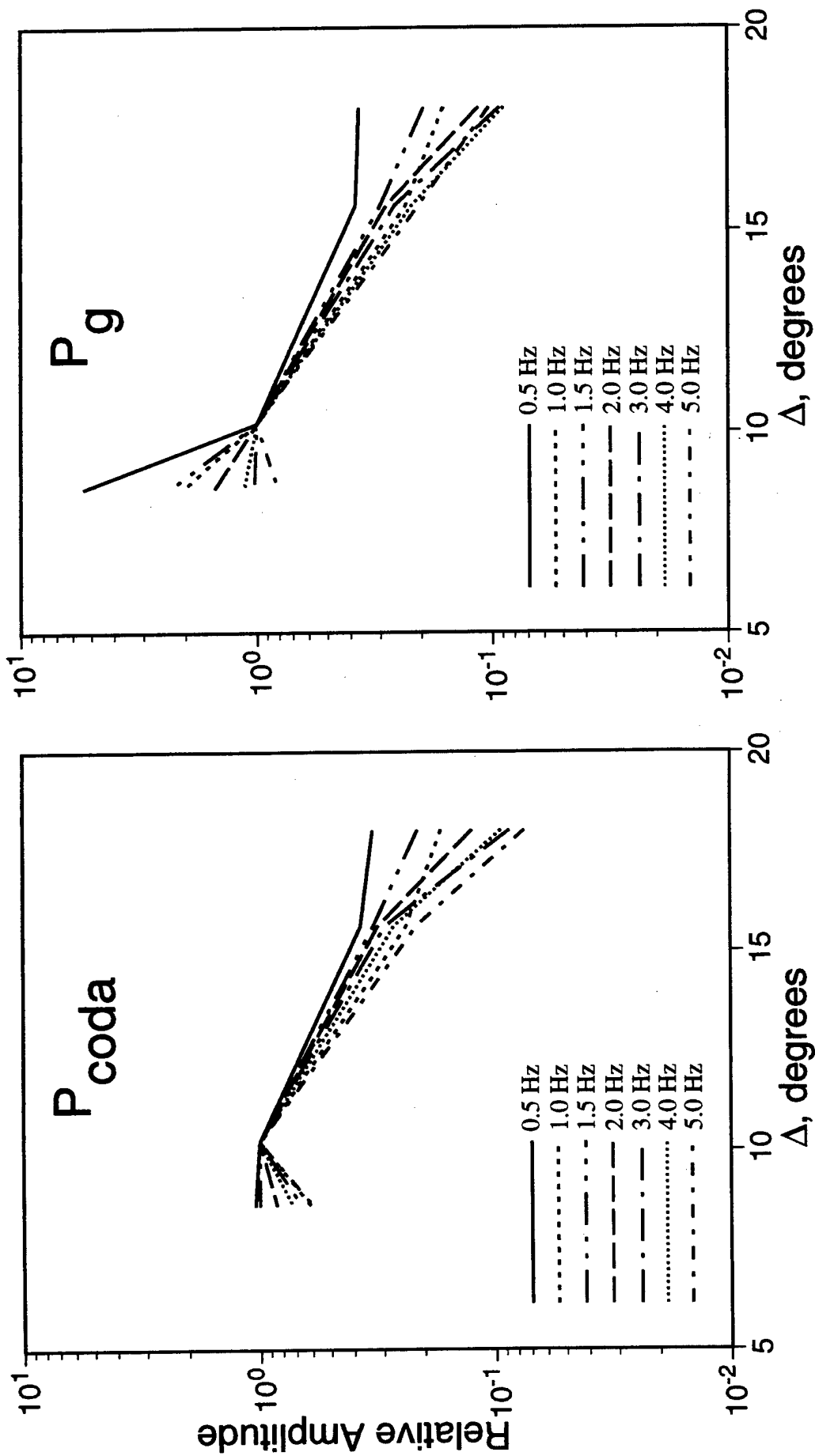


Figure 13. Frequency dependent amplitude attenuation as a function of frequency relative to Group II ( $\bar{\Delta}=10.2^\circ$ ) inferred from statistical covariance analyses of Pcoda (left) and Pg (right) PNE data recorded at Borovoye.

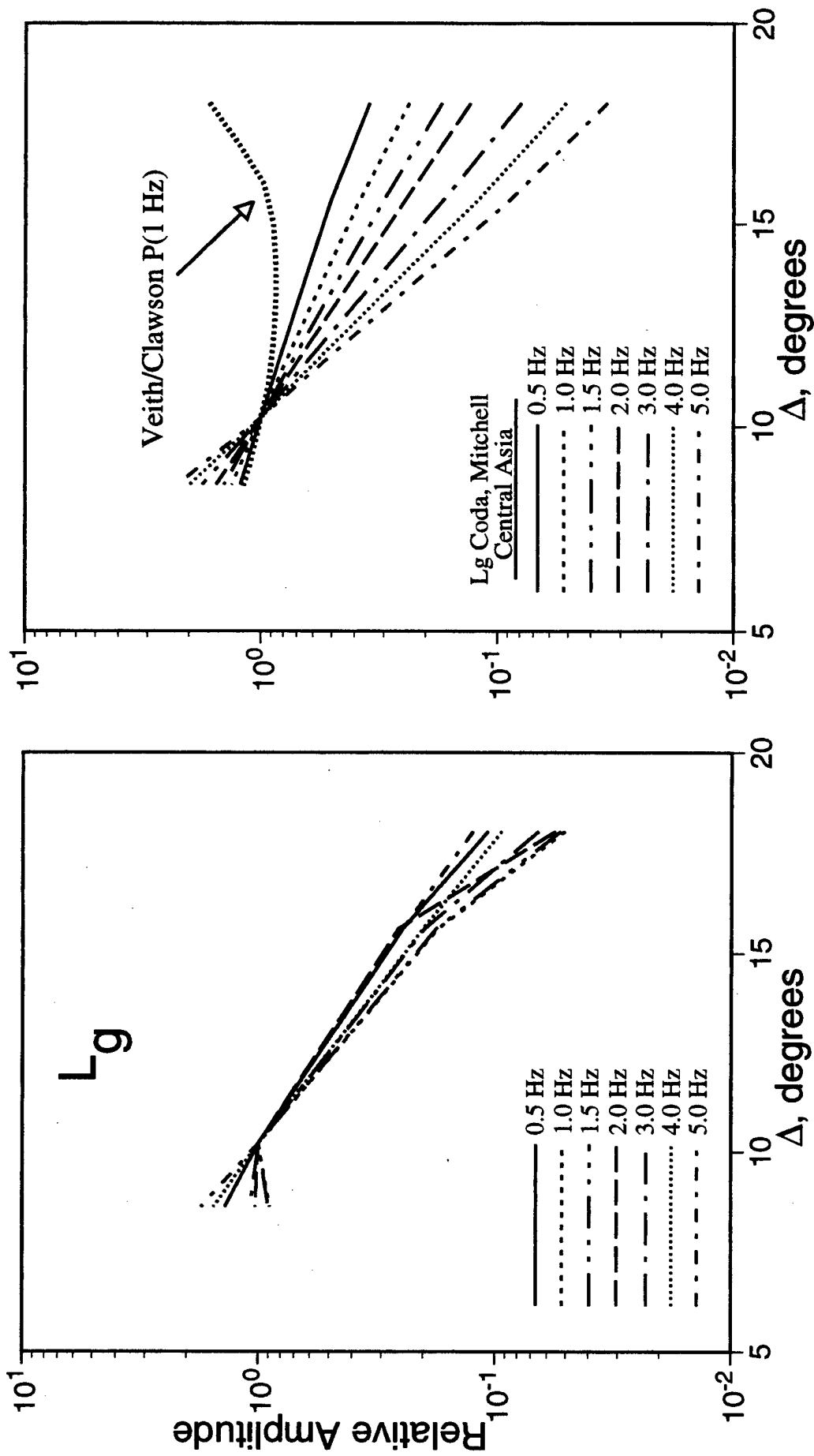


Figure 14. Comparison of the frequency dependent Lg amplitude attenuation as a function of epicentral distance relative to Group II ( $\bar{\Delta} = 10.2^\circ$ ) inferred from statistical covariance analyses of PNE data recorded at the Borovoye station (left) and from Mitchell's(1996) coda Q estimates for Central Asia (right).

the prediction of propagation path effects on the regional phase spectra expected from underground nuclear explosion sources.

Also shown for purposes of comparison on Figure 14 is the 1 Hz P wave attenuation predicted by the Veith/Clawson (1972)  $B(\Delta)$  curve over this distance range. Note with reference to Figure 12 that this predicted distance decay is reasonably consistent with the low frequency  $P_n$  attenuation inferred from the covariance analysis of the observed Borovoye data. This is unexpected given the fact that the Veith/Clawson  $B(\Delta)$  curve in this distance range is based primarily on Western U.S. data and should not be applicable to Central Asia. This apparent discrepancy is probably related, at least in part, to systematic differences in the distance attenuation of the initial, time domain P wave amplitudes used in the magnitude calculations relative to that characteristic of the longer time window RMS spectral amplitudes used in the present study. In any case, it seems clear that such nominal attenuation relations have limited applicability to the regional phase spectral parameters used for nuclear monitoring purposes.

Finally, in an attempt to assess the regional phase propagation efficiencies from the Azgir and Astrakhan sites to the Borovoye station relative to those characteristic of other NE events at the same distance outside the Caspian basin, the Group A covariance prediction equations were used to predict individual phase spectra for each of the selected Azgir and Astrakhan explosions listed in Table 1. The corresponding ratios of observed-to-predicted spectra are shown in Figures 15 and 16 for Azgir and Astrakhan, respectively. Somewhat surprisingly, the  $L_g$  spectral ratios are found to be close to 1.0 over the entire frequency band from 0.5 to 5.0 Hz for both sites, while the P wave propagation appears to be more efficient from these sites than for the propagation paths from the Group A event locations. Thus, assuming that the explosion source coupling in salt is comparable to that of the other source media sampled by the Group A explosions, which seems to be supported by the coupling analysis results presented in Table 3, the observed data from these source locations within the Caspian Basin show no obvious evidence of  $L_g$  blockage, at least along the path to Borovoye. That is, the fact that the broadband  $L_g/P$  ratios observed for the Azgir and Astrakhan explosions are lower than those observed from the Group A explosions appears to be due to the fact that their P wave propagation to Borovoye is more efficient rather than that their relative  $L_g$  propagation

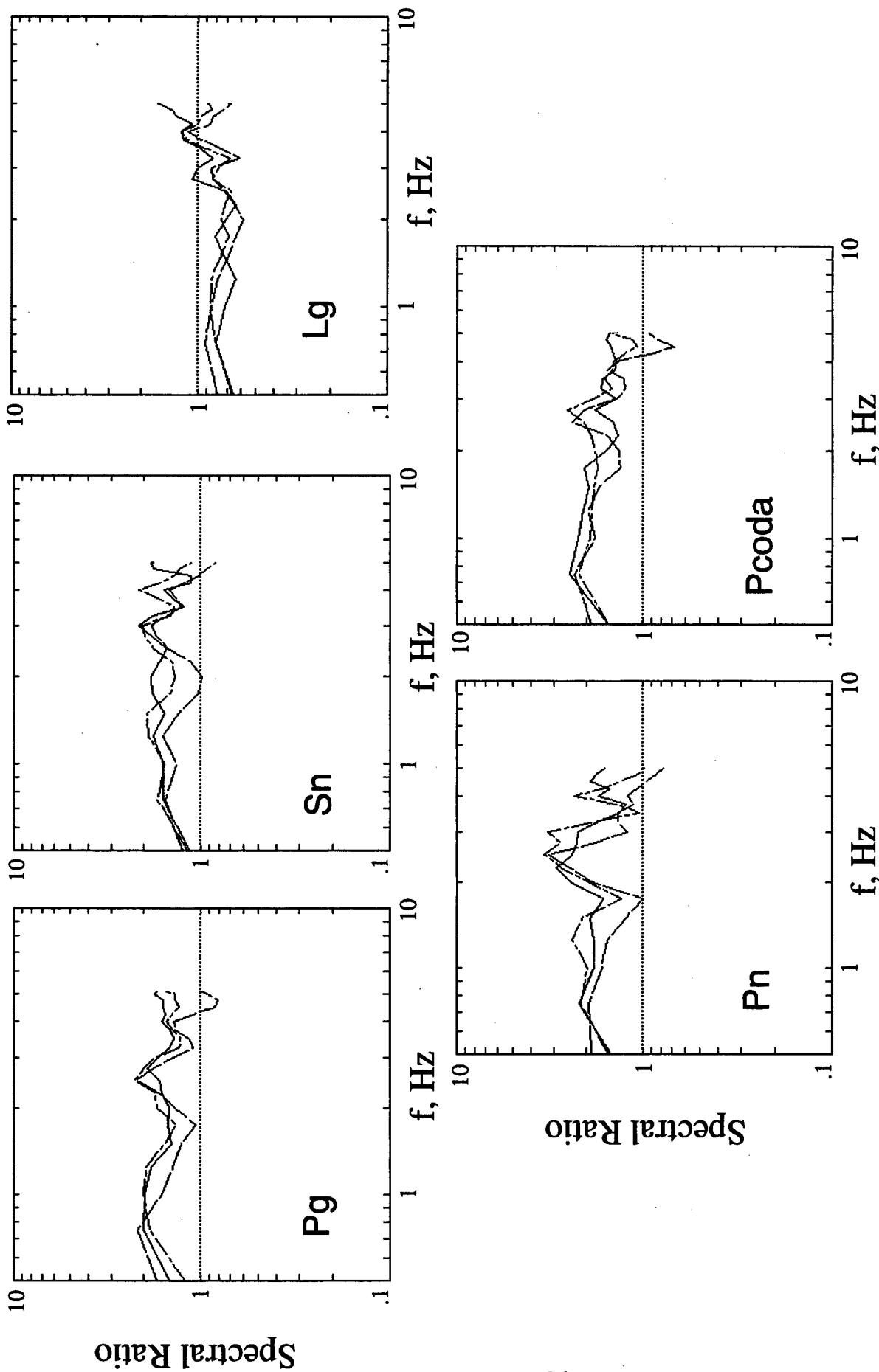


Figure 15. Ratios of observed to predicted (Group A covariance model) Borovoye regional phase spectra for selected Azgir explosions. Note that the observed Azgir Lg spectral amplitude levels are quite consistent with those of Group A explosions at comparable distances outside the Caspian Basin.

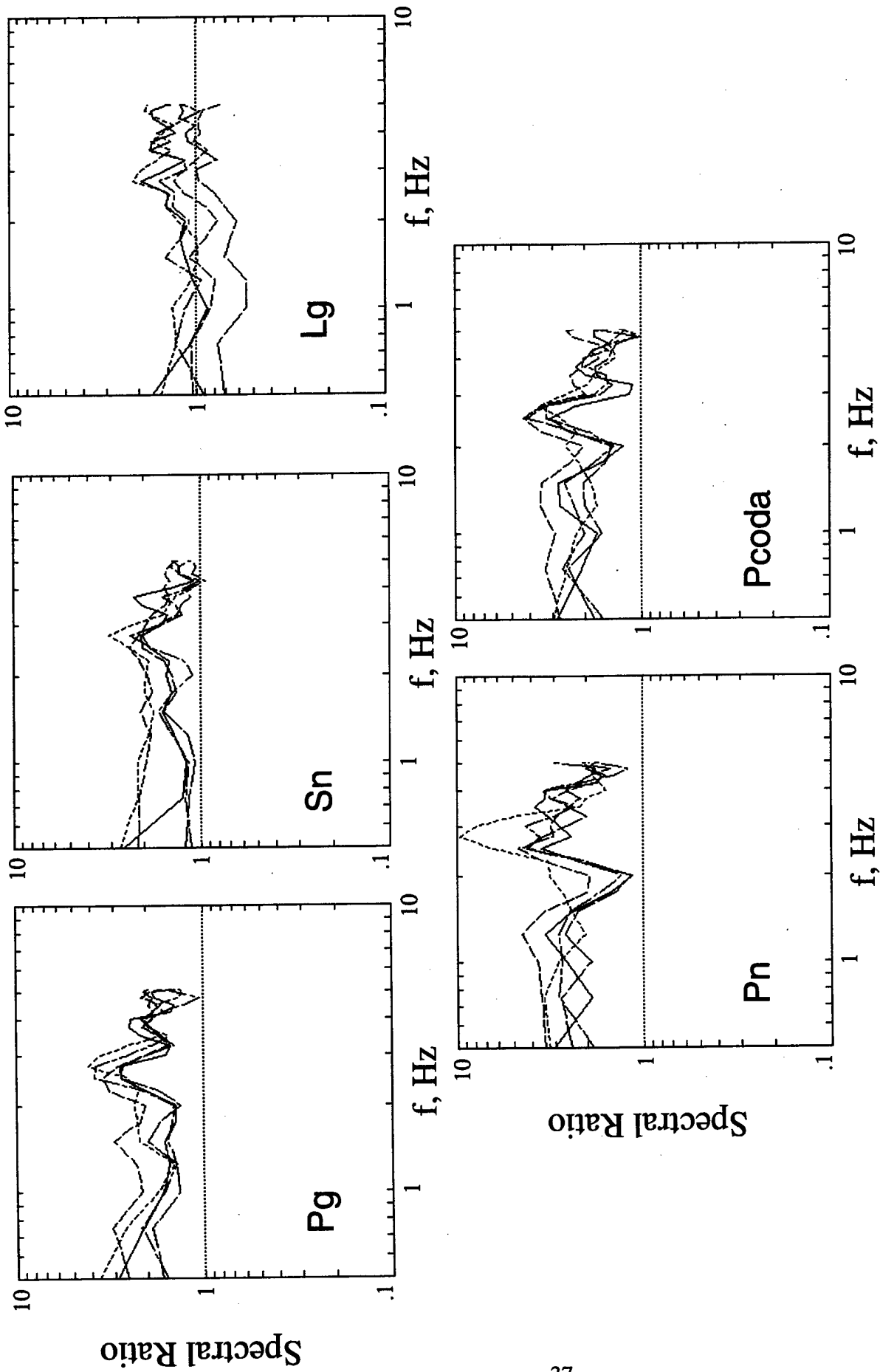


Figure 16. Ratios of observed to predicted (Group A covariance model) Borovoye regional phase spectra for selected Astrakhan explosions. Note that the observed Astrakhan Lg spectral amplitude levels are quite consistent with those of Group A explosions at comparable distances outside the Caspian Basin.

efficiency is lower. In any case, the average observed differences are only of the order of a factor of two or less, so the observed Azgir and Astrakhan regional phase spectra at Borovoye are not dramatically different from those expected for Group A explosions of comparable yield and depth of burial.

It now remains to assess the uncertainties associated with regional phase spectral amplitudes which might be predicted using the different covariance models. That is, to determine the extent to which the simple model of equation (3) can explain the observed variations in regional phase spectral amplitude levels over the ranges of explosion source parameters and propagation paths represented by our Borovoye data sample. It should be noted at the outset that any such estimates will be lower bounds in the sense that they are referenced to a single station and do not account for variable station effects. Ultimately, the additional uncertainties due to station variability will have to be either eliminated through calibration or incorporated into the final error budget. Clearly, the uncertainty will depend to some extent on the amount of calibration information which is available for the area under investigation. For example, if it is known from geologic information that clay is not present at possible explosion depths in the area, then the uncertainties associated with the non-clay covariance model of Table 3 would be preferred to those associated with the total sample covariance model of Table 2.

The residual uncertainties associated with the different covariance models have been estimated by computing observed-to-predicted regional phase spectral ratios for all the PNE events in a given sample using each model and then computing the standard deviations of the logarithms of these spectral ratios on a frequency-by-frequency basis. Three models have been analyzed which assume different levels of calibration. The first model is formulated under the assumption that explosions in clay may be possible and that the propagation path effects between the sources and station are independent of azimuth at a fixed distance. That is, for this model the explosions of Groups I and II have been combined to form a single group. For the second model, explosions in clay are also considered to be possible, but it is assumed that any systematic, azimuthally dependent propagation path effects, such as those shown for  $P_g/P_n$  in Figure 3, have been identified through calibration and accounted for. This is the model associated with the covariance coefficients of Table 2. For the third model, it is

assumed that the possibility of explosions in clay has been ruled out on the basis of geologic information and that any systematic, azimuthally dependent propagation path effects have been identified through calibration and accounted for. This is the model associated with the covariance coefficients of Table 3.

The standard deviations ( $\sigma$ ) in the covariance predictions obtained using these models are plotted versus frequency in Figure 17 where the models 1, 2 and 3 defined above are denoted as "total sample, 3 groups," "total sample, 4 groups," and "non-clay, 4 groups," respectively. It can be seen that all three of these uncertainty estimates are essentially identical above 3 Hz, but that the assumed degree of calibration has a significant effect on the uncertainty estimates at lower frequencies. The right-hand vertical axis on this figure shows the corresponding  $10^{2\sigma}$  values, which represent rough 95% uncertainty bounds on the mean predictions. It can be seen that in the absence of calibration, the 95% uncertainty bound on the covariance model prediction is about a factor of 3 above and below the mean, independent of frequency. However, with extensive calibration of the type represented by model 3 (i.e., Table 3), this 95% uncertainty bound drops to a factor of about 2.5 between 1.5 and 3.0 Hz, and drops further to about a factor of 2 between 0.5 and 1.5 Hz. These results provide some quantitative measure of the overall uncertainties associated with predicting regional phase spectral amplitudes using models of the type represented by Eq. (3) and of the potential value of calibration information, at least for the range of explosive source and propagation path conditions represented by our Borovoye data sample.

The implications of the Borovoye PNE data analysis results with respect to the transportability of regional phase spectral ratio discriminants are summarized in Figures 18-21 which show the  $L_g$  to P ( $P_n$  and  $P_g$ ) and  $S_n$  to P spectral ratios derived from the Borovoye recordings of the Soviet PNE events of Table 1. It can be seen from these figures that although there is considerable scatter in the data, these spectral ratios generally decrease to values of 1 or less at frequencies above about 3 Hz, consistent with the expected values of the regional phase spectral ratio discriminants for underground nuclear explosion sources. Note that the ratios computed with respect to the  $P_g$  phase (Figures 19 and 21) show much less scatter within groups than do the corresponding ratios computed with respect to the  $P_n$  phase (Figures 18 and 20). This is perhaps not unexpected given

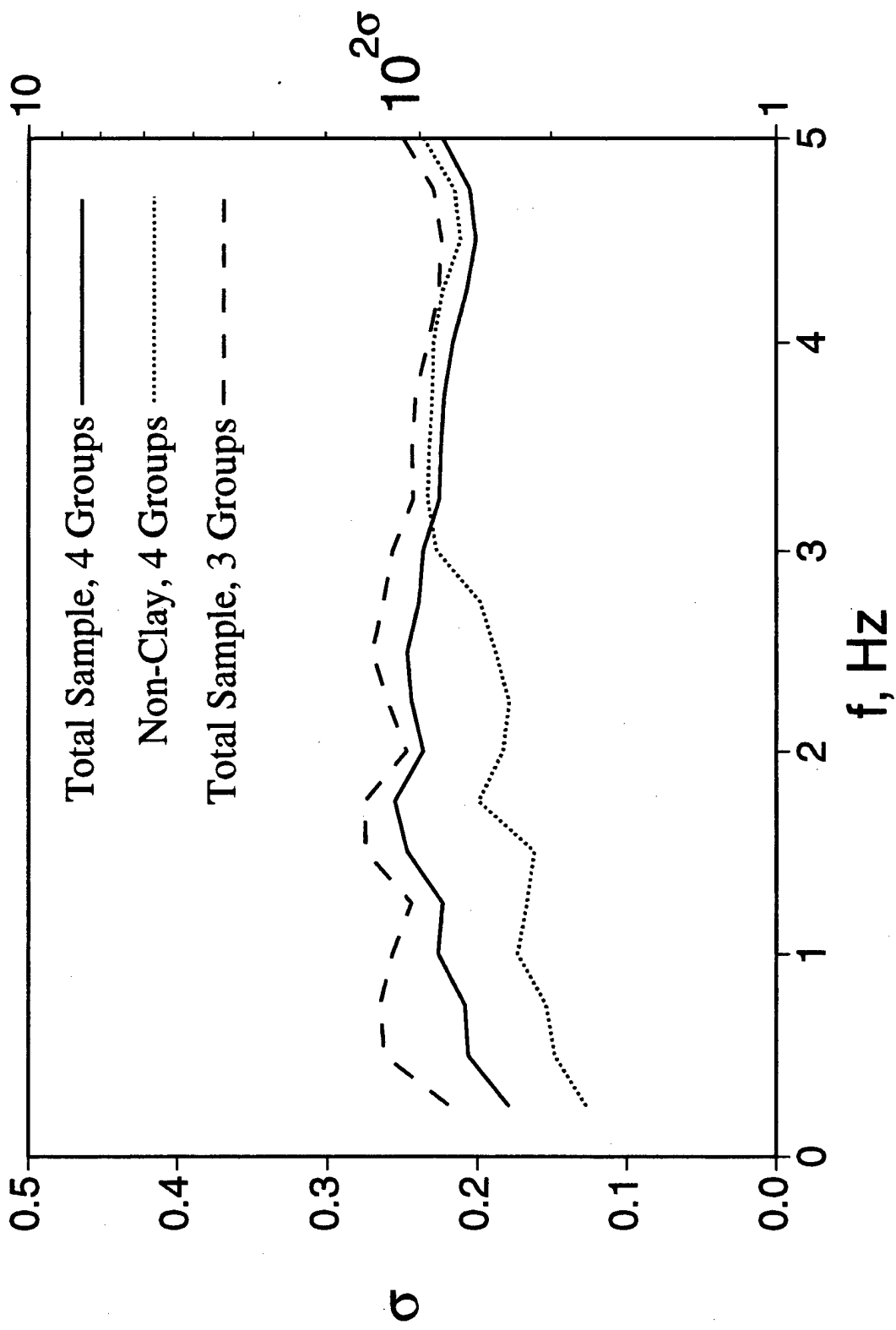


Figure 17. Comparison of estimates of covariance model prediction uncertainties ( $\sigma$ ) versus frequency for various assumed levels of regional calibration.

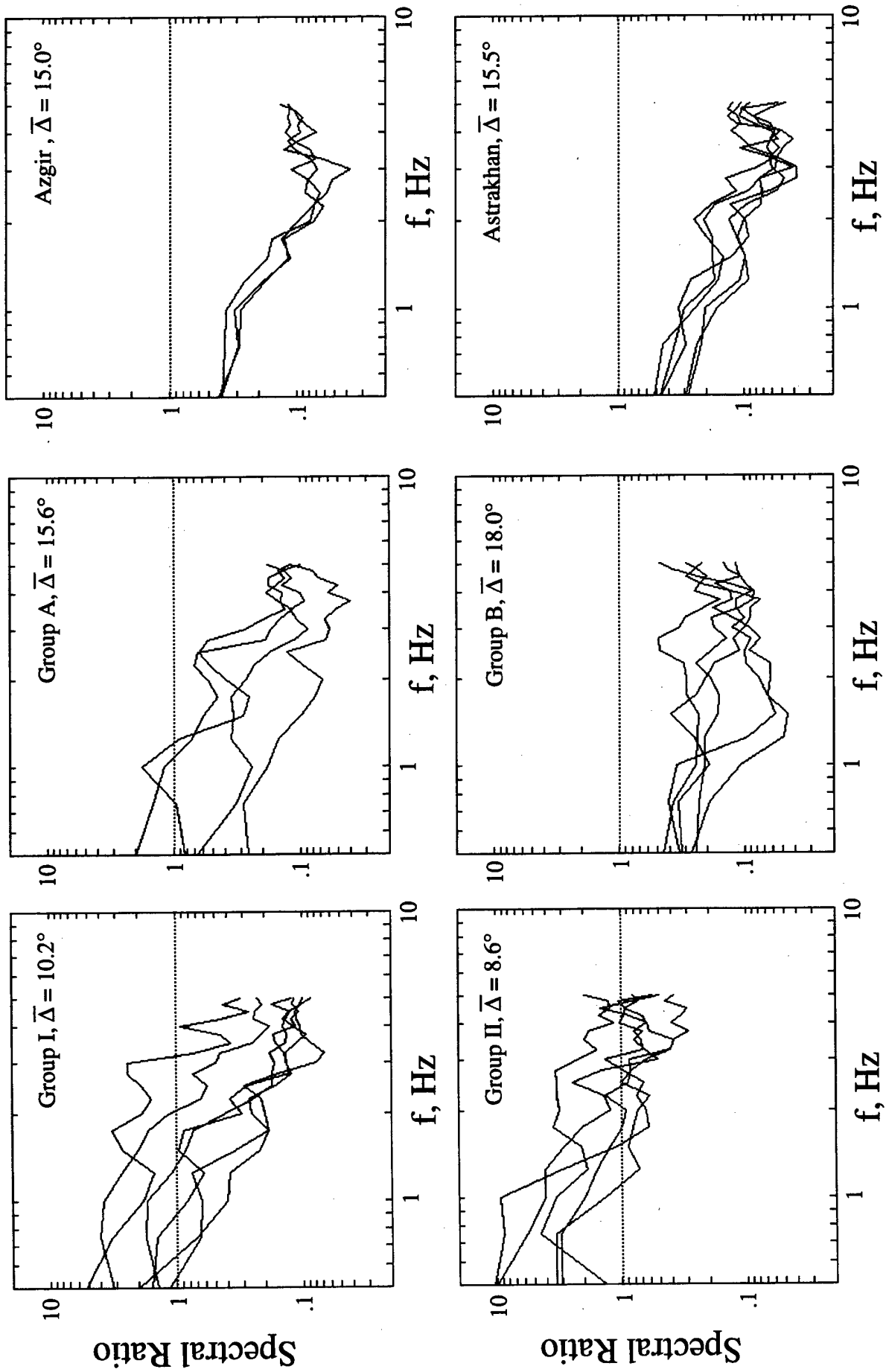


Figure 18. Observed Lg/Pn spectral ratios corresponding to the different groups of Soviet PNE events recorded at the Borovoye station.

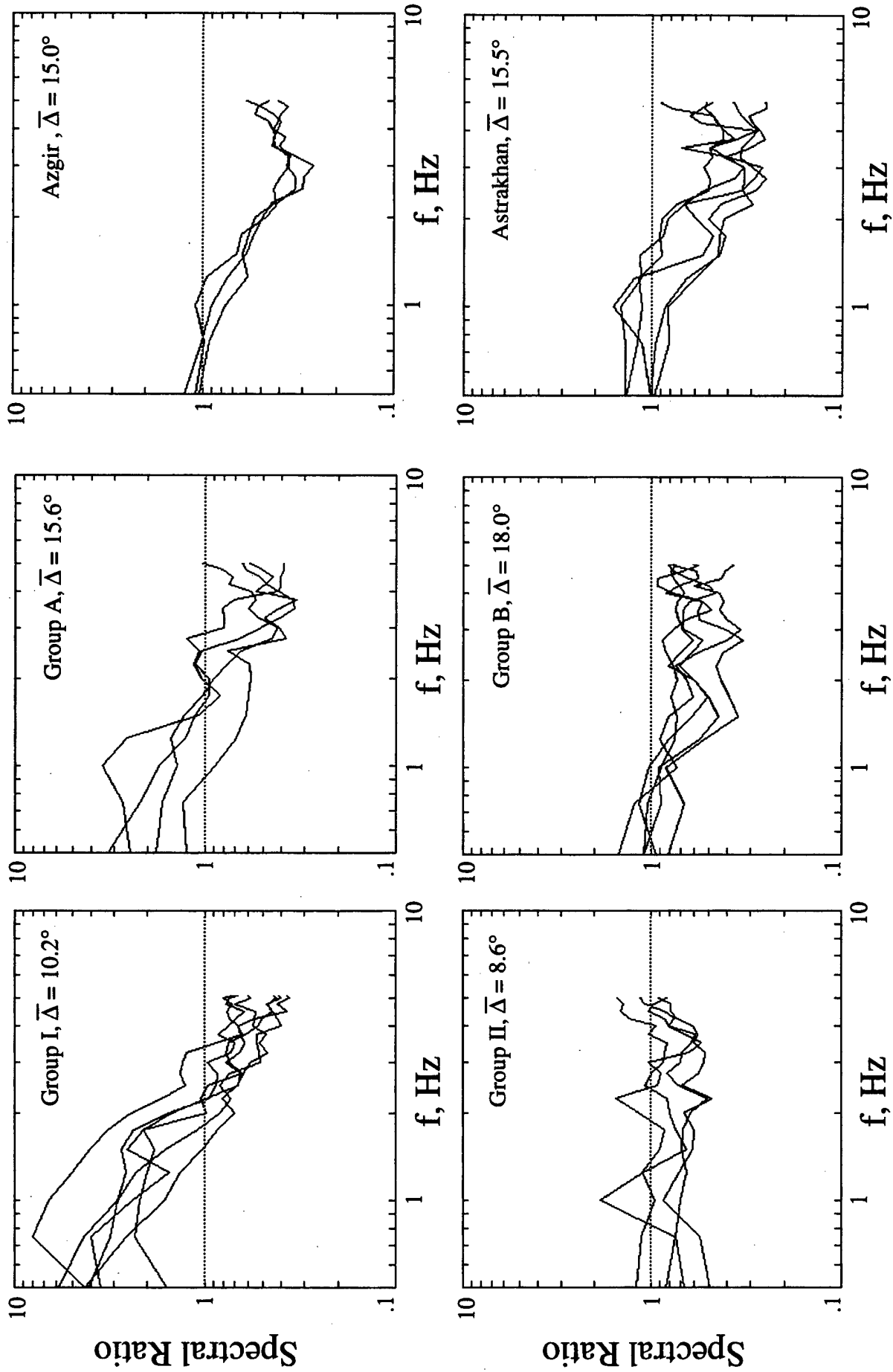


Figure 19. Observed Lg/Pg spectral ratios corresponding to the different groups of Soviet PNE events recorded at the Borovoye station.

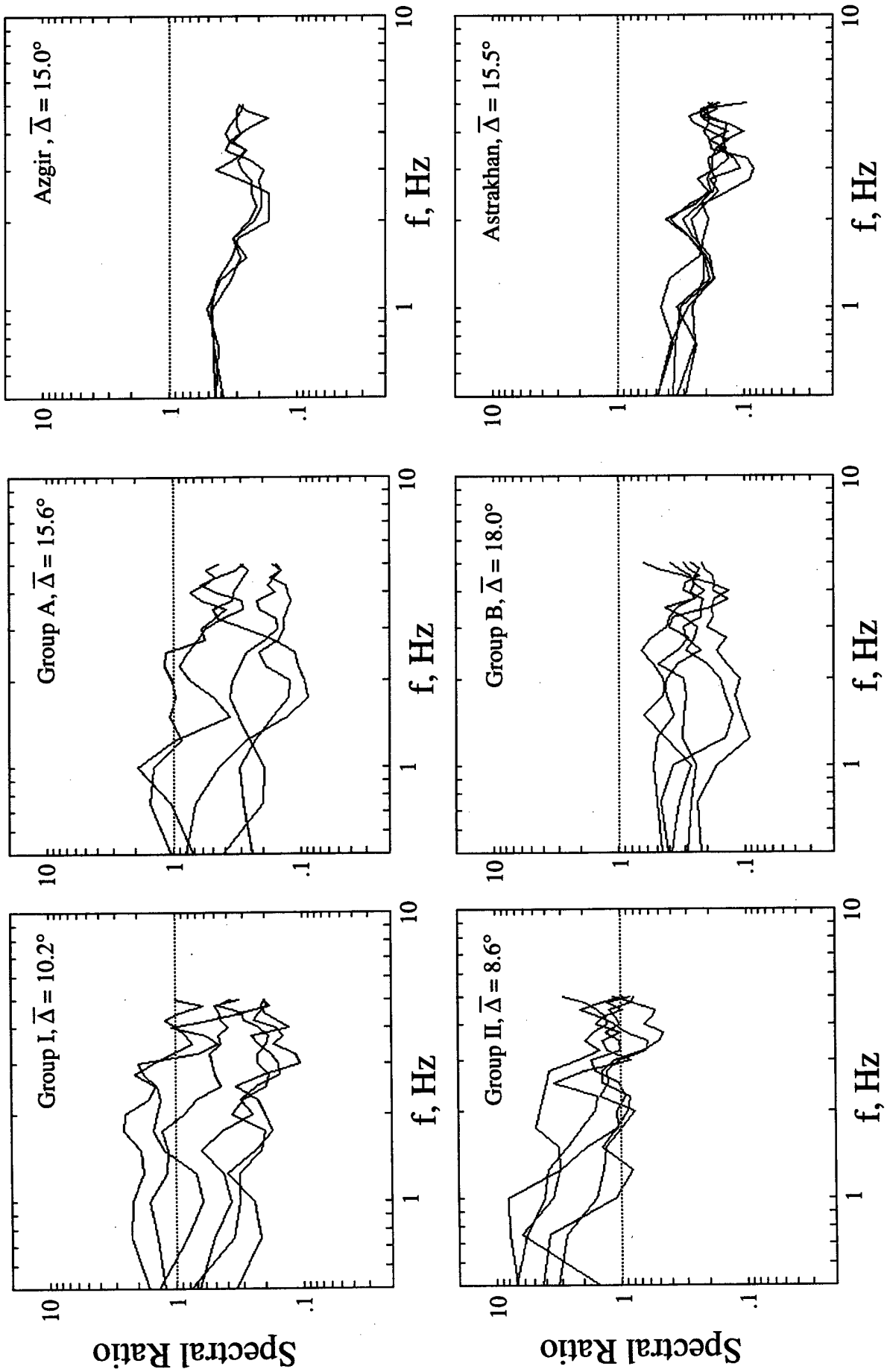


Figure 20. Observed Sn/Pn spectral ratios corresponding to the different groups of Soviet PNE events recorded at the Borovoye station.

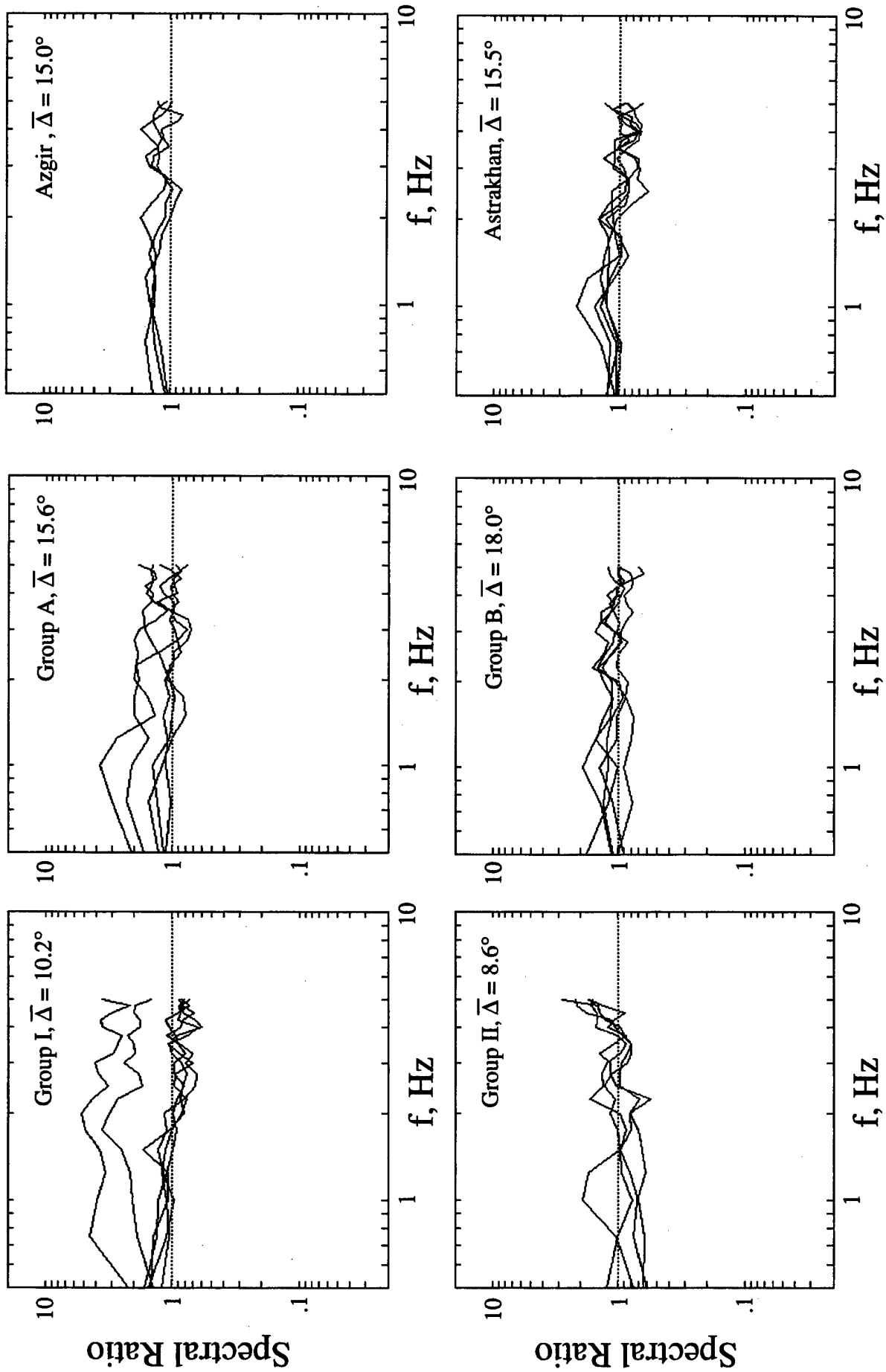


Figure 21. Observed Sn/Pg spectral ratios corresponding to the different groups of Soviet PNE events recorded at the Borovoye station.

the documented sensitivity of  $P_n$  characteristics to details of the upper mantle velocity structure along the propagation path. The standard deviations of the logarithms of the ratios of the observed phase spectral ratios to the corresponding average phase spectral ratios predicted for the different groups by the covariance model are plotted as functions of frequency in Figure 22. This display provides quantitative confirmation of the fact that the ratios computed with respect to  $P_n$  show significantly more scatter on a group-by-group basis than do those computed with respect to  $P_g$ . Note also that in this context, the  $S_n/P_g$  ratios appear to be about as stable as the  $L_g/P_g$  ratios. However, with reference to Figure 21, it can be seen that the  $S_n/P_g$  ratios frequently trend to values somewhat greater than 1 at high frequency and show very little frequency dependence, which may render them less diagnostic for event discrimination purposes. On balance, the  $L_g/P_g$  spectral ratios of Figure 19 seem to provide the most robust regional discriminant for explosion identification in that they consistently approach explosion-like values of 1 or less at high frequencies over the entire sampled epicentral distance range extending from 7.2 to 19.1 degrees. Once again, the right hand vertical axis on Figure 22 shows the corresponding  $10^{2\sigma}$  values, which represent rough 95% uncertainty bounds on the average spectral ratios. It can be seen that above 3 Hz, the 95% uncertainty bound on the average  $L_g/P_g$  spectral ratios predicted by the covariance model averages to about a factor of 1.7.

The average  $L_g/P_g$  spectral ratios for the four groups are shown in Figure 23 where it can be seen that they show no obvious distance dependence over the sampled range extending from 7.2 to 19.1 degrees. Moreover, they are consistent in that in all four cases, the ratios decrease to a value of less than 1.0 above about 2 Hz. These average ratios, together with the associated  $L_g/P_g$  95% uncertainty bounds from Figure 22, provide a quantitative basis for assessing regional discrimination capability with respect to underground nuclear explosions conducted under a wide variety of source conditions, at least for regional propagation paths comparable to those sample by these Borovoye data.

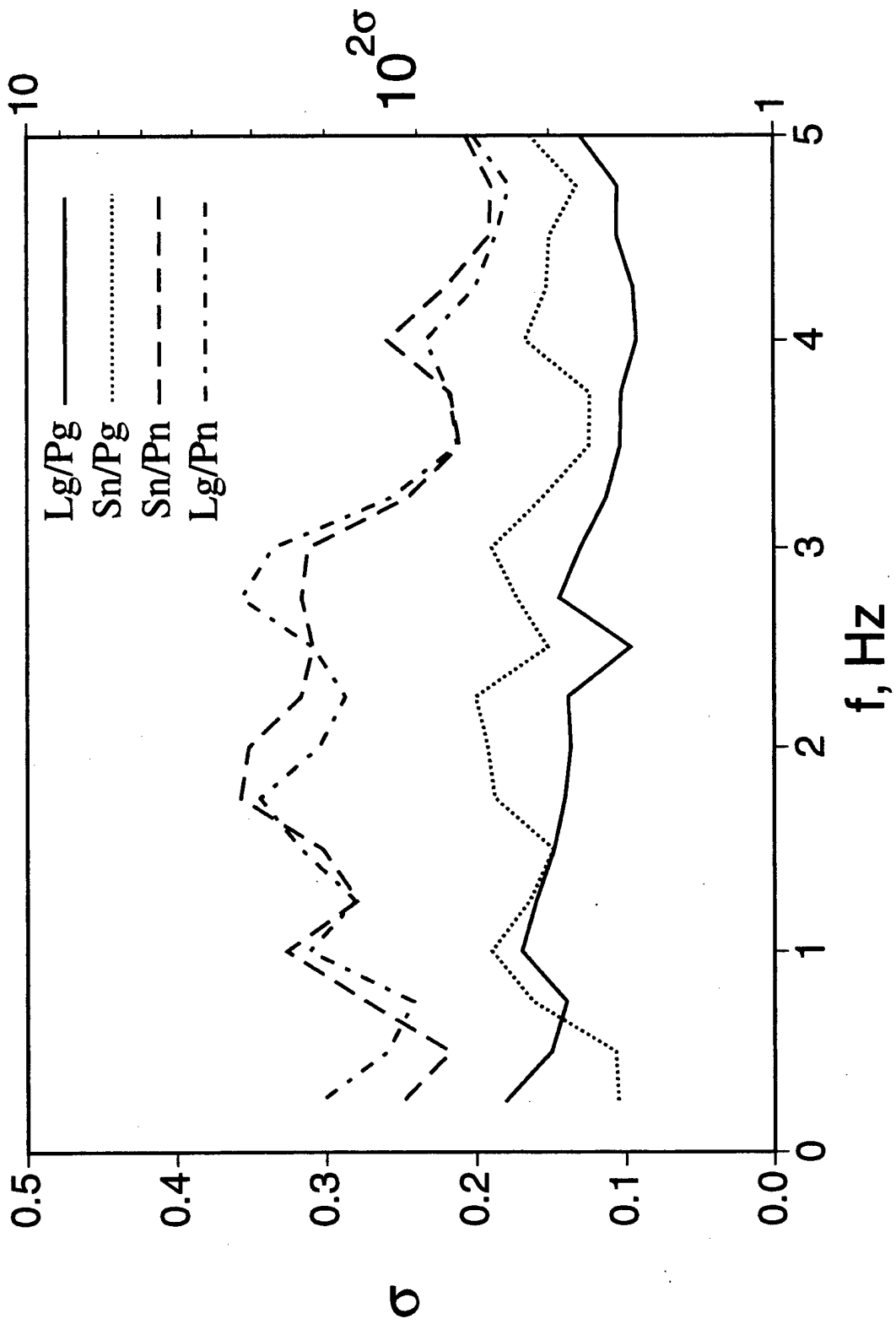


Figure 22. Comparison of estimates of covariance model prediction uncertainties ( $\sigma$ ) versus frequency for the different regional phase spectral ratios.

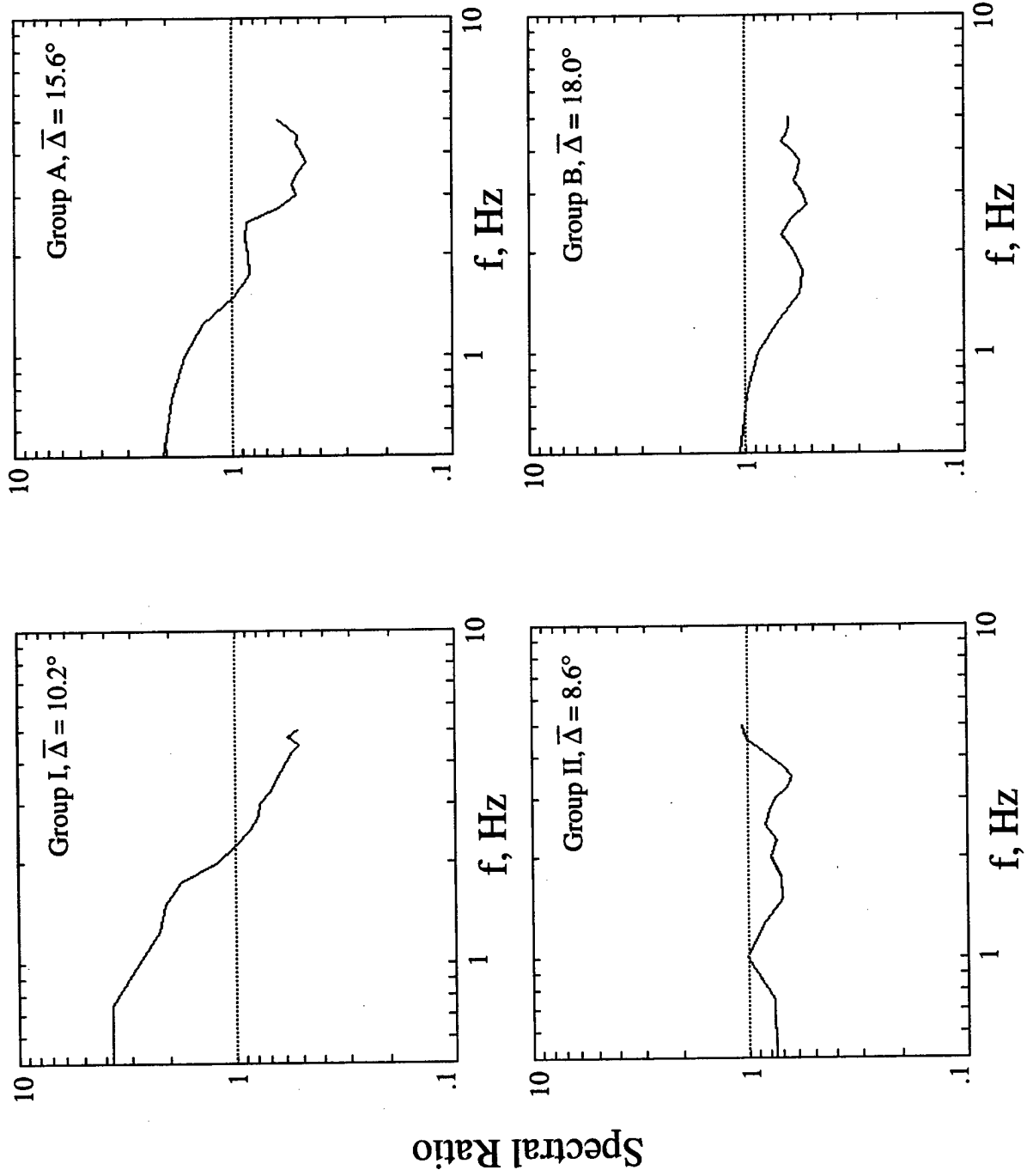


Figure 23. Average Lg/Pg spectral ratios corresponding to the different groups of Soviet PNE events recorded at the Borovoye station.

#### **4. THEORETICAL MODELING ANALYSIS OF NEAR-REGIONAL SEISMIC DATA RECORDED FROM SELECTED PNE EVENTS**

In addition to the regional data recorded at the Borovoye station, the IDG has also recorded and digitized near-regional ( $\Delta < 25$  km) seismic data from a number of Soviet PNE events. Since these data are unaffected by the variations in the long regional propagation paths to Borovoye, they provide an opportunity to test the validity of our statistical covariance decomposition of the source and propagation path effects on the observed Borovoye data. That is, if it can be verified that these near-regional data scale with explosion yield and depth of burial in the same manner as that inferred from the analysis of the Borovoye regional data, then the confidence in the covariance decomposition will be greatly increased. Unfortunately, a direct comparison of these two source scaling estimates is not possible at this time, because there is currently little overlap between the PNE events represented in the Borovoye and near-regional data samples. However, since the source scaling inferred from the Borovoye covariance analysis was found to be generally consistent with the predictions of the Mueller/Murphy model, it is of interest to assess how well that approximate source model can account for the available near-regional PNE data. That is, if it can be shown that the Mueller/Murphy source model can account for the observed variations in the near-regional PNE data, then that will provide additional support for the validity of the source scaling inferred from the covariance analysis of the Borovoye data. For this reason, near-regional data observed from selected PNE events have been theoretically simulated using the Mueller/Murphy explosion source model in an attempt to test the applicability of that model over the ranges of yield, depth of burial and source media represented by these explosions.

The source parameters of the 9 PNE events which have been selected for theoretical simulation analysis are listed in Table 5 where it can be seen that they sample yield values in the range from 2.5 to 14 kt and depths of burial in the range from 98 to 2859 m for explosions in salt, granite, limestone and sandstone source media. As was noted previously, a comparison of Table 5 with Table 1 indicates that only two of these selected events (i.e., 7/21/84 and 6/18/85) correspond to explosions for which Borovoye regional data are currently

available. However, the explosions of Table 5 do sample ranges of source parameters which are consistent with those represented in the Borovoye sample of Table 1 and, consequently, the source scaling inferred from these two data sets should be roughly comparable.

**Table 5. Source Parameters of Soviet PNE Events Used in the Theoretical Modeling Study of Near-Regional Seismic Data**

Date	Latitude	Longitude	W, kt	h, m	Medium
07/21/84	51.36	53.32	13.5	846	Salt
08/10/77	50.92	110.76	8.5	499	Granite
09/17/84	55.87	87.45	10	557	Granite
07/18/85	65.97	40.86	8.5	772	Granite
10/02/74	66.10	112.65	1.7	98	Limestone
09/02/69	57.42	54.86	7.6	1212	Limestone
04/11/72	37.38	62.00	14	1720	Limestone
04/18/87	60.25	57.08	3.2	2055	Limestone
06/18/85	60.17	72.50	2.5	2859	Sandstone

The subsurface propagation path models used in the theoretical simulation analyses are listed in Table 6 for each of the 9 selected PNE events of Table 5. These plane-layered models were developed on the basis of P and S wave velocity ( $\alpha, \beta$ ) and density ( $\rho$ ) data obtained from logging of the explosion emplacement holes, supplemented by regional geophysical data as required for the deeper structures. The listed values for the associated P and S wave anelastic attenuation parameters ( $Q_\alpha, Q_\beta$ ) were estimated for each layer using nominal values for the various rock types as a function of depth in the different source regions. Obviously, these plane-layered models provide only rough approximations to the actual propagation paths in many cases, but they are generally consistent with the type of information which might be available in a verification context. Therefore, it is relevant to attempt to assess the degree to which such simple models can be used to simulate the characteristics of the observed data.

**Table 6. Subsurface Velocity Models Used in the Theoretical Modeling Study of Near-Regional Seismic Data**

<u>7/21/84</u>						
Medium	Thickness,km	$\alpha$ ,km/sec	$\beta$ ,km/sec	$\rho$ ,gm/cm <sup>3</sup>	$Q_{\alpha}$	$Q_{\beta}$
Clay	0.068	1.50	0.60	2.00	40	25
Sandstone	0.160	2.20	0.95	2.00	60	35
Anhydrite	0.107	5.00	2.78	2.70	200	150
Salt	0.365	4.00	2.20	2.20	150	100
Anhydrite	0.050	5.00	2.78	2.70	200	150
Salt	0.055	4.10	2.22	2.20	150	100
Anhydrite	0.027	5.50	2.90	2.70	200	150
Salt	3.000	4.30	2.10	2.20	150	100
Basement	-	5.20	2.95	2.30	600	500

<u>8/10/77</u>						
Medium	Thickness,km	$\alpha$ ,km/sec	$\beta$ ,km/sec	$\rho$ ,gm/cm <sup>3</sup>	$Q_{\alpha}$	$Q_{\beta}$
Alluvium	0.025	1.70	0.50	1.50	40	30
Sandstone	0.130	2.90	1.20	2.00	60	45
Granite	-	6.20	3.40	2.70	200	150

<u>9/17/84</u>						
Medium	Thickness,km	$\alpha$ ,km/sec	$\beta$ ,km/sec	$\rho$ ,gm/cm <sup>3</sup>	$Q_{\alpha}$	$Q_{\beta}$
Fractured Granite	0.050	4.20	2.20	2.50	60	40
Granite	-	5.40	3.20	2.55	200	150

<u>7/18/85</u>						
Medium	Thickness,km	$\alpha$ ,km/sec	$\beta$ ,km/sec	$\rho$ ,gm/cm <sup>3</sup>	$Q_{\alpha}$	$Q_{\beta}$
Clay	0.050	1.88	0.50	1.50	60	45
Argillite	0.530	4.50	2.20	2.00	60	45
Sandstone	0.270	3.60	1.80	2.00	150	100
Granite	-	6.00	3.70	2.50	200	150

Table 6. Continued

<u>10/02/74</u>						
Medium	Thickness,km	$\alpha$ ,km/sec	$\beta$ ,km/sec	$\rho$ ,gm/cm <sup>3</sup>	$Q_{\alpha}$	$Q_{\beta}$
Marl	0.082	2.30	1.30	2.30	160	145
Limestone	-	3.80	2.30	2.50	200	150
<u>9/02/69</u>						
Medium	Thickness,km	$\alpha$ ,km/sec	$\beta$ ,km/sec	$\rho$ ,gm/cm <sup>3</sup>	$Q_{\alpha}$	$Q_{\beta}$
Sediments	0.040	1.00	0.30	2.20	20	10
Dolomite	0.240	3.25	1.60	2.40	100	60
Limestone	0.690	5.00	2.75	2.55	100	60
Dolomite	0.060	3.50	1.60	2.58	100	60
Limestone	0.270	5.60	3.20	2.65	100	60
Dolomite	0.060	3.50	1.60	2.47	100	60
Limestone	0.690	5.80	3.30	2.58	100	60
Dolomite	0.360	3.65	1.90	2.59	100	60
Limestone	2.500	5.50	3.25	2.60	200	100
Basement	-	5.80	3.40	2.80	200	100
<u>4/11/72</u>						
Medium	Thickness,km	$\alpha$ ,km/sec	$\beta$ ,km/sec	$\rho$ ,gm/cm <sup>3</sup>	$Q_{\alpha}$	$Q_{\beta}$
Clay	0.250	1.80	0.80	2.00	60	45
Sandstone	0.900	2.20	1.30	2.20	160	145
Marl	0.100	3.25	1.70	2.50	200	150
Limestone	0.550	2.85	1.50	2.30	200	150
Marl	0.450	3.20	1.70	2.50	200	150
Marl	0.450	3.50	1.75	2.50	200	150
Marl	6.000	4.50	2.30	2.60	200	150
Basement	-	6.22	3.40	2.70	400	300

**Table 6. Continued**

<u>4/18/87</u>						
Medium	Thickness,km	$\alpha$ ,km/sec	$\beta$ ,km/sec	$\rho$ ,gm/cm <sup>3</sup>	$Q_{\alpha}$	$Q_{\beta}$
Sand	0.250	1.80	0.90	2.00	50	25
Clay	0.250	1.80	0.90	2.00	50	25
Clay	0.300	4.00	2.10	2.30	100	50
Dolomite	0.100	5.00	2.90	2.40	100	50
Limestone	1.600	5.70	3.20	2.60	200	100
Sandstone	-	3.00	1.70	2.60	200	100

<u>6/18/85</u>						
Medium	Thickness,km	$\alpha$ ,km/sec	$\beta$ ,km/sec	$\rho$ ,gm/cm <sup>3</sup>	$Q_{\alpha}$	$Q_{\beta}$
Sandstone	2.700	3.60	2.10	2.50	160	145
Clay	0.100	2.44	1.50	2.30	60	40
Sandstone	-	3.80	2.30	2.55	2.00	150

The seismic signals corresponding to the near-regional observations from the selected PNE events of Table 5 have been theoretically simulated using the frequency-wavenumber integration algorithm developed by Bouchon (1981). In this approach, compressional point sources equivalent to the Mueller/Murphy explosive source approximations are embedded at the appropriate depths in the associated plane-layered subsurface models for the sites listed in Table 6, and the exact theoretical seismic signals corresponding to the selected source/receiver configurations are synthesized using the referenced frequency-wavenumber integration algorithm. Since our principal interest in the present study lies in assessing the adequacy of the source approximation, the comparative analyses described below have been focused on the initial arrivals contained in the first few seconds of the observed and simulated waveforms.

The observed and synthetic vertical component displacement waveforms for the PNE explosion of 7/21/84 are compared at the same absolute amplitude scales in Figure 24. This explosion had a yield of 13.5 kt and was detonated at a depth of 846 m in salt in the Karachaganak gas condensate field located in the Uralsk District of the former Soviet Union for the purpose of cavity creation. It

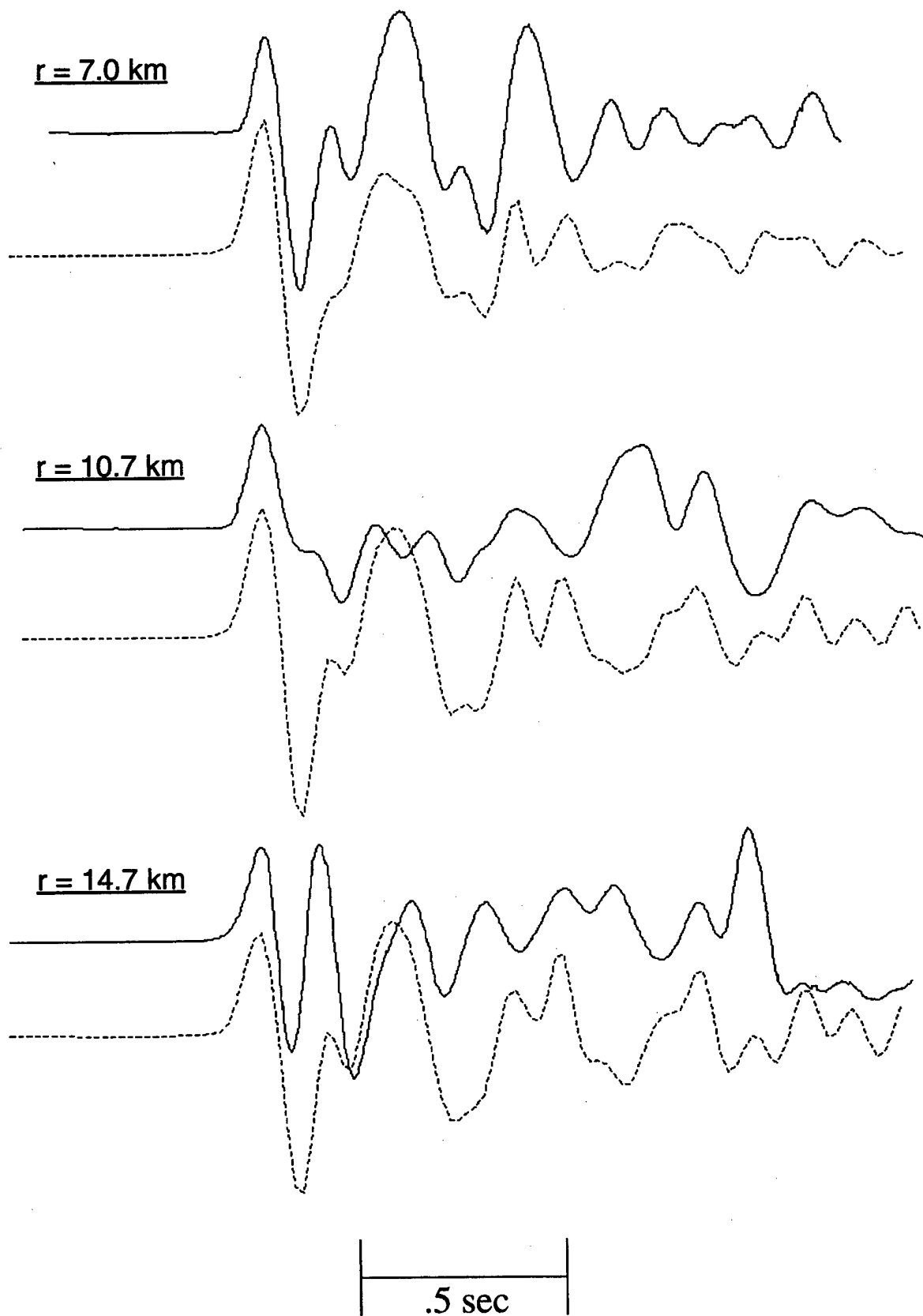


Figure 24. Comparison of observed (solid) and synthetic (dashed) near-regional, vertical component displacements for the PNE event of 7/21/84, which was a 13.5 kt explosion at a depth of 846 m in salt.

can be seen from this figure that the observed and theoretically simulated waveforms agree quite well in this case with respect to overall amplitude level and frequency content for these three stations at distances of 7.0, 10.7 and 14.7 km from the source.

Similar comparisons of simulated and observed waveforms for the 8/10/77, 9/17/84 and 7/18/85 PNE explosions in granite are shown in Figures 25-27. These explosions had similar yields of 8.5, 10 and 8.5 kt, respectively, and were conducted for the purpose of providing sources of seismic waves for Deep Seismic Sounding (DSS) experiments. It can be seen from these figures that the agreement between the synthetic and observed vertical component displacement waveforms is again quite reasonable for all three explosions at these stations in the 3 to 25 km distance range. This suggests that the Mueller/Murphy model provides adequate explosion seismic source approximations for these three widely separated granitic source environments.

Comparisons of the simulated and observed vertical displacement waveforms for the 10/02/74, 9/02/69, 4/11/72 and 4/18/87 PNE events in limestone are presented in Figures 28-31, respectively. It can be seen with reference to these figures that for the first three of these explosions, the agreement between predicted and observed amplitude levels and dominant

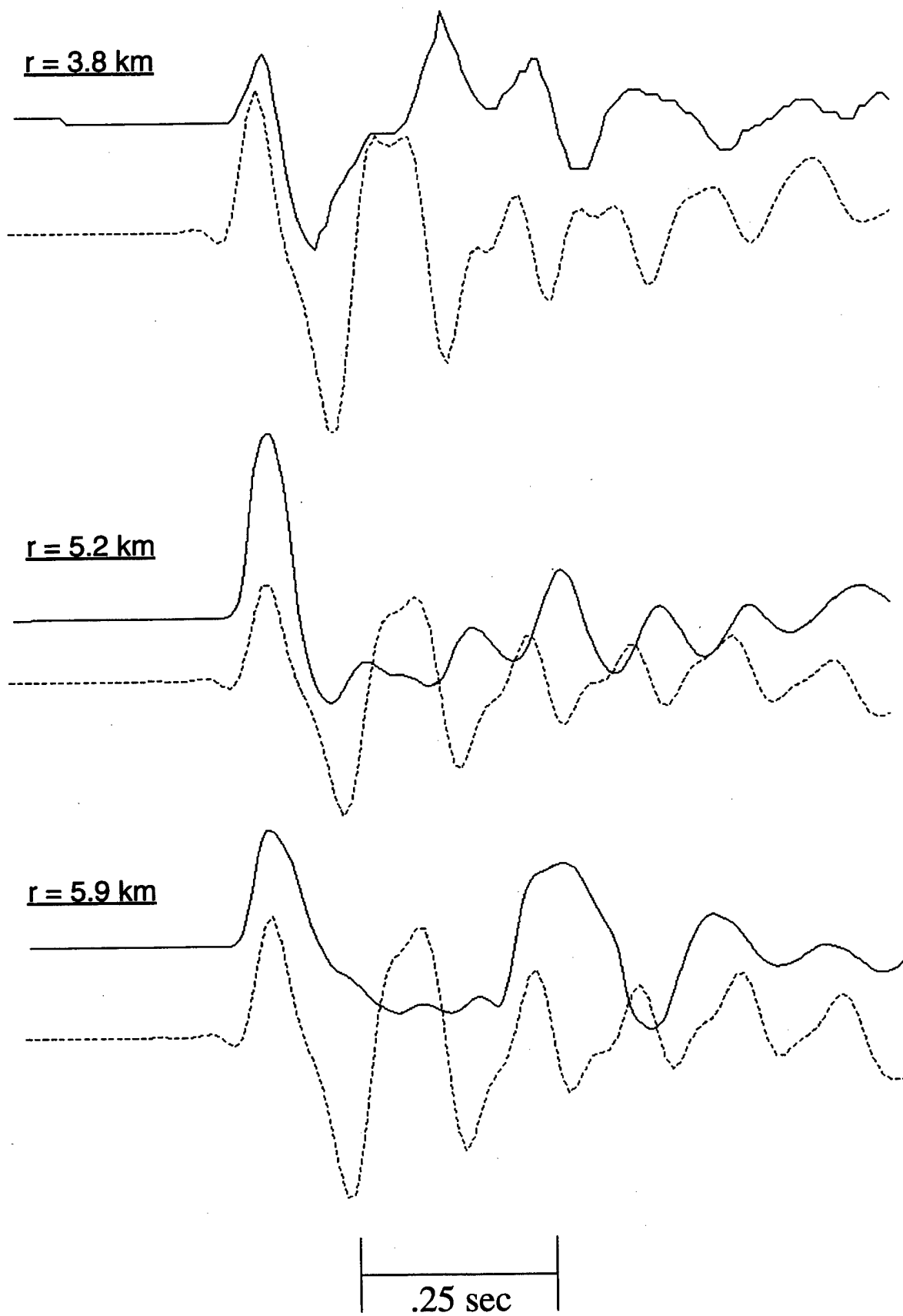


Figure 25. Comparison of observed (solid) and synthetic (dashed) near-regional, vertical component displacements for the PNE event of 8/10/77, which was an 8.5 kt explosion at a depth of 499 m in granite.

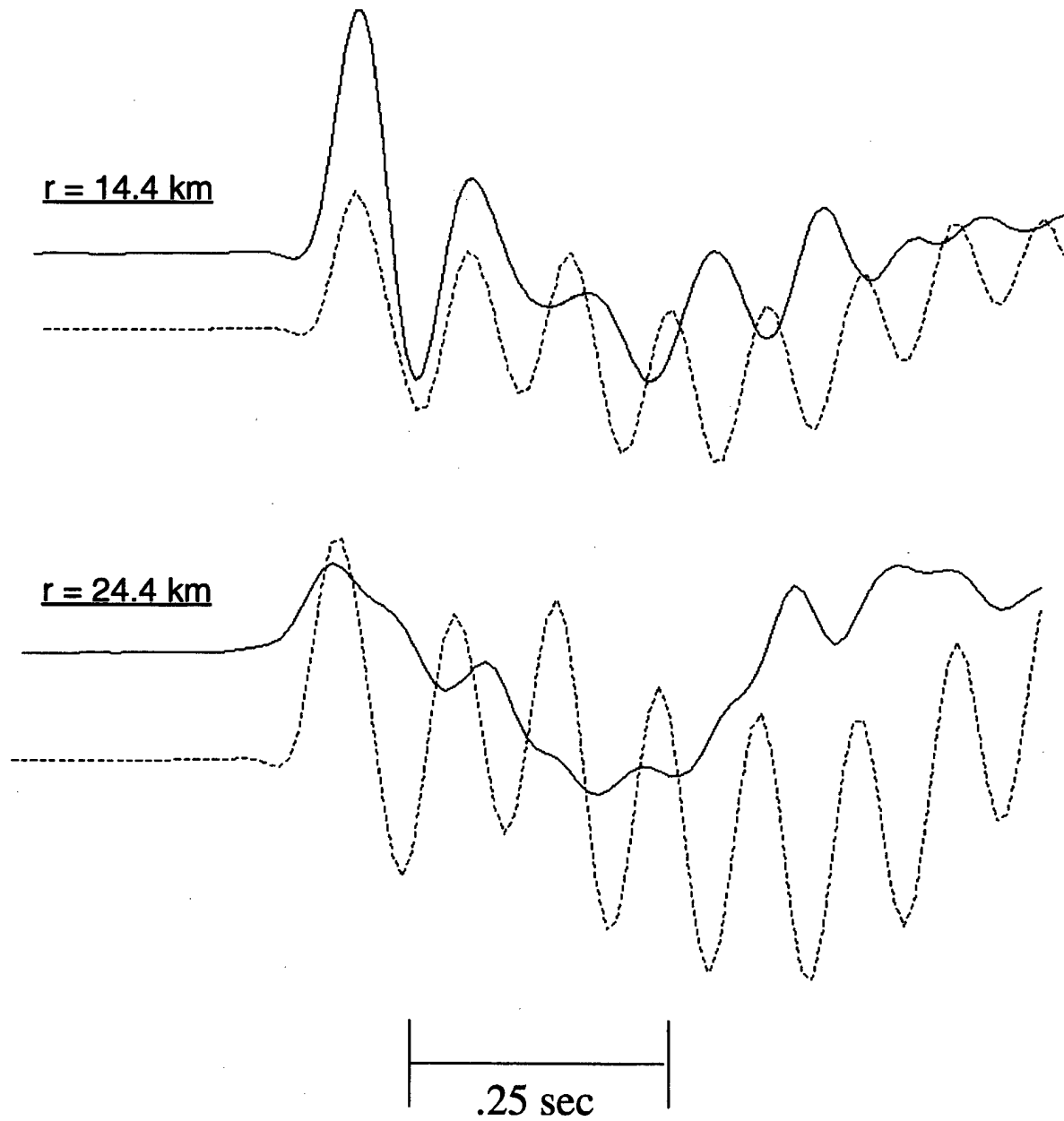


Figure 26. Comparison of observed (solid) and synthetic (dashed) near-regional, vertical component displacements for the PNE event of 9/17/84, which was a 10 kt explosion at a depth of 557 m in granite.

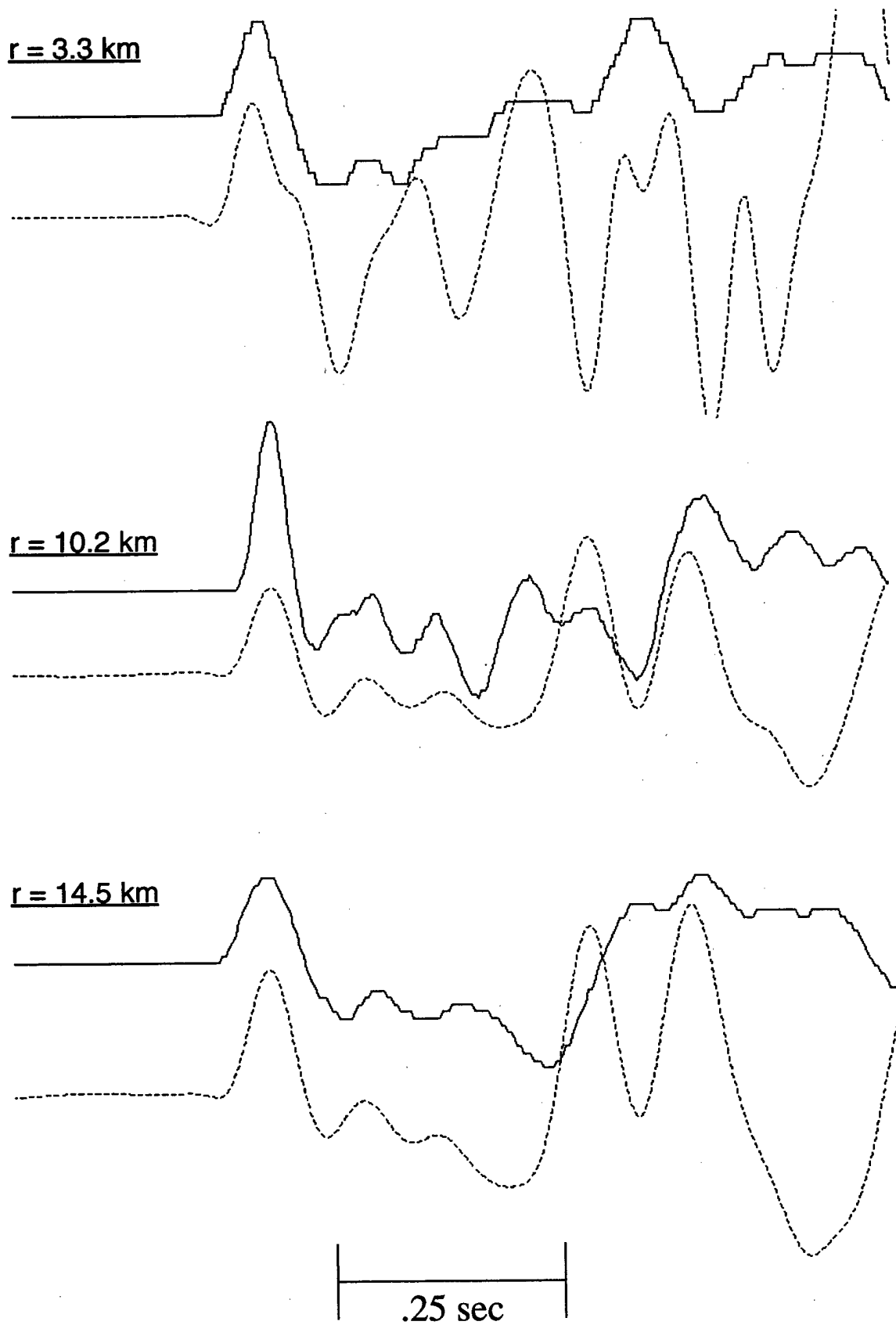


Figure 27. Comparison of observed (solid) and synthetic (dashed) near-regional, vertical component displacements for the PNE event of 7/18/85, which was an 8.5 kt explosion at a depth of 772 m in granite.

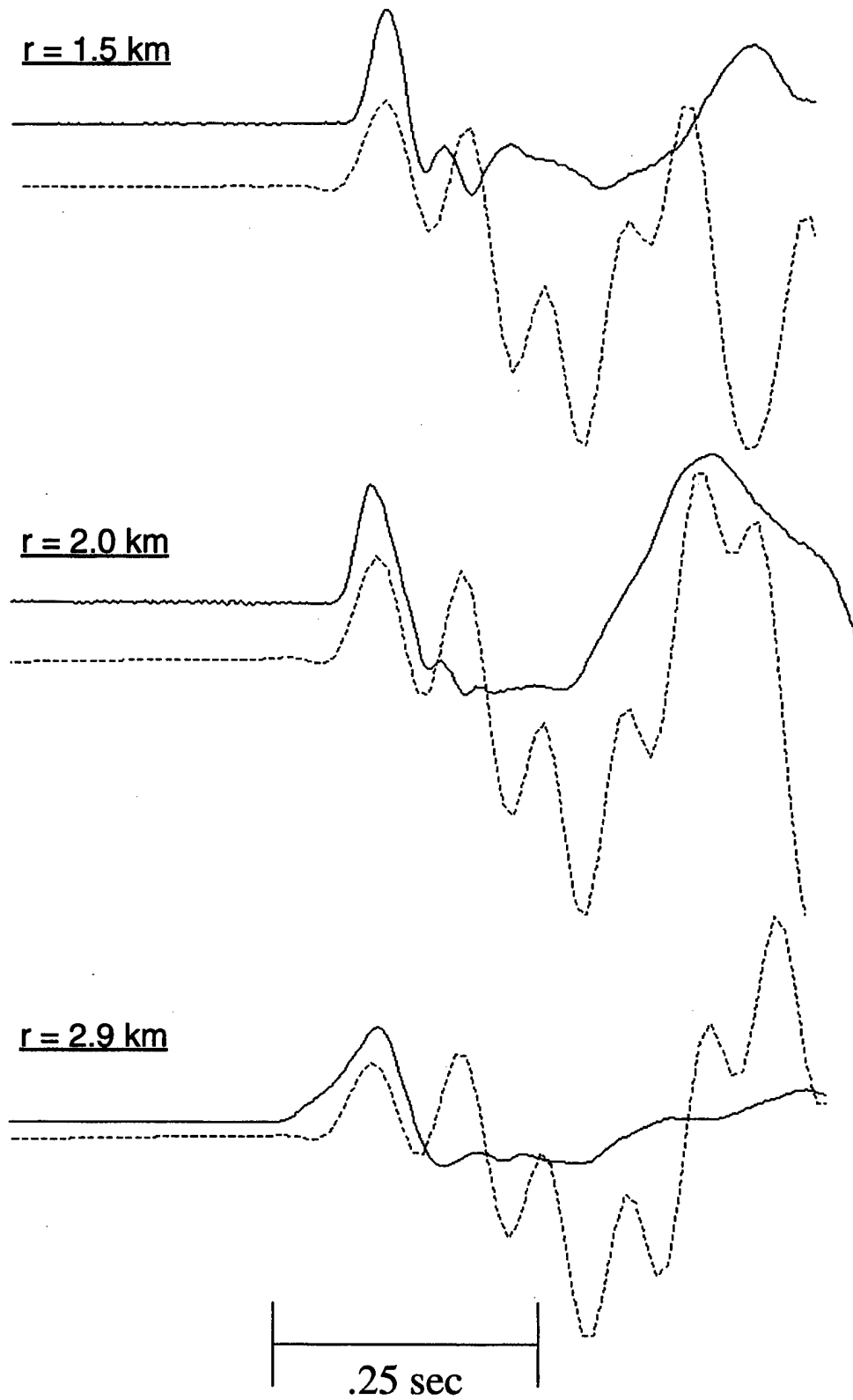


Figure 28. Comparison of observed (solid) and synthetic (dashed) near-regional, vertical component displacements for the PNE event of 10/02/74, which was a 1.7 kt explosion at a depth of 98 m in limestone.

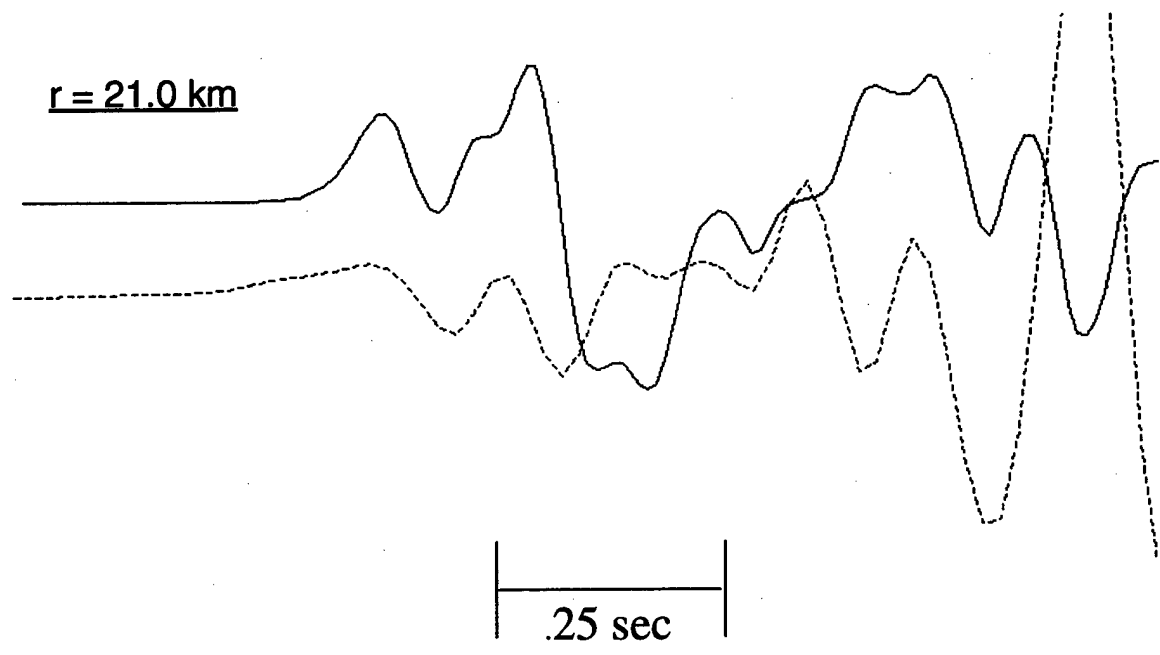


Figure 29. Comparison of observed (solid) and synthetic (dashed) near-regional, vertical component displacements for the PNE event of 9/02/69, which was a 7.6 kt explosion at a depth of 1212 m in limestone.

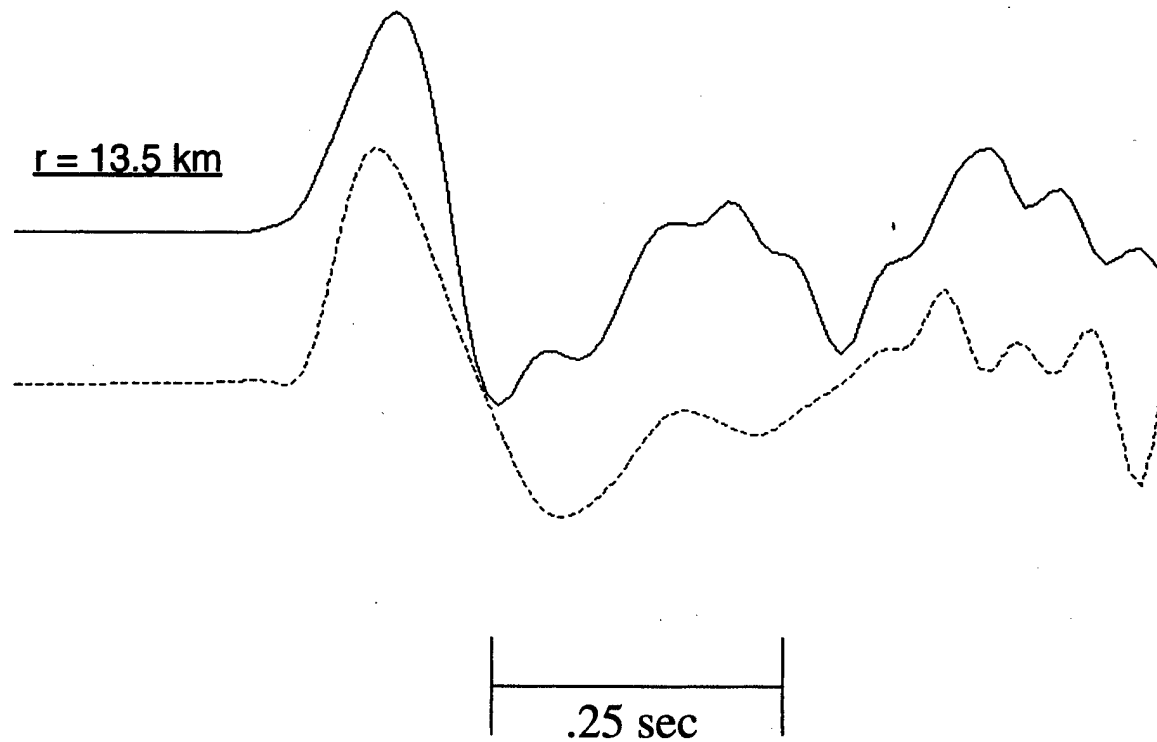


Figure 30. Comparison of observed (solid) and synthetic (dashed) near-regional, vertical component displacements for the PNE event of 4/11/72, which was a 14 kt explosion at a depth of 1720 m in limestone.

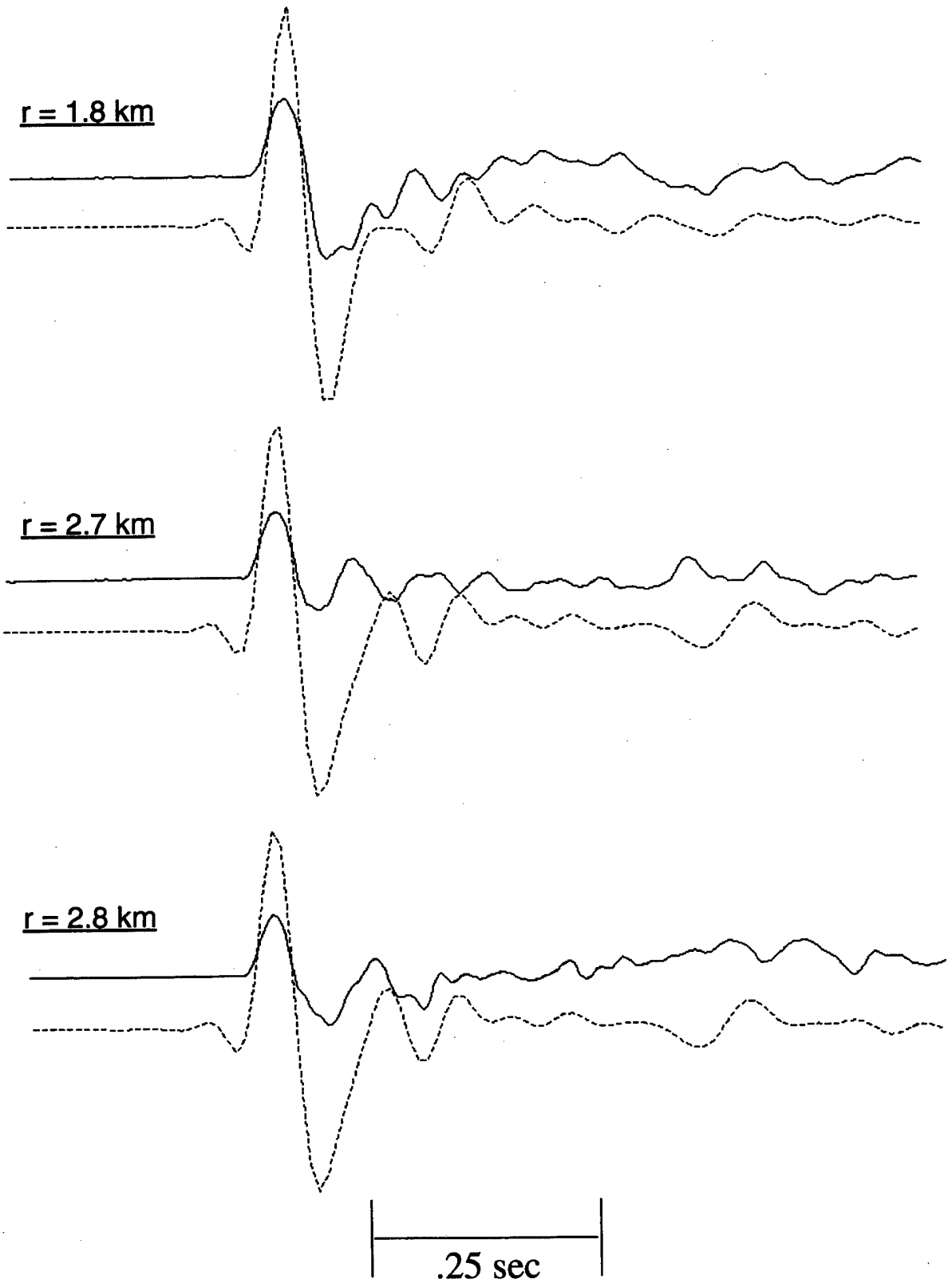


Figure 31. Comparison of observed (solid) and synthetic (dashed) near-regional, vertical component displacements for the PNE event of 4/18/87, which was a 3.2 kt explosion at a depth of 2055 m in limestone.

frequencies is quite reasonable, at least for the initial arrivals. However, the comparisons for the PNE event of 4/18/87 are less satisfactory in that the predicted amplitude levels are found to be 3 to 5 times larger than the observed at the three stations in the narrow distance range extending from 1.75 to 2.82 km. This is puzzling, particularly in view of the fact that the observed dominant frequency of the initial arrivals is well matched by the synthetics, which would not be expected if the actual source coupling was significantly different than predicted. While it is the deepest of the four explosions in limestone, it is not significantly deeper than the 4/11/72 explosion (i.e., 2055 versus 1720 m) for which the amplitude levels of the observed and synthetic waveforms are in good agreement (cf. Figure 30). It may be that there is some unaccounted for local receiver site attenuation in this case, but there are no data currently available to test this hypothesis. Thus, there is no obvious explanation for this discrepancy at the present time.

The final comparison is presented in Figure 32 which shows the observed and synthetic vertical component displacement waveforms for the 6/18/85 2.5 kt PNE event in sandstone. At an announced depth of 2859 m, this is the deepest known nuclear explosion conducted to date. Therefore, it is particularly significant that the synthetic waveforms predicted using the Mueller/Murphy source model provide such excellent fits to the observed amplitude levels and dominant frequencies at these three stations in the distance range extending from 1.41 to 6.00 km from this deeply overburied explosion.

In summary, considering the simplicity of the source and propagation path models employed, the overall agreement between the synthetic and observed waveforms shown in Figures 24-32 is quite remarkable and seems to confirm the fact that the Mueller/Murphy source approximation can generally account for the observed variations in seismic source coupling over the ranges of explosion yield, depth of burial and source media considered in this study. Moreover, although the data overlap between the PNE events represented in the near-regional and Borovoye regional data sets is not extensive enough to provide a definitive test of the covariance decomposition of the source and propagation path effects on the Borovoye data, the analyses have demonstrated that both data sets are generally consistent with the source yield and depth of burial scaling predicted by the

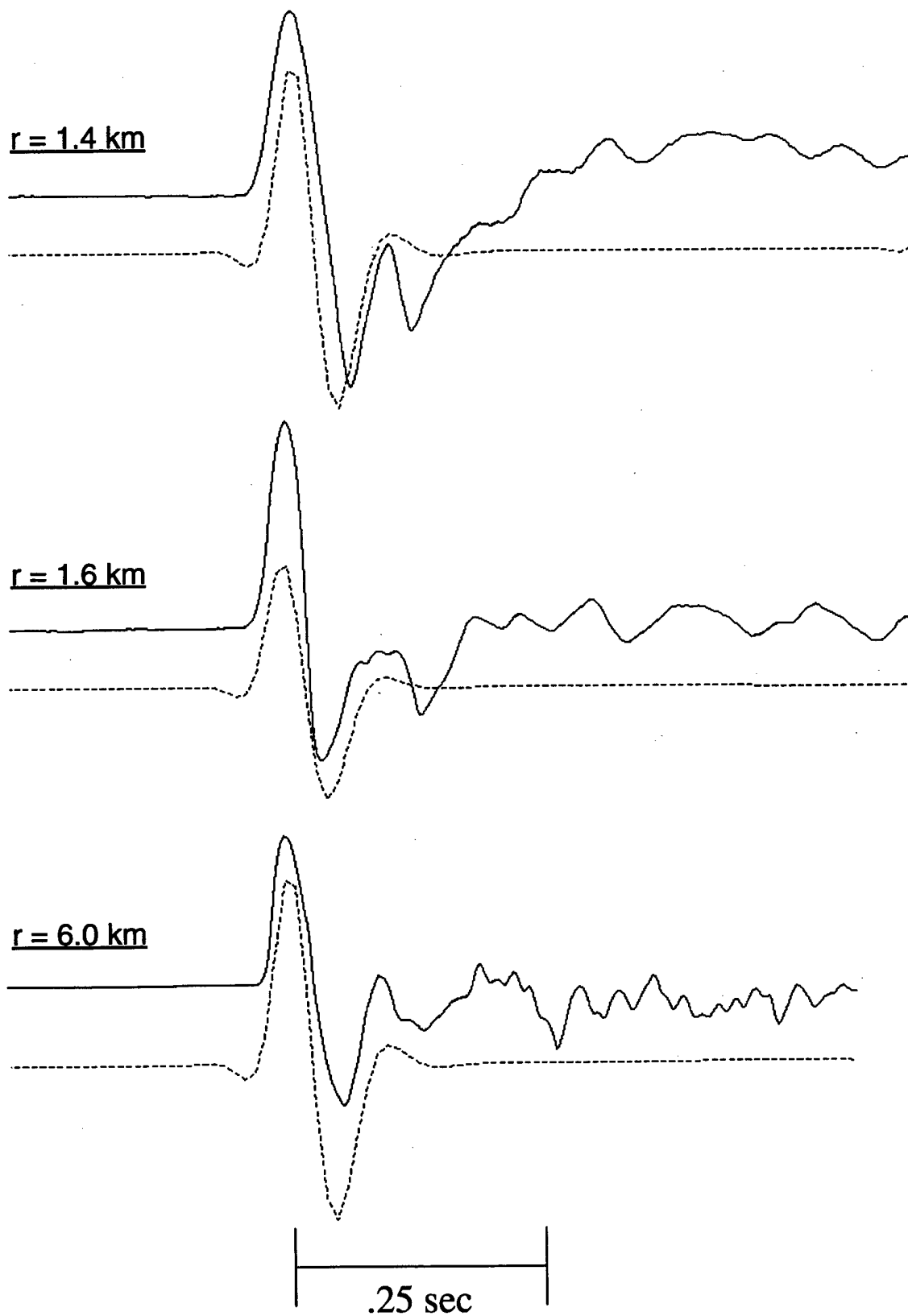


Figure 32. Comparison of observed (solid) and synthetic (dashed) near-regional, vertical component displacements for the PNE event of 6/18/85, which was a 2.5 kt explosion at a depth of 2859 m in sandstone.

Mueller/Murphy model, which supports the applicability of the proposed covariance model.

## **5. SUMMARY AND CONCLUSIONS**

### **5.1 Summary**

This report has provided a summary of the results of a joint research program which has been carried out by scientists from Maxwell Technologies, Inc. and the Russian Institute for Dynamics of the Geospheres (IDG) in an attempt to derive improved, quantitative constraints on the transportability of various regional discriminants as they apply to the identification of underground nuclear explosions under the CTBT. In particular, regional seismic data recorded at the Borovoye Geophysical Observatory in Central Asia from selected Soviet PNE tests have been collected and analyzed in detail in order to better define the ranges of seismic signal characteristics which could be expected from underground nuclear explosions conducted under the wide variety of source and propagation path conditions which must be considered in global test monitoring.

The characteristics of the 29 selected PNE events located in the regional distance range extending from 7.2 to 19.1 degrees from Borovoye were described in Section 2, where the corresponding seismic data recorded at that station were also reviewed and analyzed. It was noted there that these explosions encompass wide ranges in source medium (sandstone, clay, salt, limestone/dolomite, argillite and gabbro), yield (2.5-37.6 kt) and source depth (554-2859 m) and, therefore, that they can provide valuable insight into the effects of explosion source conditions on seismic discrimination capability. Waveform data from a selected subset of these explosions located in a narrow distance band extending from 7.2 to 11 degrees from the Borovoye station were also analyzed in some detail and it was demonstrated that the regional phase characteristics of these data show some pronounced dependence on source to station azimuth. An attempt was made to correlate this dependence with changes in crustal structure across the area which have been inferred from previous analyses of DSS data, but no significant structural variations could be identified

which might explain the observed differences in regional phase propagation efficiency.

The spectral characteristics of the selected subsample of Borovoye data were analyzed in Section 3 where these data were bandpass filtered through a Gaussian comb of filters spaced at intervals of 0.25 Hz between 0.5 and 10 Hz. These filter outputs were then used to estimate the spectral composition of the recorded signals in group velocity time windows corresponding to five different regional phases (i.e.,  $P_n$ ,  $P_{\text{coda}}$ ,  $P_g$ ,  $S_n$  and  $L_g$ ). These spectral data were then statistically analyzed to define their dependencies on the various source and propagation path variables and a model was developed for estimating the spectral compositions of the different regional phases over the sampled ranges of these variables. In addition, these data were used to assess the transportability of various proposed regional phase spectral ratio discriminants with respect to applications to data recorded from underground nuclear explosions conducted under a wide range of possible test conditions.

In Section 4 the analysis was extended by conducting theoretical simulations of near-regional seismic data recorded from selected PNE tests. As a result of this analysis, it was demonstrated that a number of important features of these observed data could be accounted for by a simple seismic source model which is consistent with that inferred from the statistical covariance analysis of the corresponding Borovoye regional data. This was interpreted as additional evidence of the validity of the covariance decomposition of source and propagation path effects on the Borovoye regional data recorded from the selected sample of Soviet PNE events.

## 5.2 Conclusions

The research summarized above supports the following conclusions regarding the dependence of the regional phase spectral characteristics of underground nuclear explosions on source and propagation path conditions.

- 1) Statistical covariance analyses of the observed Borovoye PNE regional phase spectral data indicate that, with the exception of explosions in clay, the seismic source coupling in all the other sampled source media

(i.e., salt, sandstone, limestone, dolomite, tuff, gabbro, argillite) is approximately the same. Moreover, the observed frequency dependent variations of the regional phase spectra with explosion yield and depth of burial have been shown to be generally consistent with the predictions of the Mueller/Murphy explosion source model.

- 2) The associated regional propagation path effects inferred from the covariance analyses are complex and do not appear to be easily explainable in terms of simple regionalized models of the study area. For example, the estimated frequency dependence of the attenuation of the  $L_g$  phase over the sampled distance range extending from about 7 to 20 degrees is much less pronounced than that predicted using Mitchell's coda Q values for Central Asia and the observed azimuthal dependence of the relative regional phase propagation efficiency shows no simple correlation with variations in crustal structure inferred from DSS data collected in the region surrounding the Borovoye station.
- 3) These results indicate that extrapolations and interpolations of the results of analyses of limited seismic calibration data and regional geophysical models may be subject to significant uncertainties which will have to be factored into the event screening process under the CTBT.
- 4) The observed spectral amplitude levels of the regional phase signals observed from the PNE events at the Azgir and Astrakhan test sites are not dramatically different from those observed from other PNE events at similar distances from the Borovoye station outside the Caspian Basin and show no evidence of  $L_g$  blockage, at least along this path.
- 5) The residual uncertainties associated with the derived covariance models depend on both frequency and the assumed degree of calibration. With a reasonable level of calibration, the 95% uncertainty bounds on the mean model predictions decrease from about a factor of 3 above and below the mean in the 3.0 to 5.0 Hz frequency band to about a factor of 2 between 0.5 and 1.5 Hz, at least for the range of source and propagation path conditions represented by our Borovoye data sample.

- 6) Despite the relatively high degree of variability of the regional signals observed at Borovoye from Soviet PNE events, the analysis results suggest that the corresponding spectral ratio discriminant values are fairly consistent and explosion-like at high frequencies. Spectral ratios computed with respect to the  $P_g$  phase show much less scatter than do the corresponding ratios computed with respect to the  $P_n$  phase. Moreover,  $L_g/P$  ratios are found to be more diagnostic than  $S_n/P$  ratios in that they more consistently decrease to explosion-like values at high frequencies.
- 7) The average  $L_g/P$  spectral ratios determined for the different groups of PNE events recorded at Borovoye show no obvious distance dependence over the sample range extending from 7.2 to 19.1 degrees. Moreover, they are consistent in that, for all the distance groups, the average ratios decrease to values of less than 1.0 above about 2 Hz, where the associated 95% uncertainty bound on the average ratios is about a factor of 1.7.
- 8) Simulation analyses of near-regional ( $\Delta < 25$  km) data observed from selected Soviet PNE events indicate that the Mueller/Murphy source model can be used to provide reasonable descriptions of the absolute amplitudes and frequency contents of these data. These results, taken together with those obtained from the covariance analyses of the corresponding Borovoye regional data, lead us to conclude that the Mueller/Murphy source model can be used to reliably estimate the expected variations in regional phase spectral composition over the range of explosion source conditions of potential interest in CTBT monitoring.

## REFERENCES

- Adushkin, V. V. and V. A. An (1990), "Seismic Observations and Monitoring of Underground Nuclear Explosions at Borovoye Geophysical Observatory," *Izv. Acad. Sci. USSR, Phys. Solid Earth*, No. 12, 1023-1031.
- Barker, T. G., S. M. Day, K. L. McLaughlin, B. Shkoller, and J. L. Stevens (1990), "An Analysis of the Effects of Spall on Regional and Teleseismic Waveforms Using Two-Dimensional Numerical Modeling of Underground Explosions," GL-TR-90-0126, ADA226921.
- Baumgardt, D. R. (1990), "Investigation of Teleseismic  $L_g$  Blockage and Scattering Using Regional Arrays," *Bull. Seism. Soc. Am.*, 80, pp. 2261-2281.
- Belousov, V. V., N. I. Pavlenkova and G. N. Kvyatkovskaya (1991), U.S.S.R. Deep Structure, Nauka, Moscow.
- Bennett, T. J. and J. R. Murphy (1986), "Analysis of Seismic Discrimination Capabilities Using Regional Data From Western U.S. Events," *Bull. Seism. Soc. Am.*, 76, 1069-1086.
- Bennett, T. J., J. R. Murphy, M. E. Marshall and B. W. Barker (1993), "A Preliminary Regional Seismic Discrimination Analysis of the Novaya Zemlya Event of December 31, 1992," in *The Novaya Zemlya Event of 31 December 1992 and Seismic Identification Issues*, edited by A. S. Ryall, 15th Annual Seismic Research Symposium, PL-TR-93-2160, ADA271458.
- Blandford, R. and P. Klouda (1980), "Magnitude-Yield Results at the Tonto Forest Observatory," in *Studies of Seismic Wave Characteristics at Regional Distances*, Teledyne-Geotech Report AL-80-1, Teledyne-Geotech, Alexandria, Virginia.
- Blandford, R. R. (1981), "Seismic Discrimination Problems at Regional Distances, in *Identification of Seismic Sources - Earthquake or Underground Explosion*, D. Reidel Publishing Company, Boston, Massachusetts.
- Bouchon, M. (1981), "A Simple Method to Calculate Green's Functions For Elastic Layered Media," *Bull. Seism. Soc. Am.*, 71, 959-971.
- Chael, E. P. (1988), "Spectral Discrimination of NTS Explosions and Earthquakes in the Southwestern United States Using High-Frequency Regional Data," *Geophys. Res. Lett.*, 15, pp. 625-628.
- Kim, W-Y and G. Ekström (1996), "Instrument Responses of Digital Seismographs at Borovoye, Kazakhstan, by Inversion of Transient Calibration Pulses," *Bull. Seism. Soc. Am.*, 86, 191.

- Laushkin, V. A., S. I. Oreshin and V. M. Ovtchinnikov (1995), "Regional Analysis of Former Soviet Union Peaceful Nuclear Explosions Recorded in the Former Soviet Union," EOARD Report SPC-94-4065.
- McLaughlin, K. L., J. L. Stevens, T. G. Barker, S. M. Day, and B. Shkoller (1993), "2D and 3D Numerical Modeling of Seismic Waves from Explosion Sources," in *Proceedings of the Numerical Modeling for Underground Nuclear Test Monitoring Symposium*, Editors: S. R. Taylor, and J. R. Kamm, LANL Report LA-UR-93-3839.
- Mitchell, B. J., Y. Pan and J. Xie (1996), "The Variation of  $L_g$  Coda Q across Eurasia and its Relation to Continental Evolution," PL-TR-96-2154, ADA317387.
- Mueller, R. A. and J. R. Murphy (1971), "Seismic Characteristics of Underground Nuclear Detonations. Part I. Seismic Spectrum Scaling," *Bull. Seism. Soc. Am.*, 61, 1975.
- Murphy, J. R. (1977), "Seismic Source Functions and Magnitude Determinations for Underground Nuclear Detonations," *Bull. Seism. Soc. Am.*, 67, 135-158.
- Murphy, J. R. and L. J. O'Brien (1977), "The Correlation of Peak Ground Acceleration Amplitude With Seismic Intensity and Other Physical Parameters," *Bull. Seism. Soc. Am.*, 67, 877-915.
- Murphy, J. R. and T. J. Bennett (1982), "A Discrimination Analysis of Short-Period Regional Seismic Data Recorded at Tonto Forest Observatory," *Bull. Seism. Soc. Am.*, 72, pp. 1351-1366.
- Murphy, J. R., B. W. Barker and A. O'Donnell (1989), "Network-Averaged Teleseismic P-Wave Spectra For Underground Explosions. Part I. Definitions and Examples," *Bull. Seism. Soc. Am.*, 79, 141-155.
- Murphy, J. R. and B. W. Barker (1994), "Application of Network-Averaged Teleseismic P Wave Spectra to an Analysis of the Seismic Source Characteristics of Soviet PNE Explosions," S-CUBED Report SSS-FR-94-14528.
- Murphy, J. R., D. D. Sultanov, B. W. Barker, I. O. Kitov and M. E. Marshall (1996), "Application of Soviet PNE Data to the Assessment of the Transportability of Regional Discriminants," PL-TR-96-2290, ADA323142.
- Murphy, J. R., I. O. Kitov, N. Rimer, D. D. Sultanov, B. W. Barker, J. L. Stevens, V. V. Adushkin and K. H. Lie (1996), "Further Studies of the Seismic Characteristics of Russian Explosions in Cavities: Implications For Cavity Decoupling of Underground Nuclear Explosions," PL-TR-96-2017, ADA305955.
- Ringdal, F. and B. K. Hokland (1987), "Magnitudes of Large Semipalatinsk Explosions Using P Coda and  $L_g$  Measurements at NORSAR," in *NORSAR Semiannual Technical Summary*, 1 April - 30 September 1987, Rept. 1-87/88.

- Constraint of the Physical Source Mechanisms," in *Explosion Source Phenomenology, Geophysical Monograph 65*, AGU, Washington, DC.
- Sultanov, D. D., Kh. D. Rubinshtein, E. N. Ferapontova, P. B. Kaazik, O. P. Kuznetsov, I. O. Kitov, N. I. Nedoshivin, V. M. Ovtchinnikov, Yu., K. Malyshev and O. P. Willemson (1993), "Investigation of Seismic Efficiency of Soviet Peaceful Nuclear Explosions Conducted in Various Geological Conditions," Institute for Dynamics of the Geospheres, Russian Academy of Sciences Report dated July 29, 1993.
- Taylor, S. R., N. W. Sherman and M. D. Denny (1988), "Spectral Discrimination Between NTS Explosions and Western United States Earthquakes at Regional Distances," *Bull. Seism. Soc. Am.*, 78, pp. 1563-1579.
- Taylor, S. R. and G. E. Randall (1989), "The Effects of Spall on Regional Seismograms," *Geophys. Res. Lett.*, 16, 211-214.
- Taylor, S. R. and M. D. Denny (1991), "An Analysis of Spectral Differences Between Nevada Test Site and Shagan River Nuclear Explosions," *J. Geophys. Res.*, 96, pp. 6237-6245.
- Veith, K. F. and G. E. Clawson (1972), "Magnitude From Short-Period P-Wave Data," *Bull. Seism. Soc. Am.*, 62, 435-452.
- Zverev, S. M. and I. P. Kosminskaya (1980), Seismic Models For Lithosphere Beneath Principal Gestructures of the U.S.S.R. Territory, Nauka, Moscow.

THOMAS AHRENS  
SEISMOLOGICAL LABORATORY 252-21  
CALIFORNIA INSTITUTE OF TECHNOLOGY  
PASADENA, CA 91125

AIR FORCE RESEARCH LABORATORY  
ATTN: VSOE  
29 RANDOLPH ROAD  
HANSCOM AFB, MA 01731-3010 (2 COPIES)

AIR FORCE RESEARCH LABORATORY  
ATTN: RESEARCH LIBRARY/TL  
5 WRIGHT STREET  
HANSCOM AFB, MA 01731-3004

AIR FORCE RESEARCH LABORATORY  
ATTN: AFRL/SUL  
3550 ABERDEEN AVE SE  
KIRTLAND AFB, NM 87117-5776 (2 COPIES)

RALPH ALEWINE  
NTPO  
1901 N. MOORE STREET, SUITE 609  
ARLINGTON, VA 22209

MUAWIA BARAZANGI  
INSTITUTE FOR THE STUDY OF THE CONTINENTS  
3126 SNEE HALL  
CORNELL UNIVERSITY  
ITHACA, NY 14853

T.G. BARKER  
MAXWELL TECHNOLOGIES  
8888 BALBOA AVE.  
SAN DIEGO, CA 92123-1506

DOUGLAS BAUMGARDT  
ENSCO INC.  
5400 PORT ROYAL ROAD  
SPRINGFIELD, VA 22151

THERON J. BENNETT  
MAXWELL TECHNOLOGIES  
11800 SUNRISE VALLEY DRIVE SUITE 1212  
RESTON, VA 22091

WILLIAM BENSON  
NAS/COS  
ROOM HA372  
2001 WISCONSIN AVE. NW  
WASHINGTON DC 20007

JONATHAN BERGER  
UNIVERSITY OF CA, SAN DIEGO  
SCRIPPS INSTITUTION OF OCEANOGRAPHY IGPP, 0225  
9500 GILMAN DRIVE  
LA JOLLA, CA 92093-0225

ROBERT BLANDFORD  
AFTAC  
1300 N. 17TH STREET  
SUITE 1450  
ARLINGTON, VA 22209-2308

LESLIE A. CASEY  
DEPT. OF ENERGY/NN-20  
1000 INDEPENDENCE AVE. SW  
WASHINGTON DC 20585-0420

CENTER FOR MONITORING RESEARCH  
ATTN: LIBRARIAN  
1300 N. 17th STREET, SUITE 1450  
ARLINGTON, VA 22209

ANTON DAINTY  
HQ DSWA/PMP  
6801 TELEGRAPH ROAD  
ALEXANDRIA, VA 22310-3398

CATHERINE DE GROOT-HEDLIN  
UNIVERSITY OF CALIFORNIA, SAN DIEGO  
INSTITUTE OF GEOPHYSICS AND PLANETARY PHYSICS  
8604 LA JOLLA SHORES DRIVE  
SAN DIEGO, CA 92093

DEFENSE TECHNICAL INFORMATION CENTER  
8725 JOHN J. KINGMAN ROAD  
FT BELVOIR, VA 22060-6218 (2 COPIES)

DIANE DOSER  
DEPARTMENT OF GEOLOGICAL SCIENCES  
THE UNIVERSITY OF TEXAS AT EL PASO  
EL PASO, TX 79968

MARK D. FISK  
MISSION RESEARCH CORPORATION  
735 STATE STREET  
P.O. DRAWER 719  
SANTA BARBARA, CA 93102-0719

LORI GRANT  
MULTIMAX, INC.  
311C FOREST AVE. SUITE 3  
PACIFIC GROVE, CA 93950

HENRY GRAY  
SMU STATISTICS DEPARTMENT  
P.O. BOX 750302  
DALLAS, TX 75275-0302

I. N. GUPTA  
MULTIMAX, INC.  
1441 MCCORMICK DRIVE  
LARGO, MD 20774

DAVID HARKRIDER  
BOSTON COLLEGE  
INSTITUTE FOR SPACE RESEARCH  
140 COMMONWEALTH AVENUE  
CHESTNUT HILL, MA 02167

THOMAS HEARN  
NEW MEXICO STATE UNIVERSITY  
DEPARTMENT OF PHYSICS  
LAS CRUCES, NM 88003

MICHAEL HEDLIN  
UNIVERSITY OF CALIFORNIA, SAN DIEGO  
SCRIPPS INSTITUTION OF OCEANOGRAPHY IGPP, 0225  
9500 GILMAN DRIVE  
LA JOLLA, CA 92093-0225

DONALD HELMBERGER  
CALIFORNIA INSTITUTE OF TECHNOLOGY  
DIVISION OF GEOLOGICAL & PLANETARY SCIENCES  
SEISMOLOGICAL LABORATORY  
PASADENA, CA 91125

EUGENE HERRIN  
SOUTHERN METHODIST UNIVERSITY  
DEPARTMENT OF GEOLOGICAL SCIENCES  
DALLAS, TX 75275-0395

ROBERT HERRMANN  
ST. LOUIS UNIVERSITY  
DEPARTMENT OF EARTH & ATMOSPHERIC SCIENCES  
3507 LACLEDE AVENUE  
ST. LOUIS, MO 63103

VINDELL HSU  
HQ/AFTAC/TTR  
1030 S. HIGHWAY A1A  
PATRICK AFB, FL 32925-3002

RONG-SONG JIH  
HQ DSWA/PMP/CTBT  
6801 TELEGRAPH ROAD  
ALEXANDRIA, VA 22310-3398

THOMAS JORDAN  
MASSACHUSETTS INSTITUTE OF TECHNOLOGY  
EARTH, ATMOSPHERIC & PLANETARY SCIENCES  
77 MASSACHUSETTS AVENUE, 54-918  
CAMBRIDGE, MA 02139

LAWRENCE LIVERMORE NATIONAL LABORATORY  
ATTN: TECHNICAL STAFF (PLS ROUTE)  
PO BOX 808, MS L-175  
LIVERMORE, CA 94551

LAWRENCE LIVERMORE NATIONAL LABORATORY  
ATTN: TECHNICAL STAFF (PLS ROUTE)  
PO BOX 808, MS L-208  
LIVERMORE, CA 94551

LAWRENCE LIVERMORE NATIONAL LABORATORY  
ATTN: TECHNICAL STAFF (PLS ROUTE)  
PO BOX 808, MS L-202  
LIVERMORE, CA 94551

LAWRENCE LIVERMORE NATIONAL LABORATORY  
ATTN: TECHNICAL STAFF (PLS ROUTE)  
PO BOX 808, MS L-195  
LIVERMORE, CA 94551

LAWRENCE LIVERMORE NATIONAL LABORATORY  
ATTN: TECHNICAL STAFF (PLS ROUTE)  
PO BOX 808, MS L-205  
LIVERMORE, CA 94551

LAWRENCE LIVERMORE NAT'L LABORATORY  
ATTN: TECHNICAL STAFF (PLS ROUTE)  
PO BOX 808, MS L-200  
LIVERMORE, CA 94551

LAWRENCE LIVERMORE NAT'L LABORATORY  
ATTN: TECHNICAL STAFF (PLS ROUTE)  
PO BOX 808, MS L-221  
LIVERMORE, CA 94551

THORNE LAY  
UNIVERSITY OF CALIFORNIA, SANTA CRUZ  
EARTH SCIENCES DEPARTMENT  
EARTH & MARINE SCIENCE BUILDING  
SANTA CRUZ, CA 95064

ANATOLI L. LEVSHIN  
DEPARTMENT OF PHYSICS  
UNIVERSITY OF COLORADO  
CAMPUS BOX 390  
BOULDER, CO 80309-0309

JAMES LEWKOWICZ  
WESTON GEOPHYSICAL CORP.  
325 WEST MAIN STREET  
NORTHBORO, MA 01532

LOS ALAMOS NATIONAL LABORATORY  
ATTN: TECHNICAL STAFF (PLS ROUTE)  
PO BOX 1663, MS F659  
LOS ALAMOS, NM 87545

LOS ALAMOS NATIONAL LABORATORY  
ATTN: TECHNICAL STAFF (PLS ROUTE)  
PO BOX 1663, MS F665  
LOS ALAMOS, NM 87545

LOS ALAMOS NATIONAL LABORATORY  
ATTN: TECHNICAL STAFF (PLS ROUTE)  
PO BOX 1663, MS D460  
LOS ALAMOS, NM 87545

LOS ALAMOS NATIONAL LABORATORY  
ATTN: TECHNICAL STAFF (PLS ROUTE)  
PO BOX 1663, MS C335  
LOS ALAMOS, NM 87545

GARY MCCARTOR  
SOUTHERN METHODIST UNIVERSITY  
DEPARTMENT OF PHYSICS  
DALLAS, TX 75275-0395

KEITH MCLAUGHLIN  
CENTER FOR MONITORING RESEARCH (SAIC)  
1300 N. 17TH STREET, SUITE 1450  
ARLINGTON, VA 22209

BRIAN MITCHELL  
DEPARTMENT OF EARTH & ATMOSPHERIC SCIENCES  
ST. LOUIS UNIVERSITY  
3507 LACLEDE AVENUE  
ST. LOUIS, MO 63103

RICHARD MORROW  
USACDA/IVI  
320 21ST STREET, N.W.  
WASHINGTON DC 20451

JOHN MURPHY  
MAXWELL TECHNOLOGIES  
11800 SUNRISE VALLEY DRIVE SUITE 1212  
RESTON, VA 22091

JAMES NI  
NEW MEXICO STATE UNIVERSITY  
DEPARTMENT OF PHYSICS  
LAS CRUCES, NM 88003

ROBERT NORTH  
CENTER FOR MONITORING RESEARCH  
1300 N. 17th STREET, SUITE 1450  
ARLINGTON, VA 22209

OFFICE OF THE SECRETARY OF DEFENSE  
DDR&E  
WASHINGTON DC 20330

JOHN ORCUTT  
INSTITUTE OF GEOPHYSICS AND PLANETARY PHYSICS  
UNIVERSITY OF CALIFORNIA, SAN DIEGO  
LA JOLLA, CA 92093

PACIFIC NORTHWEST NATIONAL LABORATORY  
ATTN: TECHNICAL STAFF (PLS ROUTE)  
PO BOX 999, MS K6-48  
RICHLAND, WA 99352

PACIFIC NORTHWEST NATIONAL LABORATORY  
ATTN: TECHNICAL STAFF (PLS ROUTE)  
PO BOX 999, MS K6-40  
RICHLAND, WA 99352

PACIFIC NORTHWEST NATIONAL LABORATORY  
ATTN: TECHNICAL STAFF (PLS ROUTE)  
PO BOX 999, MS K6-84  
RICHLAND, WA 99352

PACIFIC NORTHWEST NATIONAL LABORATORY  
ATTN: TECHNICAL STAFF (PLS ROUTE)  
PO BOX 999, MS K5-12  
RICHLAND, WA 99352

FRANK PILOTTE  
HQ AFTAC/TT  
1030 S. HIGHWAY A1A  
PATRICK AFB, FL 32925-3002

KEITH PRIESTLEY  
DEPARTMENT OF EARTH SCIENCES  
UNIVERSITY OF CAMBRIDGE  
MADINGLEY RISE, MADINGLEY ROAD  
CAMBRIDGE, CB3 0EZ UK

JAY PULLI  
BBN SYSTEMS AND TECHNOLOGIES, INC.  
1300 NORTH 17TH STREET  
ROSSLYN, VA 22209

DELAINE REITER  
SENCOM CORP.  
73 STANDISH ROAD  
WATERTOWN, MA 02172

PAUL RICHARDS  
COLUMBIA UNIVERSITY  
LAMONT-DOHERTY EARTH OBSERVATORY  
PALISADES, NY 10964

MICHAEL RITZWOLLER  
DEPARTMENT OF PHYSICS  
UNIVERSITY OF COLORADO  
CAMPUS BOX 390  
BOULDER, CO 80309-0309

DAVID RUSSELL  
HQ AFTAC/TTR  
1030 SOUTH HIGHWAY A1A  
PATRICK AFB, FL 32925-3002

CHANDAN SAIKIA  
WOODWARD-CLYDE FEDERAL SERVICES  
566 EL DORADO ST., SUITE 100  
PASADENA, CA 91101-2560

SANDIA NATIONAL LABORATORY  
ATTN: TECHNICAL STAFF (PLS ROUTE)  
DEPT. 5704  
MS 0979, PO BOX 5800  
ALBUQUERQUE, NM 87185-0979

SANDIA NATIONAL LABORATORY  
ATTN: TECHNICAL STAFF (PLS ROUTE)  
DEPT. 9311  
MS 1159, PO BOX 5800  
ALBUQUERQUE, NM 87185-1159

SANDIA NATIONAL LABORATORY  
ATTN: TECHNICAL STAFF (PLS ROUTE)  
DEPT. 5704  
MS 0655, PO BOX 5800  
ALBUQUERQUE, NM 87185-0655

SANDIA NATIONAL LABORATORY  
ATTN: TECHNICAL STAFF (PLS ROUTE)  
DEPT. 5736  
MS 0655, PO BOX 5800  
ALBUQUERQUE, NM 87185-0655

THOMAS SERENO JR.  
SCIENCE APPLICATIONS INTERNATIONAL  
CORPORATION  
10260 CAMPUS POINT DRIVE  
SAN DIEGO, CA 92121

AVI SHAPIRA  
SEISMOLOGY DIVISION  
THE INSTITUTE FOR PETROLEUM RESEARCH AND  
GEOPHYSICS  
P.O.B. 2286 NOLON 58122 ISRAEL

ROBERT SHUMWAY  
410 MRAK HALL  
DIVISION OF STATISTICS  
UNIVERSITY OF CALIFORNIA  
DAVIS, CA 95616-8671

DAVID SIMPSON  
IRIS  
1200 NEW YORK AVE., NW  
SUITE 800  
WASHINGTON DC 20005

JEFFRY STEVENS  
MAXWELL TECHNOLOGIES  
8888 BALBOA AVE.  
SAN DIEGO, CA 92123-1506

BRIAN SULLIVAN  
BOSTON COLLEGE  
INSITUTE FOR SPACE RESEARCH  
140 COMMONWEALTH AVENUE  
CHESTNUT HILL, MA 02167

TACTEC  
BATTELLE MEMORIAL INSTITUTE  
505 KING AVENUE  
COLUMBUS, OH 43201 (FINAL REPORT)

NAFI TOKSOZ  
EARTH RESOURCES LABORATORY, M.I.T.  
42 CARLTON STREET, E34-440  
CAMBRIDGE, MA 02142

LAWRENCE TURNBULL  
ACIS  
DCI/ACIS  
WASHINGTON DC 20505

GREG VAN DER VINK  
IRIS  
1200 NEW YORK AVE., NW  
SUITE 800  
WASHINGTON DC 20005

FRANK VERNON  
UNIVERSITY OF CALIFORNIA, SAN DIEGO  
SCRIPPS INSTITUTION OF OCEANOGRAPHY IGPP, 0225  
9500 GILMAN DRIVE  
LA JOLLA, CA 92093-0225

TERRY WALLACE  
UNIVERSITY OF ARIZONA  
DEPARTMENT OF GEOSCIENCES  
BUILDING #77  
TUCSON, AZ 85721

JILL WARREN  
LOS ALAMOS NATIONAL LABORATORY  
GROUP NIS-8  
P.O. BOX 1663  
LOS ALAMOS, NM 87545 (5 COPIES)

DANIEL WEILL  
NSF  
EAR-785  
4201 WILSON BLVD., ROOM 785  
ARLINGTON, VA 22230

RU SHAN WU  
UNIVERSITY OF CALIFORNIA SANTA CRUZ  
EARTH SCIENCES DEPT.  
1156 HIGH STREET  
SANTA CRUZ, CA 95064

JIAKANG XIE  
COLUMBIA UNIVERSITY  
LAMONT DOHERTY EARTH OBSERVATORY  
ROUTE 9W  
PALISADES, NY 10964

JAMES E. ZOLLWEG  
BOISE STATE UNIVERSITY  
GEOSCIENCES DEPT.  
1910 UNIVERSITY DRIVE  
BOISE, ID 83725